OPTIMIZATION OF PARAMETERS FOR DRILLING OF HARD ROCKS IN PETROLEUM EXPLORATION

A PROJECT THESIS

Submitted by

SHAHID SADIQ

(2010-NUST-MS-IME-14)

In partial fulfillment of the requirements of the Higher Education Commission, Pakistan

PROJECT SUPERVISOR

DR. SYED HUSSAIN IMRAN JAFFERY

PROJECT Co-SUPERVISOR

DR. MUSHTAQ KHAN

SCHOOL OF MECHANICAL & MANUFACTURING ENGINEERING,

NATIONAL UNIVERSITY OF SCIENCES & TECHNOLOGY

ACKNOWLEDGEMENTS

Thanks to Allah Almighty for bringing me to this stage and my supervisors for guiding me through the process.

ABSTRACT

Pakistan's economy is experiencing a steady growth and the industrial sector is poised to contribute significantly towards the economy. In this context, the availability of energy at competitive rates is vital for Pakistan's industry in order for it to compete internationally. The role of petroleum based fuels in powering the economy is significant and evident from the fact that out of 20.4 GW of installed electricity generation capacity in Pakistan, thermal power plants account for 66% of this figure as against 32% contributed by hydal power generation.

With the electricity requirements increasing in the country, most of the thermal power is generated by fuel oil and natural gas. Out of these, fuel oil is mostly imported while natural gas reserves in the country are limited and expected to be depleted by 20 years owing to heavy industrial and domestic usage. It is therefore expedient to explore new deposits of petroleum resources in the country, so as to reduce the import bill and provide fuel at economic price to enable industrial growth.

In Pakistan, petroleum deposits are often found in hard rock formations as well as greater depths. There is therefore a strong need to optimize the drilling process by identifying the key process variables that contribute towards drill bit wear and drill life. Based on this analysis and field data, the drill life can be mapped against the dominant process parameters so that a window of optimal performance can be identified.

Furthermore, drill wear mechanisms can also be identified by performing scale-down model testing in laboratory conditions that would ultimately lead to the development of more efficient drilling bits. Ultimately the project aims to help local mining and exploration industry like OGDCL reduce operating cost.

TABLE OF CONTENTS

LIST OF FIGURES

LIST OF TABLES

LIST OF ABBREVIATIONS

Abbreviation	Expanded form
2D	Two dimensional
3D	Three dimensional
AC	Alternating Current
ASTM	American Standard Testing Methods
DLC	Diamond Like Carbon
EDS	Energy Dispersive Spectrometer
HSS	High speed steel
MEMS	Micro Electro Mechanical Systems
MRR	Material Removal Rate
N/A	Not Applicable
OGDCL	Oil and Gas Development Corporation Limited.
PID	Proportional Integral Differential (Controller)
SEM	Scanning Electron Microscopy
SiC	Silicon Carbide
SiO_2	Silica
SMME	School of Mechanical and Manufacturing Engineering
SS	Stainless Steel
TEM	Transmission Electron Micrography
TiN	Titatnium Nitride
XRD	X-Ray Diffractometer

LIST OF SYMBOLS

Roman Symbols

Symbol	Description
Al_2O_3	Aluminum Oxide
B	Bit efficiency co-efficient
P	Applied load
$h_x\ (x = o, W, f)$	Depth (o=Original, W=worn, f=scar surface)
d, D	Diameter
F	Force
Mg-Al-Zn	Magnesium-Aluminum-Zinc Alloy
m	Mass
MoS_2	Molybdenum Sulfide
I	Moment of Inertia
$r, R_x\ (x = o, W, f)$	Radius (o=Original, W=worn, f=scar surface)
SiO_2	Silica
SiC	Silicon Carbide
T	Torque
V	Volume
W	Width of wear scar

Greek Symbols

Symbol	Description
α	Rotational acceleration
μ	Co-efficient of friction
$\omega_x\ (x = \theta, z)$	Frequency (θ=rotational, z=normal)

CHAPTER 1: INTRODUCTION

The engineering problem of wear has been known to mankind since antiquity (1) . Lubricants such as animal fat were used in axles of chariots to reduce friction and to avoid the excessive material-loss which is when dry surfaces rub together. Modern engineering approach has gone a step further and looked into the mechanisms of wear such as wear caused by adhesion, abrasion, oxidation, delaminating and melting.

Various researchers have looked into wear mechanisms for different metal cutting processes like drilling, milling and turning. Such research has contributed tremendously towards the development of more effective tools and tool coatings, leading to enhanced tool life and greater productivity. Ultimately, such developments have contributed to reduced process costs and enhanced process efficiency.

The process of oil drilling is analogous to the process of metal drilling, albeit on a much larger scale. The tools used in this process are also of similar categories, that include high speed steel (HSS), carbide (tungsten carbide), diamond (various grades of diamond) and coated tools. However, as compared with metal cutting, very few researchers have reported work done on the wear.

The more we can characterize the full scale problem the easier it becomes to ensure that the bench tests we run will provide useful information. Critical to the characterization process and ultimately to the interpretation of the test results, is the determination of the mechanisms of wear at work in the contact interface.

Wear processes must be analyzed and defined before they can be modeled, for example abrasion, erosion, corrosion or other chemical action, de-lamination or adhesive wear, the involvement of wear debris identified, the appearance of failed surfaces established (for example, cracking, phase transformations, melting, chemical layers).

The type of wear process will, to a large extent, govern whether it can be modeled at reduced scale and whether accelerated testing is valid. As a rule, contacts involving both sliding friction and wear can be modeled at reduced scale and with accelerated testing. This is because it is usually possible to increase the loading conditions in the contact without changing the wear regime.

Processes involving surface fatigue can in some cases be modeled at reduced scale, but for obvious reasons, not at a reduced number of cycles. These processes include rolling contact fatigue and fretting.

The demand for fossil fuels is rising and along with their prices. Furthermore, with no economically viable renewable energy alternative to fossil fuels, hydro-carbon fuels remain the primary source of energy that powers human civilization today. Since hydro-carbon based fuels are nonrenewable, new reservoirs are continuously being explored.

In this context, certain reservoirs are found in hard rock formations that are difficult to drill, rendering them economically unfeasible to extract. In order to analyze wear mechanisms, the first step would be to analyze tool wear rates at known conditions and to determine the optimal conditions for operating existing tools against known rock samples. This research therefore looks towards determining wear rates of these tool materials when worked against hard rock formations.

The breakdown of this thesis is as follows: Chapter 2 is a literature review of rock drilling, tribological investigations performed for rock drilling, uses and modifications of the pin-on-disk tribometer for different purposes, other tribometers used for tribology studies, the techniques employed for determining the wear rates involved, and the methodologies used for identifying different wear mechanisms and constructing wear maps from the acquired data. Chapter 3 is a review of the methodology used in this study; Chapter 4 is the detailed description of the experimental setup, including the fixture design, motor and controller selection, and sample preparation for performing the experiments; following that are the results obtained from the experimentation performed and a discussion of the results, ending with concluding remarks and suggestions for future work.

CHAPTER 2: LITERATURE REVIEW

2.1. DRILLING OF HARD ROCKS

2.1.1. Techniques for rock drilling

Drilling of rocks is a specialized process and requires special techniques and equipment. There are many different techniques for drilling of rocks. The two most commonly employed methods based upon the type of force applied are:

a. Rotary percussive drilling method: in which the rock is crushed into smaller fragments through repeated impact with the bit rotating slightly with each impact, used for hard rocks. (2) (3)
b. Rotary cutting method: In which the drill bit rotates and cuts into the rock, used for soft rocks, such as coal or limestone; but these rocks are encountered rarely, and therefore it's not a common method. (2) (3)

The percussive drilling technique is further classified into:

i. Top-hammer, in which the impact is applied on the drill rod, which transmits the impact (2)
ii. Down-the-hole drilling, in which the impact is applied by the drill bit directly on the rock. (2)

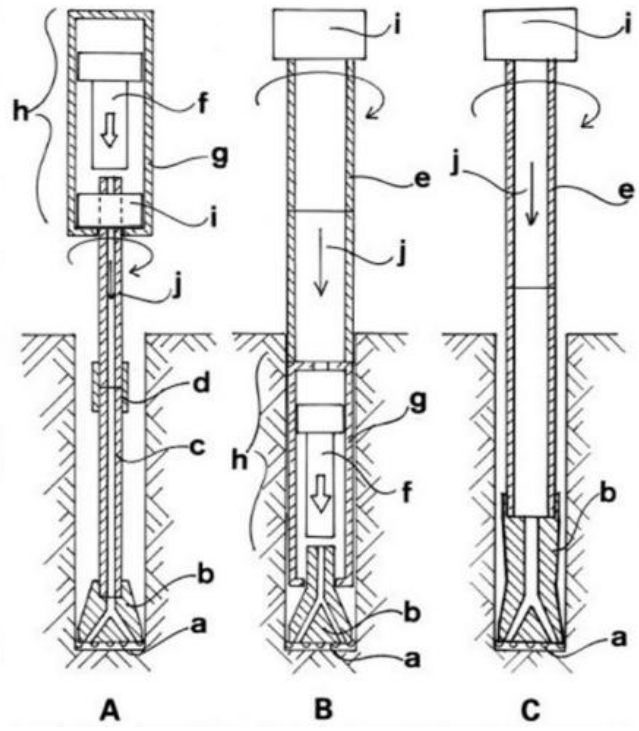

Figure 1 Schematic drawing of 3 types of drills A) Top hammer, B) Down-the-hole, C) Simple Rotary Drill with (a) tip, (b)bit, (c)rod, (d) sleeve, (e) drill pipe, (f) piston, (g) cylinder, (h) percussion mechanism, (i) rotation mechanism and (j) flushing from Watanabe (2)

The rotary cutting technique may be performed via air circulation, water circulation, or mud circulation. The percussive techniques require harder drill bits, and may use pneumatic or hydraulic sources of impact. Sonic drilling, flame jet drilling, and other less frequently used techniques are also used for rock drilling, but the most common type used for drilling hard rocks is the percussive technique. The percussive drilling techniques employ cemented carbide buttons, diamond enhanced buttons (4) or brazed inserts on the high speed steel pins, or diamond cores. (3) (5)

2.1.2. Tribological studies of rock drilling

Beste et al. (5) have experimentally identified that during drilling the rock fragments integrate into the surface of the carbide buttons, either by partially covering the surface, forming an intermixed layer, or forming channels that penetrate deeper into the carbide material. These experiments were performed using repeated drilling experiments on different rock samples.

Oskarsson (6) developed some wear tests for simulating the rotary-percussive technique for drilling rocks. This technique involves bringing spring-loaded drill bit inserts into contact

with a rotating rock-cylinder with an axial feed to compensate for the wear loss, and adding water and slurry to the process to vary the abrasion conditions.

Angseryd et al. (7) have used the rotating-cylinder method (6) to test the wearing behavior of carbide coated drill bits used in rock-drilling. It was found, as by Beste et al. (5) that the rock debris adheres to the surface of the drill bits. This rock debris created abrasion and reduced the life of the drill bit. Wet drilling was found to create more wear in the inserts than dry drilling. (7)

The different mechanisms of rock wear can be identified using the apparatus suggested in this study. The literature study shows that for the optimization of rock drilling, the pin wear must be decreased, with improved ability to create wear and destruction in the rock.

2.2. THE PIN-ON-DISK TRIBOMETER

The tribometer selected for development in this study is the standard pin-on-disk tribometer. It consists of a disc sample rotated at a given frequency, and a loaded pin brought into contact with the rotating disc. This contact brings about wear of both the contacting surfaces; this wear is recorded, and wear-mechanism maps are constructed based upon different experimental iterations with varying conditions. Some example uses of the pin-on-disk apparatus modified for different tribological investigations are as follows:

2.2.1. Example uses of the pin-on-disk apparatus

Magnetic recording media

The pin-on-disk tribometer has been used in different tribological experiments, the most common of which is for the magnetic recording media industry. Experiments have been carried out by Khurshudove et al. (8) ,Kim et. Al (9), Xu and Bhushan (10), and others for identifying the wear behavior of magnetic disk sliders, identifying the mechanisms of wear in these cases and thus different methods have been suggested by them for the improvement of performance and reliability of magnetic discs and magnetic disc sliders. Khurshudov et al. (8) compared the wear behavior of SiC and alumina spherical sliders observed the formation of agglomerated ceramic wear particles for both materials, whereas a longer life was observed for SiC sliders. Kim et al. (9) found that the wear in the head-disk-interface is due to wear particle contamination, and suggested the use of micro-grooves, particle trappings and organic ultra-thin film for reduction of the contact energy at the interface.

Gatzen and Beck (11) modified the standard pin-on-disk tribometer for tribological investigations for comparing Silicon sliders to Altic sliders, used on DLC coated metal discs for the recording head industry. This tribometer was used to run low-velocity friction tests. The testing arrangement consists of a high inertia rotary table fitted with an air bearing, which, due to its enormous mass rotates at low velocities of range 0.1-0.2rpm, and very smooth rotation. This table is driven by a commuting motor via a friction drive. The test-head is fitted in a stage with an adjustable z-height. The arrangement is also equipped with a commercial optical frictional force measurement system, which measures the degree of deflection in the direction of the head's frictional load through a fiberoptic system. A gram load cell is used for verifying and adjusting the nominal force of the test head. In this way friction tests were performed for loads of the range 10-60mN. (11)

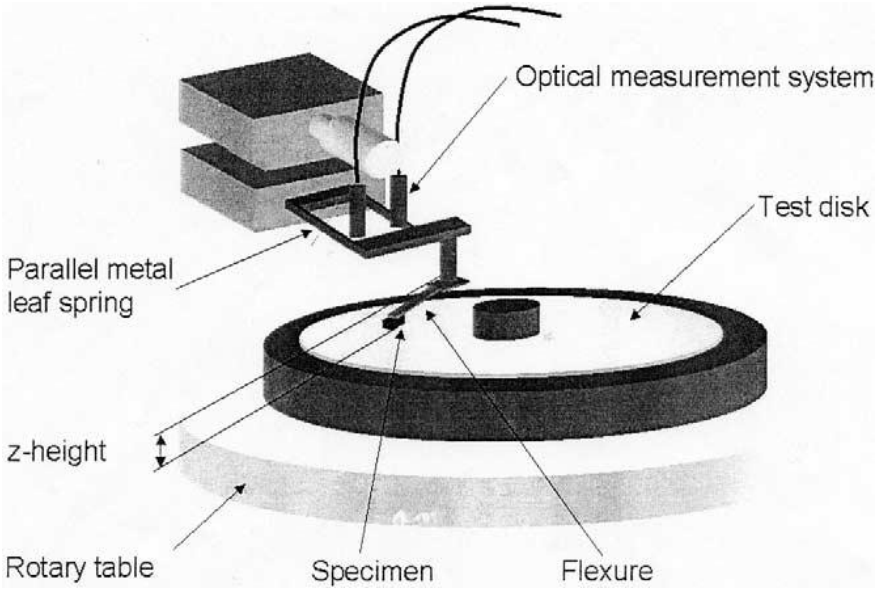

Figure 2 The pin-on-disk apparatus used by Gatzen and Beck

All of the above have employed the standard pin-on-disk apparatus accompanied with some accessories, for carrying out those experiments.

Thermochemical environment tribological investigations

Environmental tribometers which control the thermal and environmental aspects of the experiment are not very common because of the technological complexity involved. (12) Adamou et al. (12) identifies two such types of environmental tribometers:

a. Tribometers which control the chemical environment of the contact interface. These consist of a chamber which can reach upto 10^{-6} mbar of vacuum, therefore the tightness of the chamber requires a magnetic coupling to facilitate the rotation of the disc (12). These types of apparatus are limited to very low loads (~0.06N), and low velocities (0.05m/sec) (12)
b. Tribometers which control both the chemical and thermal environment of the experimentation. These tribometers consist of a heating element, which involves complicated technology for the structure. Tests can be performed at temperatures as low as 77K (13) and as high as 1600K (14) (15) ,and even above 2000K (16). Inductive furnaces were used in these studies, however, inductive furnaces are seldom used in the case of a "controlled" atmosphere. (12)

A design for an environmental tribometer is presented by Adamou et. Al (12) for testing rubber surfaces in contact in a controlled environment. The setup is enclosed in a chamber which can sustain upto 10^{-6} mbar vacuum pressure, and gaseous media other than ambient air can be introduced. The apparatus can be placed in a heating furnace to reach temperatures upto 900 °C. The sliding velocity can vary between 0.05m/sec to 1.5m/sec, and normal load can be applied in the range of 5 to 100N. The accessories and instrumentation of the tribometer can measure normal and tangential loads, temperature in the contact vicinity, pressure of the chamber, and electrical resistance of the contact. In this apparatus the pin and disc are carried by a shaft loaded by polymeric bearings which can withstand vacuum environment and zero lubrication conditions. A radiative furnace is used for heating the test chamber, whereas a water circulation network is used to maintain the temperature of the environment. The chamber is contained by vacuum rings to keep it air-free. A vane pump linked to a secondary molecular turbo pump is used to inject the required gases into the test chamber. This design is used to perform pin-on-disk tests for Inconel 718 alloy, at atmospheric pressure, primary vacuum (0.13 mbar) and secondary vacuum (7.2 e^{-5} mbar) at a temperature of 650°C, load of 15N and sliding speed of 0.75m/sec to showcase the working capabilities of the tribometer. (12)

Wear tests for locomotive industry

Pin-on-disk tribometers have been used for performing different tests in the locomotive industry. Sundh et al. (17) performed pin-on-disk sliding wear tests for determining the wear rates for stick-slip and sliding behavior of lubricated wheel-rail contacts. These tests have been performed with the standard pin-on-disk apparatus placed in an environmental chamber

for varying loads, humidity conditions, lubricants, lubrication conditions, and contact conditions.

2.2.2. Friction-induced Oscillations in pin-on-disk tribometers

Oscillations are usually observed while running unlubricated or boundary lubricated tribology experiments on a standard pin-on-disc tribometer apparatus, which result in some uncertainty in the obtained values of the co-efficient of friction for the aforementioned experiments.

Traditionally, friction-induced oscillations have been reported to be associated with the mechanisms of:

- slip-dependence of the coefficient of friction (18), (19), (20)
- Velocity-dependence of the coefficient of friction (18), (19), (20)

The abovementioned mechanisms, although being able to explain *dynamic instabilities*, are insufficient to explain,

- the modes of friction vibrations occurring at high surface speeds (21)
- Correlation between friction-induced oscillations and the dynamic characteristics of the system (21)

Tolstoi (22) shows that for some dry metallic surfaces the apparent difference between the static and kinetic coefficients of friction is not an intrinsic property of the interface, but rather a result of additional vibrations and separation of the surfaces during sliding.

Godfrey (23) and Tworzydlo et al. (21) have performed experiments to determine the reason behind such friction oscillation. Furthermore, in another study, Tworzydlo et al. (24) have numerically modeled the friction induced oscillations arising in pin-on-disk tribometers.

The apparatus used by Godfrey for the experimentation consisted of a standard pin-on-disc tribometer, a pulley and weight pan arrangement for loading the pin, and a commercial force transducer attached to the pin-holder via a jeweller's chain (23). Different material combinations for the pin and disc were experimented upon at different speeds, loads and lubrication states. It was observed that in some cases, the friction oscillations were dependant upon rotation rates, however they were observed to be independent of the materials, lubrication or operating conditions (temperature, pressure, etc). (23)

According to the study conducted by Tworzydlo et al., self-excited oscillations are attributed to friction-induced dynamic coupling between certain degrees of freedom of the system, with or without presence of velocity-dependent friction (21). In the studies carried out by Tworzydelo et al., to perform the verifying tests, a standard pin-on-disk apparatus, with mild-steel discs and Ultimo 4 carbon tool steel pins, was fitted with a load cell consisting of an array of six accelerometers further attached to the pin-slider for observing the frictional and normal forces at the interface (21). A controlled hammer impact was applied to the pin to measure the slider response and therefore to obtain the modes of the slider. (21)

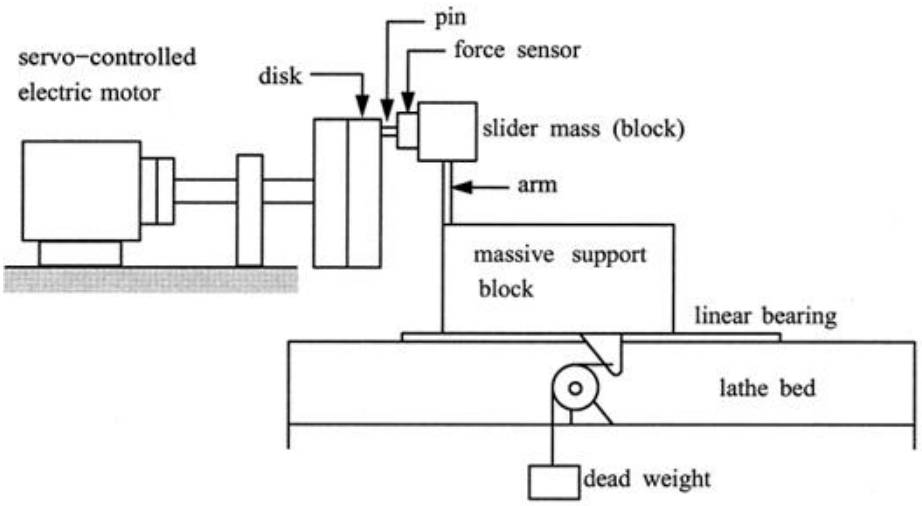

Figure 3 A schematic representation of the POD Appartus used by Tworzydlo et al. (21)

It was observed that the offset of the pin relative to the center of mass of the block is one of major factors affecting the stability of sliding (21). Irregular bursts of violent instabilities were observed with increasing Surface damage on the pin and disk (21). As shown by Figure, friction was found to couple the normal and rotational modes at most levels of normal load (21). This coupling is claimed to cause the slider to undergo self-excited vibrations of a frequency close to the rotational natural frequency of the slider (24). This instability, although apparently causing a reduction in the observed co-efficient of friction can occur in the absence of explicit slip-weakening of friction between the sliding surfaces (21). Thus different kinds of unstable vibrations may be produced at high coefficients of friction corresponding to frictional seizure (21).

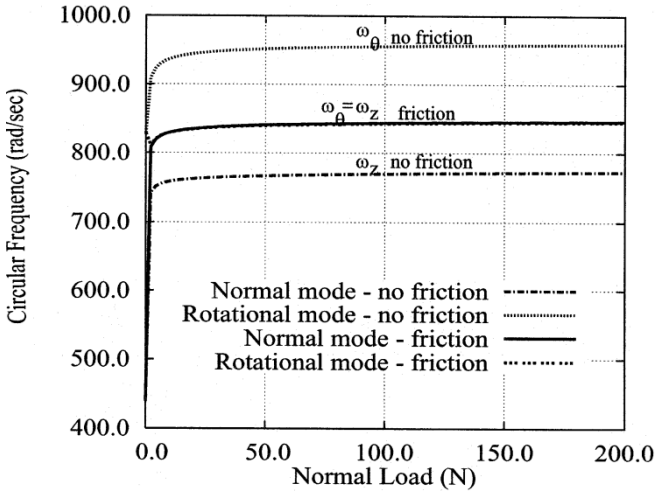

Figure 4 Coupling of normal and rotational modes in the presence of friction, as shown by Tworzydlo et al. (21)

2.3. OTHER TRIBOMETERS

Besides the pin-on-disk tribometers, some other tribometers used and developed for different tribological purposes are as follows:

2.3.1. Pin and V-blocks tribometer

Sebastian and Bhaskar (25) have suggested a modified design for the standard pin and v-blocks tribometers, compact and vacuum compatible for use in a space tribology laboratory. The suggested test rig consists of a standard pin and v-blocks arrangement suspended on a frame with two built-in transducers, one connected to screws that grip the V-blocks, for measuring the applied load *P*, and the other connected to the force sensor, via a flexible coupling, for measuring reaction torque *T* at the sliding contacts (25). Disc springs are fitted on each arm to adjust the stiffness of the loading system. (25)

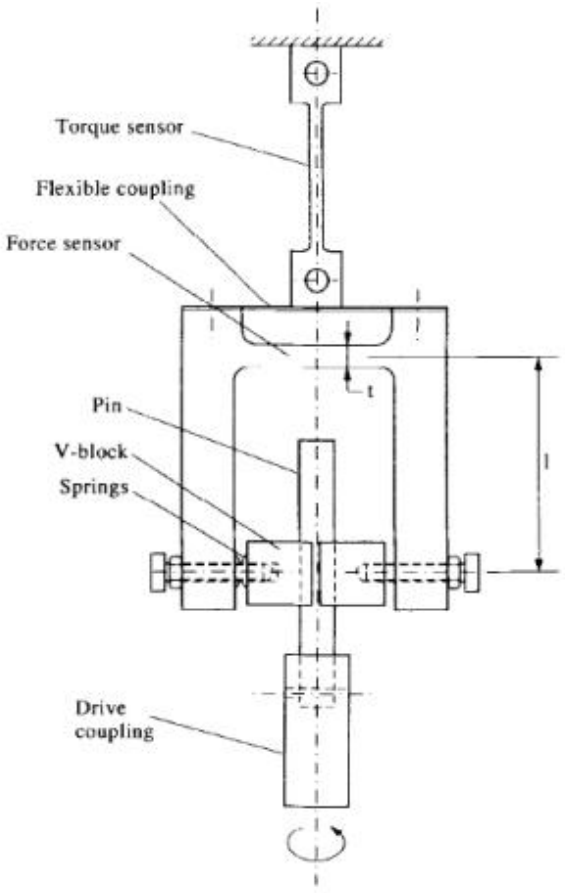

Figure 5 Pin-and-V blocks tribometer as designed by Sebastian and Bhaskar (25)

The combined wear of the pin and blocks, in the abovementioned arrangement, can be deduced from the changes in the applied load (25). Two sets of experiments, using this test rig, were performed on pins of different materials coated with silicate bonded MoS_2 film, employing unlubricated, anodized V-blocks of aluminum (6061-T6) , and the effect on the co-efficient of friction for different loads, speeds was observed at room temperature for atmospheric pressure and high vacuum environment.

2.3.2. Ball-on-disc tribometer

The ball-on-disc tribometer is another common type used for special purpose wear studies.

Subramonian and Basu (26) have presented a modified high-speed cryogenic design of the ball-on-disk tribometer for use in space tribology experiments. This design has been used by them to study the performance of ball bearings used in space shuttle main engine or high-speed cryo-turbopumps of the liquid rocket engine.

A ball-on-disc tribometer was developed by De Moerlooze et al. (27) as a novel tribometer for tribological experiments. The test rig consists of a servo-driven main shaft supported by an air bearing, and upon the main shaft is bolted the tub-shaped (for the option of lubricant-use) support for the disc specimen, whereas three sample balls are glued to a sample-holder which is assembled onto the sample-holder disc allowing the arrangement to be able to trace three separate trajectories (and thus 3 different surface speeds), or a single circular track (averaging effect) (27). The load is applied on the main axis, therefore, thereby opening the option of loading each ball with a different normal load. Two S-beam dynamometers, supported by a magnetically preloaded rectangular air bearing, connected to the sample holder disk, are used to measure the frictional torque (27). An additional position measurement is introduced for measuring the relative rotation of the upper contact with respect to the lower contact, when performing experiments with sinusoidal position input (27). The wear profile is measured online via signals obtained from three capacitive distance probes, connected between the sample holder disk and the rim of the tub (27). This rig was used to measure the wear behavior of different ball samples against a steel disk. (27)

2.3.3. Mastication simulating tribometer

Sajewicz and Kulesza (28) have developed a specialized tribometer for simulating the effects of mastication (chewing) on hard teeth and dental material. The developed tribometer provides reciprocating movement and cyclic loading of the dental samples. It consists of a sample holder, a counter-sample placed in a container of artificial saliva or any other lubricating liquid, the container being attached to an oscillating disc driven by a crank-rocker mechanism connected to a motor, and a pneumatic actuator which asserts the load through a spring loaded loading beam. The loading and friction forces are detected and monitored using straing gauge (28). The loading of the pneumatic system is controlled via a closed-loop PID controller (28).

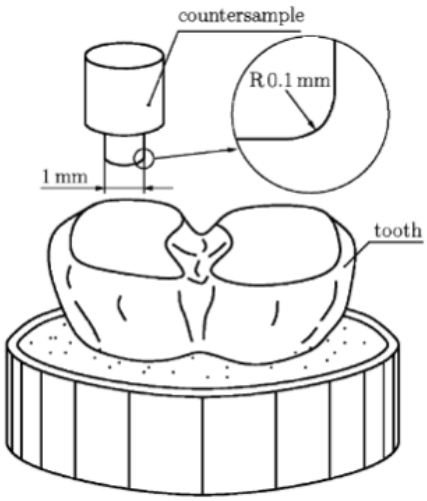

Figure 6 Schematic of the sample and countersample used in the tribometer by Sajewicz and Kulesza (28)

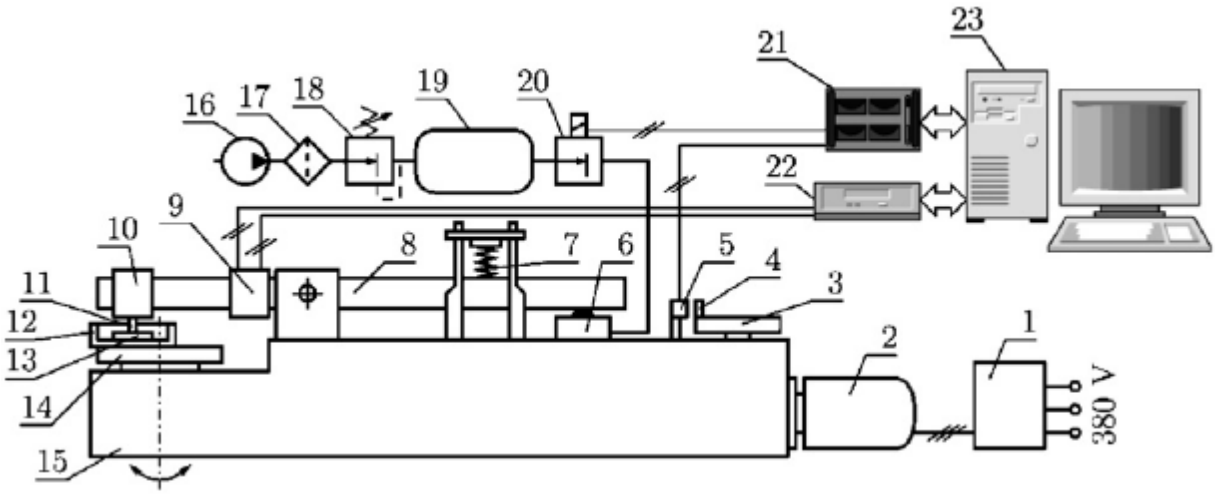

Figure 7 Schematic drawing of the tribometer by Sajewicz and Kulesza (28): (1) inverter; (2) gear-motor; (3) rotational disc; (4) permanent magnet; (5) proximity detector; (6) pneumatic actuator; (7) unloading spring; (8) loading beam; (9) strain gauges; (10) sample holder; (11)sample; (12) container; (13) countersample; (14) oscillating disc; (15) frame; (16) air compressor; (17) compressed air filter; (18) pressure valve;(19) pressurized container; (20) proportional pressure regulator; (21) PCL- 818 HG card; (22) Spider-8 amplifier; (23) computer

2.3.4. Polymer testing ring-on-disc tribometer

Tribometers used for testing wear mechanisms involved in the wear of polymeric materials require temperature monitoring to prevent the alteration of the co-efficient of friction due to melting of the polymers at raised temperatures (29). Therefore, a ring-on-disk tribometer with a water-cooling system was developed by Kashani et al. (29) for studying the wear properties of polymers. This tribometer is equipped by instrumentation to detect and monitor the

temperature at the contacting interface, and strain gauges for recording the loading and friction forces, and a quick data acquisition system (29). The tribometer can measure the static and dynamic COF from short experiments, and provide data for the calculation of wear rate by performing long term experiments (29).

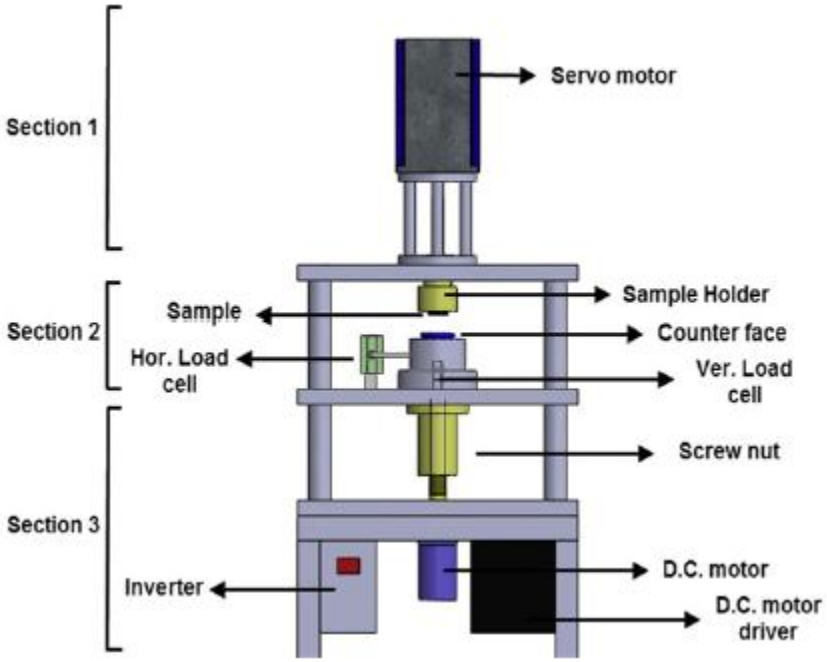

Figure 8 Schematic of the ring-on-disk tribometer developed by Kashani et al. (29)

2.3.5. Linear reciprocating tribometers

Linear reciprocating tribometers are used for simulating wear mechanisms arising during reciprocating motion. Truhan et al. (30) have designed a high-speed reciprocating tribometer for diesel engines, whereas Mohan et al. (31) have presented a low-speed linear reciprocating tribometer for studying the friction in machine tool slideways. The tribometer developed by Mohan et al. employs the principle of a slider on a flat-disk, using proximity sensors and switches to reverse the direction of translation at each reversal point (31).

2.3.6. Three-pins on disk Tribometer for friction drives

Friction drives, owing to their silent working, compactness and low power requirements, are famous in the precision works industry, watch industry, and precision positioning equipment industry. The tribometer developed by Sinha et al. (32) is used to study friction materials used in friction motors and suggest improvements for minimizing wear and enhancing the efficiency of the drives. It consists of three axisymmetrically placed pins, and a rotor with a

torsional brake, so that both normal and torsional loads can be applied: this tribometer simulates the function of an ultrasonic motor (32). It has been used to observe the stick-slip behavior in friction drives, and the wear arising thereof.

2.3.7. Three-balls-on-disc microtribometer

For studying the friction and wear arising in micro ball bearings used in MEMS applications, Olaru et al. (33) have developed a microtribometer, which consists of three microballs sandwiched between a driving disc and an inertial driven disc. The data regarding the friction between the microballs and the discs is obtained by visually monitoring the angular position of the inertial disc after an initial acceleration and then letting the disc decelerate itself due to its own inertia and the friction with the microballs, and relating it to the co-efficient of friction through a hypothetical equation (33).

2.3.8. Block on ring tribometer

To study the different wear regimes and mechanisms associated with each regime, dry sliding tests were performed by Chen and Alpas (34), using a block-on-ring tribometer. In these tribology tests, samples of Mg-Al-Zn alloy (AZ91) were prepared in the form of polished rectangular blocks, and brought into contact with slider rings of bearing steel. The wear rates were obtained from gravimetric analysis, temperature at the contact interface was monitored using thermocouples, the microstructure of the worn surfaces and wear debris was observed using SEM with EDS (energy dispersive X-ray spectrometer), and the composition of the wear debris was determined via an X-ray diffractometer (34).

2.3.9. Rotating cylinder tribometer

The rotating cylinder tribometer (6) is not a typically used apparatus. Angseryd et al. (7) used this apparatus to perform sliding wear tests on carbide coated drilling inserts used in rock-drilling. The carbide coated inserts were brought into contact via a spring, with a rotating rock cylinder, at an axial feed rate to continuously compensate for the wear loss occurring thereof (7). The tests were performed for dry and wet conditions, as well as the introduction of abrasive materials like Al_2O_3 and SiO_2. The wear loss was calculated through gravimetric analysis, and the wear debris structure and composition was observed using SEM with EDS (7).

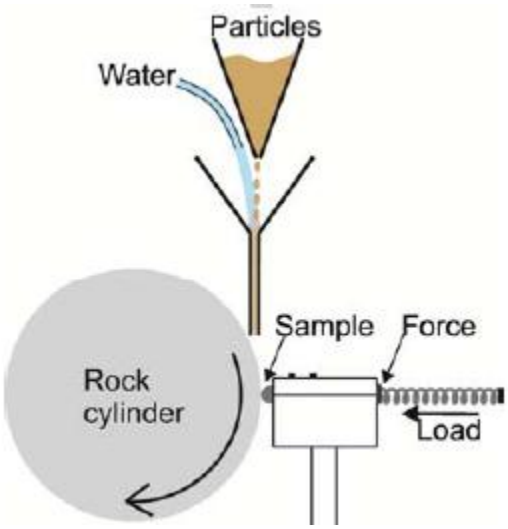

Figure 9 Pin-and-rotating cylinder tribometer used by Angseryd et al. (7)

2.4. WEAR VOLUME DETERMINATION

In pin-on-disk and other tribometry tests, the amount of wear can be determined by measuring appropriate linear dimensions of both specimens before and after the test, or by weighing both specimens before and after the test.

2.4.1. Pin-wear

Since point contact is the most commonly used form of contact in unidirectional sliding friction and wear tests, the slider tip can be considered to have either a spherical shape or compound curvatures, which after being worn out is not flat but possesses unknown curvatures.

Whitenton and Blau (35) compared three methods for determining the wear volumes of spherically tipped sliders, each having its own limitations:

a. mass loss (gravimetric measurements), which is unable to detect miniscule wear, such as that involved in friction tests of advanced wear-resistant materials (36)
b. two-dimensional (2D) analysis based on the measurements of wear scar sizes, which is valid only for flat wear scars, mostly used in cases in which the wear resistance of the disc specimen is higher than that of the slider, and the wear scar can safely be assumed to be flat. (36)

The wear volume is then implicitly expressed as, (35)

$$V = \frac{1}{3}\pi h^2(3R_o - h) \quad \textbf{1}$$

where R_o is the sphere diameter, and the wear depth h is given by (35):

$$h = R_o - \sqrt{R_o^2 - \frac{d_{scar}^2}{4}} \quad \textbf{2}$$

where d_{scar} is the wear scar diameter

c. Three-dimensional (3D) analysis which involves multi-trace stylus profile-metry, and is very accurate but also very tedious. The method has no closed-form analytical solution, and requires rigorous and complicated numerical integration. (36)

Qu and Truhan (36) have introduced the "single-trace wear volume analysis" method for accurately and quickly determining the wear volume in tribology tests.

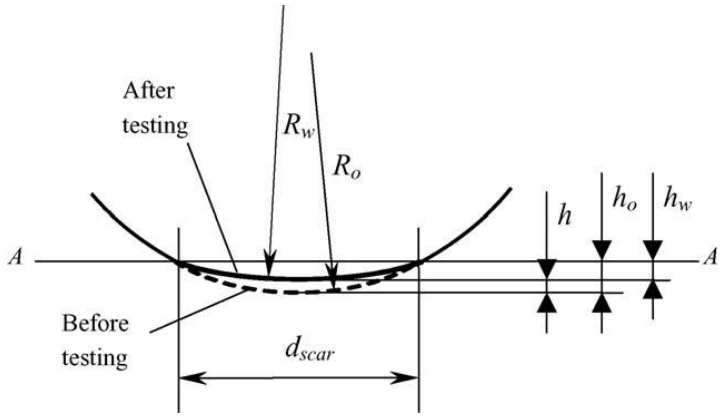

Figure 10 Sideview representation of the worn tip of a spherically tipped slider, as Qu and Truhan (36)

The Qu and Truhan single-trace method for spherically tipped sliders shows that for a system with relatively homogenous materials, surface conditions and distribution of wear debris, assuming a constant surface curvature, the wear cap can be approximately represented by a spherical surface, then the wear volume can be obtained from, (36)

V=(volume of original cap below A-A) – (volume of worn cap below plane A-A)

Thus, (36)

$$V = \frac{1}{3}\pi[h_o^2(3R_o - h_o) - h_W^2(3R_W - h_W) \quad \textbf{3}$$

$$h = h_o - h_w \quad \textbf{4}$$

Where,

$$h = R_o - \sqrt{R_o^2 - \frac{d_{scar}^2}{4}}$$

5

$$h_W = R_W - \sqrt{R_W^2 - \frac{d_{scar}^2}{4}}$$

6

Where the subscript "o" is for original, and "W" is for worn.

2.4.2. Disc-wear

Generally, the disc-wear for pin-on-disc or ball-on-disc tests, is calculated from the depth and the average cross-sectional area of the wear track. For cases in which direction reversal occurs at every stroke (30), the aforementioned method is no longer reliable when the magnitude of the wear track length is approximately the same width of the wear track (36).

The Qu and Truhan single trace method has a solution for this. A wear scar, of length L_s and width W, is divided into three regimes, a cylindrical surface sandwiched between two spherical surfaces of radius R_f. (36)

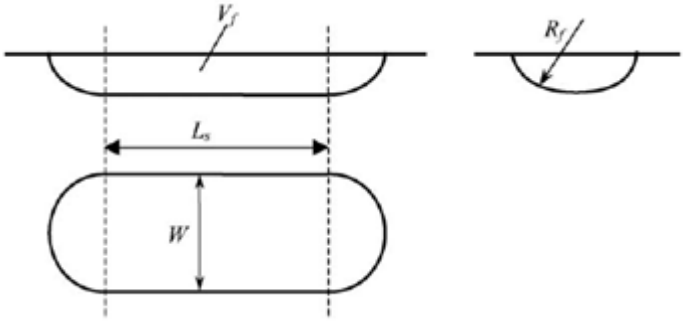

Figure 11 Wear scar on flat specimen against spherically tipped slider as shown by Qu and Truhan (36)

The wear volume, according to the single trace method, is then given by (36):

$$V_f = L_S\left[R_f^2 \sin^{-1}\left(\frac{W}{2R_f}\right) - \frac{W}{2}\left(R_f - h_f\right)\right] + \frac{\pi}{3}h_f^2\left(3R_f - h_f\right)$$

7

$$h_f = R_f - \sqrt{R_f^2 - \frac{W^2}{4}}$$

8

Although the single-trace analysis is such a reliable and time-saving technique, it is not employed in this work because profilometry technology was not easily available to the author, futhermore, the accuracy of the wear volume measurement does not lie well within the scope of this work.

The single-trace method was compared to the three most commonly used methods, for a 9.535mm diameter 440C SS bearing ball which was unidirectionally slid against the face of a rotating Ti–6Al–2Sn–4Zr–2Mo alloy disk under 10N normal load and at 0.3 m/s speed for 500 m, in ambient air without lubricant (36). For the single-trace method, a single surface profile passing through the wear scar center was measured, and the radius of the curvature of the profile was obtained by curve fitting.

The comparison of all four methods is given in the table:

Table: Wear volume measurement of the 440C stainless steel ball

Method	**Wear volume ($\times 10^{-3}$ mm^3)**	**Error compared to 3D analysis (%)**	**Time consumed (min)**
Mass loss	25.6± 12.8	-21.7	~2
2D	39.9±1.9	22.0	~3
3D	32.7	N/A	~45
Single-trace	33.1±1.6	1.2	~5

Table 1 Wear volume measurement of the 440C stainless steel ball by Qu and Truhan (36)

2.5. WEAR MECHANISM MAPS

When wear tests are performed to identify the mechanism for the wear of a certain material, wear maps are constructed. These wear plots or wear mechanism maps summarize the identification of areas of different intensity, such as ultra-mild, mild and severe wear, etc., and depending upon the scope of the research, may also identify the kind of wear that takes place in a region, such as oxidation wear, abrasion wear, etc. 2D and 3D maps can be

constructed, but 2D maps are more commonly found in literature (37). A wear map should not only present the experimental data in a summarized form but should also be able to predict wear at interpolated and extrapolated parameter values (37). Wear maps give an idea of safe-operation, and failure conditions (37) . This is made possible if extensive data is gathered from experimentation and literature, for the specific material being studied (37).

The developments in wear-mechanism mapping have been documented by Lim (37). According to the study, the earliest wear map appeared in 1941, by Okoshi and Sakai (38), where they plotted wear rate as a surface function of the sliding speed and applied load.

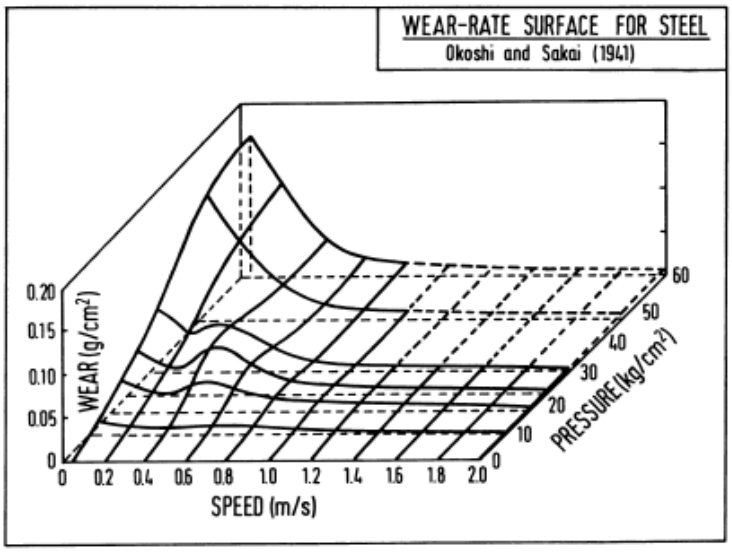

Figure 12 Wear map as proposed by Okoshi and Sakai (38)

Lim and Ashby (1) have performed significant and extensive research on the construction of wear maps for steels, identifying different regimes for different kinds of wear in steels. They have also identified the different mechanisms involved for each regime of wear. The resulting map is a contour plot superimposed on the scatter plot of the wear rates against sliding speed and applied load (1).

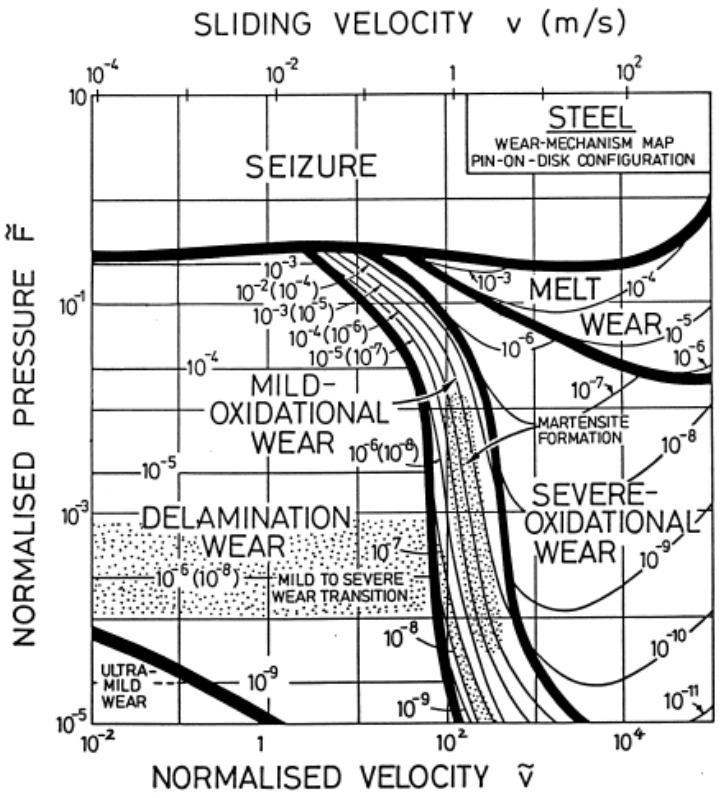

Figure 13 Wear map for steels as by Lim and Ashby

Riahi and Alpas (39) have developed wear mechanism maps for grey cast iron. In this research a block-on-ring configuration was used to perform wear tests, gravimetric analysis was used to measure wear volume loss, contact surface temperature was recorded using thermocouple probes, and the changes in morphology and compositions were monitored by using SEM, and EDS (Energy dispersion spectrometer).

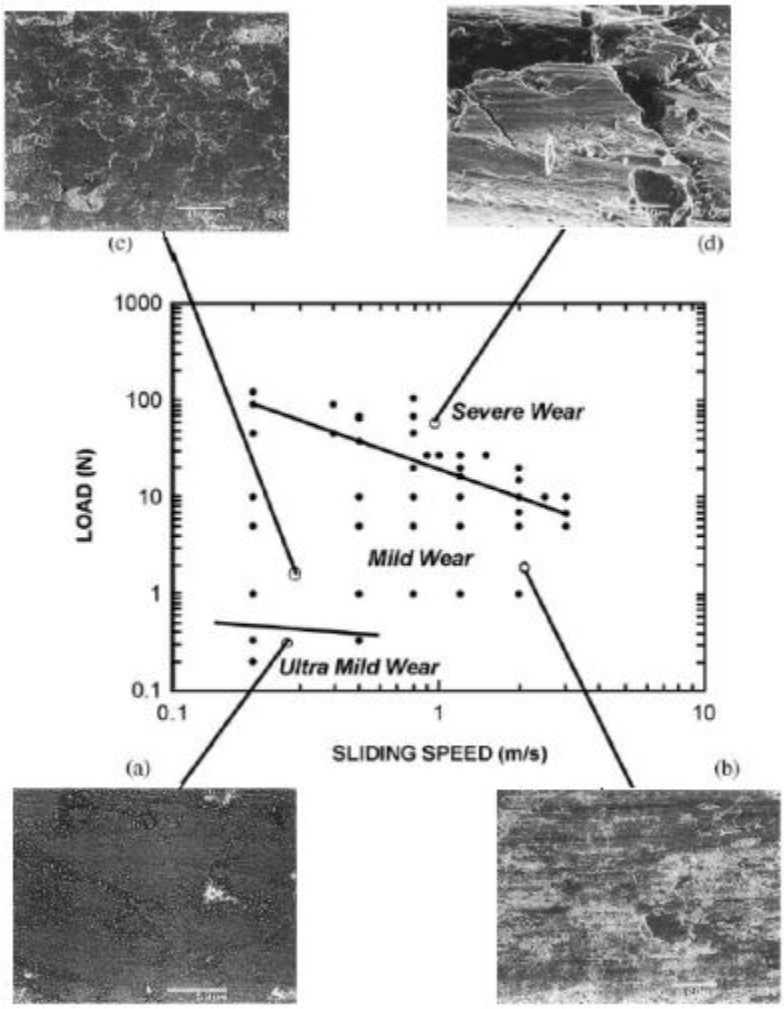

Figure 14 The surface morphologies of grey cast iron in (a) the ultra-mild regime; (b) the mild regime at low loads and high sliding speeds; (c) the mild regime at low loads and sliding speeds; and (d) the severe wear regime, as shown by Riahi and Alpas (39)

In the above map, regimes for wear of different intensities are identified. Furthermore, Riahi and Alpas have derived an empirical relationship between transition loads and transition speeds i.e. the loads and speeds at which the wear of one intensity transits into a regime of different intensity (39). The relationship is given as (39)

$$\log P_{tr} = C_1 \log V + C_2 \quad \textbf{9}$$

Where P_{tr} is the transition load in N, V the sliding speed in m/s and C_1 and C_2 are constants that can be determined from the experimental data.

Meng-Buranay et al. (40) have identified the mechanisms for ultramild and mild wear regimes of Si-Al alloys used in the automotive industry. These mechanisms were identified using focused ion beam and cross-sectional TEM investigations.

Wilson and Alpas (41) constructed wear mechanism maps for TiN-coated high speed steel, from empirical data obtained from pin-on-disk tests using HSS pins. Different intensity wear regimes were identified on the wear maps, and the mechanism of wear during transition from one regime to another were also observed (41). Four wear regimes were identified, in regime I, it was noticed that the severe wearing off of the TiN coating at low speeds occurs due to oxidation and polishing; in regime II, mild wear of the coating was accompanied by transfer of oxidized pin material to the TiN coating; in regime III, rapid wear of the coating at high loads, low speed was observed, followed by a rise in temperature; in regime IV, severe plastic deformation of the HSS pin and very mild polishing and wear of the TiN coating was observed at 300 °C (41).

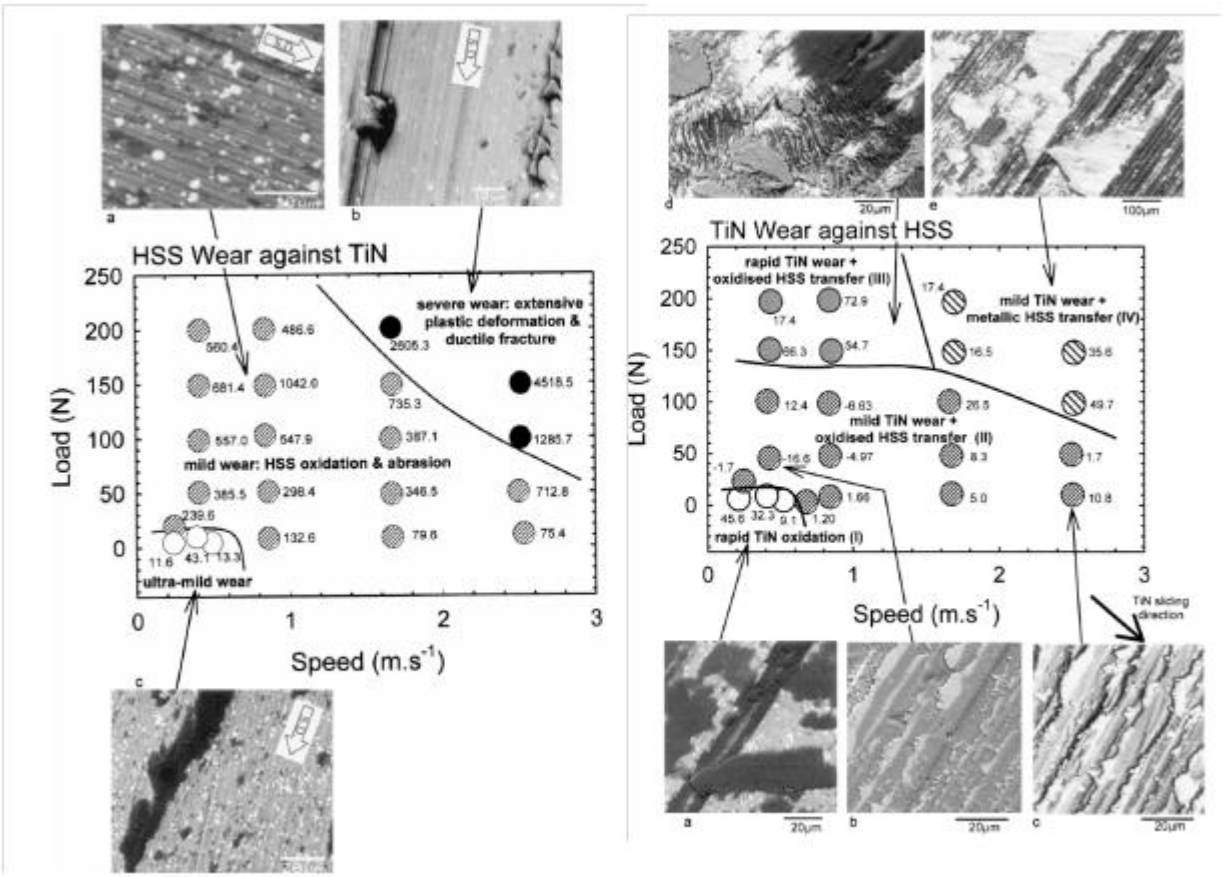

Figure 15 Left: Wear map showing wear rates, different wear regimes and micrographs for HSS pin material in dry sliding against TiN coating, Right: Wear map showing wear rates, different wear regimes and micrographs for TiN in dry sliding against HSS pin, as shown by Wilson and Alpas (41)

Chen and Alpas (34) conducted dry sliding experiments using block-on-ring tribometer, for AZ91 alloy using SAE52100 bearing steel rings, and constructed wear maps after Lim and Ashby (1), to depict the wear regimes of increasing intensity.

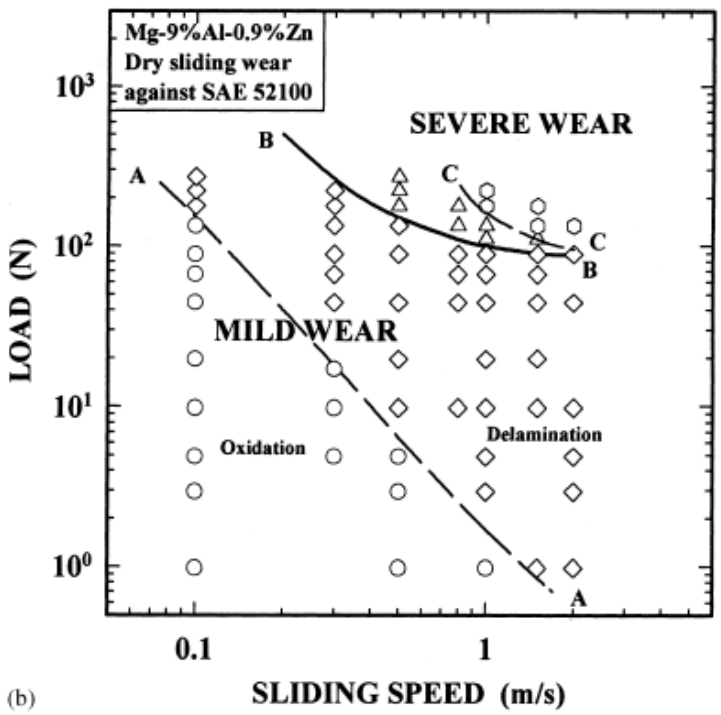

Figure 16 wear transition map for AZ91 by Chen and Alpas (34), showing the region of dominance of wear mechanisms and the transition boundaries between them: BB: mild wear to severe wear transition; AA: transition between the oxidational wear (o) and delamination (◊) wear in the mild wear regime; CC: transition between severe deformation induced wear (▲) and melt wear (○).

The research also explains the wear mechanism associated with each regime. Oxidational and delamination wear was identified in the mild-wear regime; severe plastic deformation and melt wear was identified for the severe wear regime (34). The identification of these mechanisms was made possible with the use of of X-ray diffractometry to observe the wear debris compositions and Scanning Electron Microscopy to observe wear surface morphology.

Similarly, Edrisy et al. (42) have constructed wear rate maps for low-carbon thermal steel spray coatings on aluminum alloys used in the automotive industry, using a pin-on-disk tribometer with an environmental chamber; regimes of oxidational wear and severe plastic deformation with iron splats were identified for the test samples, with the help of morphological and compositional analysis via XRD, SEM, and EDS.

A surface plot of the wear volume against load and speed was presented as a wear map for the diamond polishing process by Hird and Field (43),

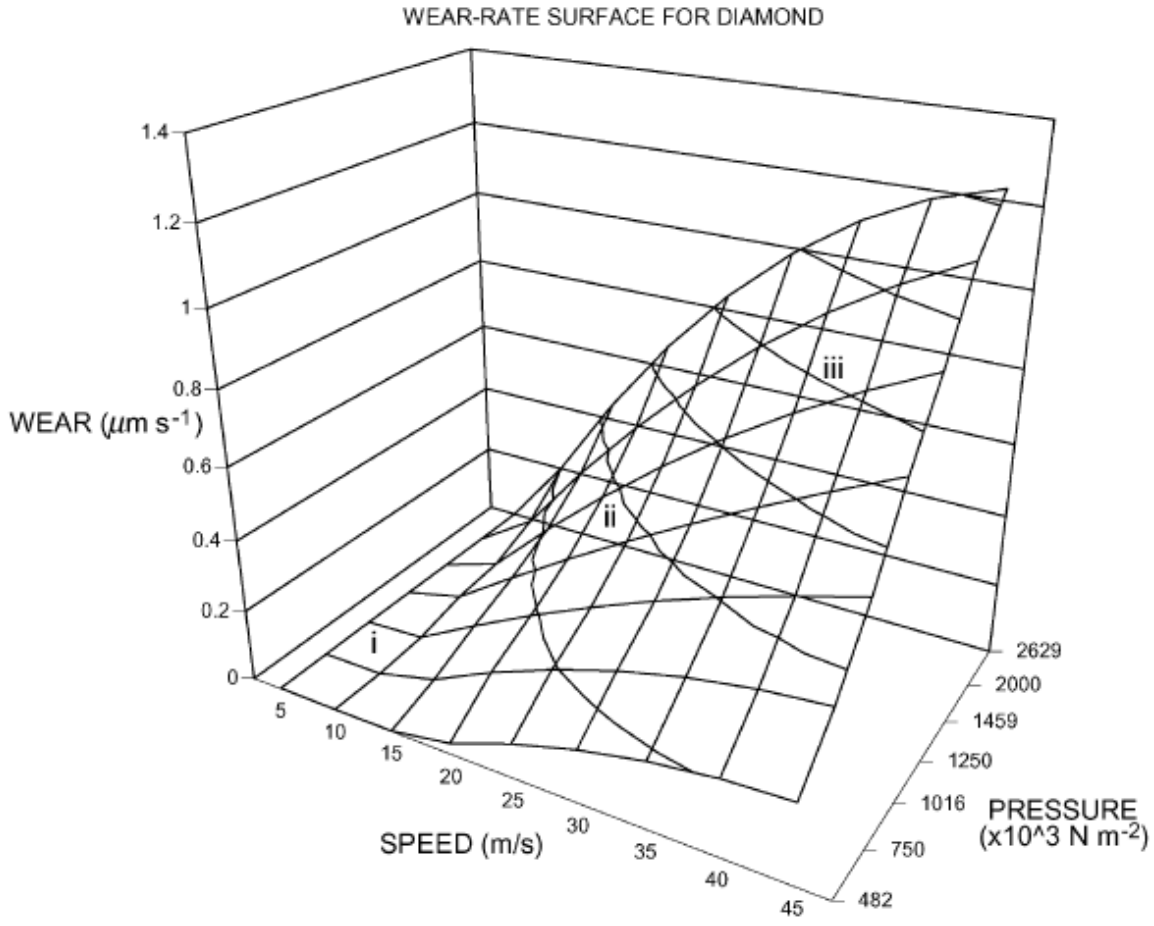

Figure 17 Surface plot of the wear volume against speed, and pressure for diamond polishing process by Hird and Field (43)

This approach is followed in the current work to plot the wear process of the sample rocks and pins experimented upon.

CHAPTER 3| METHODOLOGY

In order to analyze wear mechanisms of known tool materials drilling against rock samples, this research attempts to utilize the standard technique known as the pin-on-disk arrangement. (44)

Already, previous researchers have used this technique effectively to identify wear mechanisms for different pin-disk material arrangements. (45), (46), (47), (48), (49), (50), etc.The methodology is as follows as

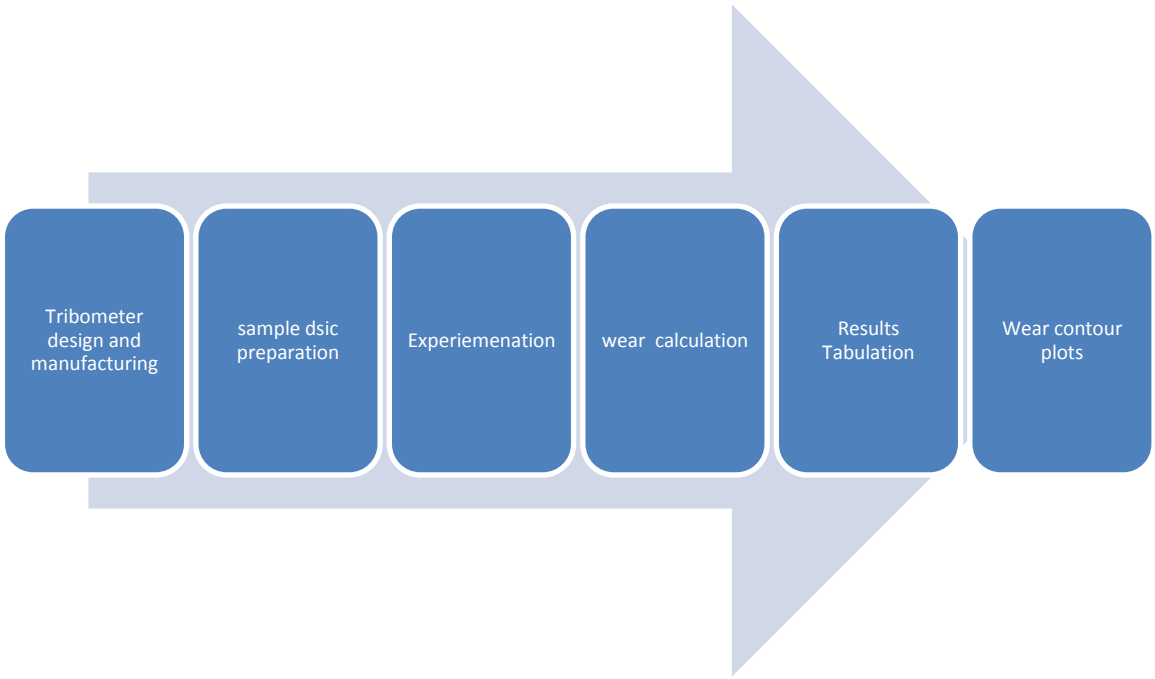

Figure 18 Methodology

The ASTM G999-05 (44) standard was followed for the purpose of finding the wear volumes form the rock samples. The method as described in the standard implies the use of subject bit on the sample discs. This was done by the use of the designed tribometer .The sample disc is rotated about its axis by means of an electric motor that is controlled by a controller. The controller provided the speed control for the mechanism.

Figure 19 Motor controller

However a tachometer was also used in the experimentation for verifying the motor's revolutions per minute.

Figure 20 Tachometer

The experimentation thus did produced scars on the disc along with wear on the bit. The vernier caliper was used for the purpose of identifying the scar depth for calculating the volume loss.

Figure 21 Vernier Caliper

The detailed construction of this specific indigenously designed rock-drilling simulating tribometer is explained in the next chapter. Samples of different types of hard rocks obtained are first prepared in disc shape, and standard bits of Carbide and HSS are used to perform the experiments at different speeds and different loads.

Figure 22 Carbide bit

Figure 23 HSS bit

Wear volume is determined by measuring the dimensions of the wear scar on the disc and the difference in length of the worn pin. This volume is then plotted against the speed and load to obtain surface and contour plots for each set of experiments (details in Chapter 6).

CHAPTER 4| EXPERIMENTAL SETUP

This research will make use of an indigenously developed pin-on-disk fixture that will allow a pin made from standard tool materials to be rubbed against various rock samples, rotating at known rpm (Figure 18).

The surface speed can be calculated using standard mechanics/physics involving linear and angular velocity. The pin will be pressed against the rotating disk with a known axial force. The resulting wear rates will be plotted against the known conditions. The calculations are shown subsequently in the motor selection section.

4.1. FIXTURE DESIGN

The apparatus design (Fig.18) requires the concept to be finalized, in order to complete the final design. The ASTM G99-05 (44) was taken as reference for the apparatus design. Pro Engineer Wildfire 5.0 was made use of for this process. The standard (44) explains the application based design of the tribometer indicating the importance of the design able to press against the disk. The design at hand was done giving special consideration for

flexibility of the tribometer for large number of sample bits and disks. The tribometer design consists of a lever arm which holds the tool post. The tool post is able to move in a dedicated cut for the purpose of bit placement. The lever arm can also move about a fixed point.

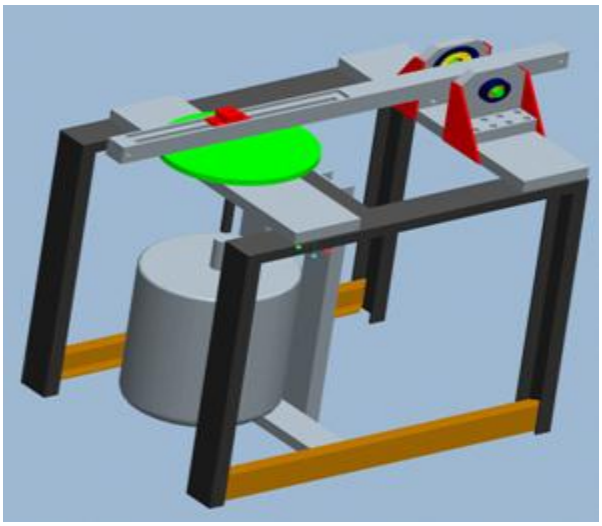

Figure 24 Pin-on-disk CAD assembly

This allows the placement of variable sample disk sizes and easy experimentation. The lever arm rests on two bearing posts by means of a shaft. The disk placement assembly consists of a round disk which acts as base with four studs protruding from it for holding the sample firmly at various different speeds.

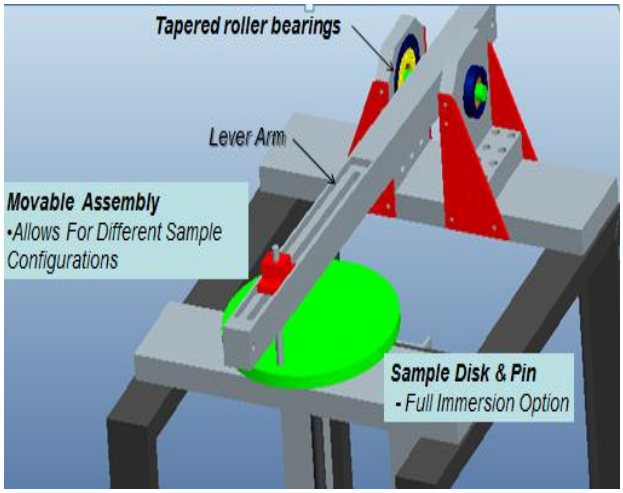

Figure 25 Pin on disk assembly tagged

This disc is rotated by motor from the motor compartment below the disc .The motor and the disc are linked together through a spider flexible coupling. This coupling prevents the transfer

of motor vibrations to the system. Also the motor mounting in the motor compartment has been done with rubber felts for damping the vibrations.

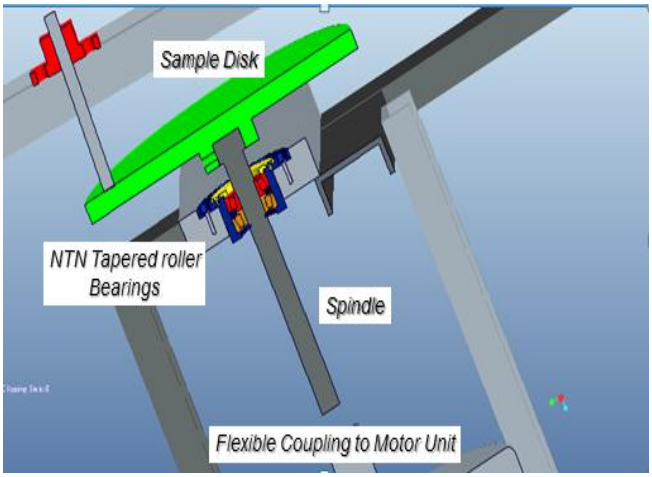

Figure 26 Pin-on-disk x-sec assembly view

The bearing assembly (Fig.19) consists of the taper roller bearings (NTN-4T30204) stacked in back to back arrangement catering for the load and along with keeping the bore size near to the calculated size. The taper roller bearings were selected for the purpose of catering for the axial and radial loads.

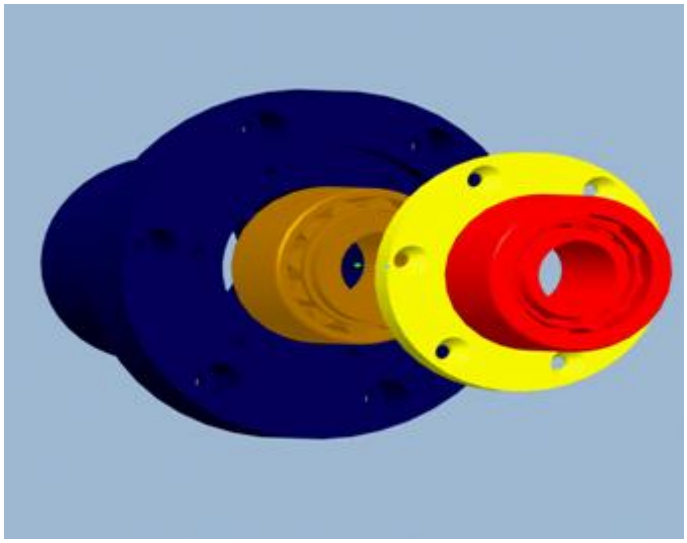

Figure 27 Bearing unit assembly (exploded view)

4.2. MOTOR SELECTION

For motor selection the first requirement is to determine the driving mechanism and its dimensions, and then to check the conditions required for the mechanism, such as the mass of the load and the speed to be reached by the motor, after which we calculate the load torque, moment of inertia and speed which are converted to those at the motor output shaft.

The required specifications such as positioning accuracy, holding of position, speed range, operating voltage and other environmental resistances for the mechanism and the machine. The calculations for calculation of torque for the motor are given as:

- Angular velocity required: 3000 rpm in 60 seconds
- Diameter of disc: 12 inches

For finding torque in case of no pin load on the disc, the relation is given as,

$$T = I \propto$$

10

The angular acceleration 'α' is obtained using the relation,

$$\alpha = \frac{\omega}{t}$$

11

For ω= 3000 rpm = 314.1592 radian/second

$$\boldsymbol{\alpha = 5.2359\ radian/sec^2}$$

12

The moment of inertia "I" is determined using the relation,

$$I = \frac{mr^2}{2}$$

13

Assuming the steel plate and rock disk as a single body,

Mass = m=15 kg,

And,

Diameter of the disk =0.3048 m → Radius, r=0.1524 m

For the above values of *m* and *r*, the moment of inertia is then calculated as,

$$\boldsymbol{I= 0.1741932\ kg\text{-}m^2}$$

14

The required torque is obtained by substituting the values of "I" and" α" in equation 10,

$$\boldsymbol{T_1=0.9120\ N\text{-}m}$$

15

Now for determining the torque in the case of P=500 N pin load on the disc, the relation is given as,

$$T = F.r$$

16

Where,

"*F*" is the friction force caused due to 1000N load, and
"*r*" is the radius of the disc (considering the load acting on the circumference of the disc).

To calculate the friction force "*F*"

$$F = \mu.P$$

17

So, for μ=0.45(steel on concrete)

F=225N

Now substituting *D*=0.3048 m →*r*=0.1524 m, and *F* in equation 16, the value of torque required to overcome this friction force,

$$\boldsymbol{T_2=34.29\ N\text{-}m}$$

18

Hence the maximum torque requirement from the motor is given by,

$$T_{max}=T_1+T_2$$

$$\boldsymbol{T_{max}=35.202\ N\text{-}m}$$

19

Now calculating the required Power using the relation below,

$$Power\ (kW) = \frac{Torque(Nm) \times 2\pi \times rotational\ speed\ (rpm)}{60000}$$

20

We get

$$\boldsymbol{Power=11.05\ KW=14.822\ HP}$$

21

Similarly the diameter of shaft can be determined using the relation given below,

$$D = 1.72 \times \left(\frac{T_{max}}{\sigma_{max}}\right)^{\frac{1}{3}}$$

22

For σ_{max}*= 345 MPa,* we get,

$$\boldsymbol{D= 8.15\ mm}$$

23

4.3. MOTOR-CONTROLLER SELECTION AND INTEGRATION

The total power required for conducting the required experiments on the apparatus required an A/C motor and a motor speed controller, as purchased. The motor is an A/C induction type squirrel cage motor manufactured by Siemens, while the controller is manufactured by Puma Pakistan Ltd.

The motor and controller connections were made in delta configurations as was mentioned in the manual. After successfully connecting the motor with the controller and the power source, the controller was tuned according to the required limits. The controller has an extensive list

of functions. The first task was to tune the controller as per required output and hardware. The connections are explained with the help of pictures in Appendix A.

4.4. FIXTURE MANUFACTURING

The design of the pin on disk mechanism modeled in Pro Engineer wildfire 5.0 was fabricated using the workshop of SMME along with small portion of the work from local market. The parts in the assembly required use of lathe and milling machines along with sheet metal welding and cutting processes. The manufacturing drawings generated using the Pro Engineer wildfire 5.0 drawing tool assistance. The local market resources were used for the purpose of finishing the task in shortest possible time.

Figure 28 Indigenously fabricated pin-on-disk tribometer for tribological studies of hard-rock drilling

Figure 29 Side view of indigenously fabricated pin-on-disk tribometer for tribological studies of hard-rock drilling

4.5. SAMPLE SELECTION AND PREPARATION

The rock samples that are part of this research are called the "Hard Rocks". The three main categories found of the hard rocks are 1) Limestone 2) Dolomite 3) Sandstone. However the samples cannot be obtained from the rig area as only the chip form is available. The experimentation will require the use of outcrop (An outcrop is a visible exposure of bedrock or ancient superficial deposits on the surface of the Earth) samples of the hard rocks. The outcrop samples can then be grinded to the slab form for experimentation.

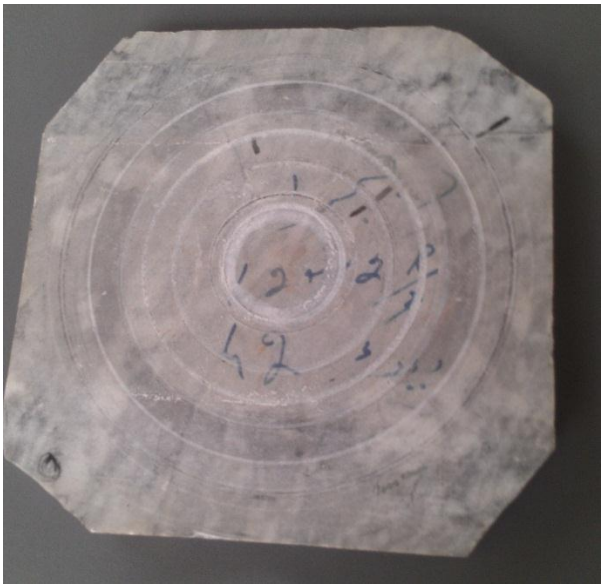

Figure 30 Rock sample "S-grey" with wear scars

Figure 31 Rock sample "Granite" with wear scars

Figure 32 Rock sample "Loralai" with wear scars

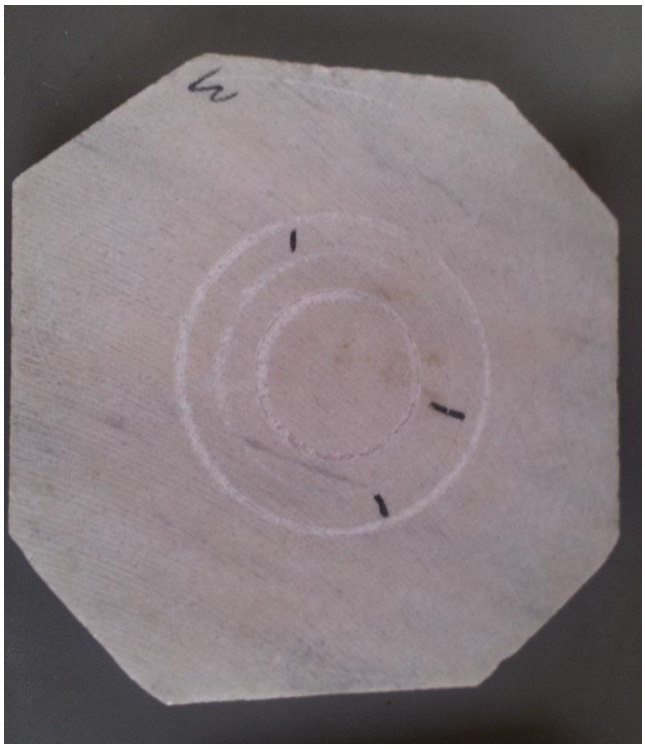

Figure 33 Rock sample "Tavera" with wear scars

CHAPTER 5| RESULTS AND DISCUSSIONS

5.1. EXPERIMENT SET A: "S-GREY" AND CARBIDE PIN

A set of experiments for varying speeds and loads were performed for a disk of rock sample "S-grey", with a Carbide pin. The experimental data is tabulated as follows:

Table: Experimental data of wear rate of Carbide pin sliding against Sample 1

Speed (mm/sec) **Load (N)**	**1000**	**1500**	**2000**
10	0.54427	0.45085	0.16954
50	0.317	0.48301	0.59811
100	0.4051	0.638	0.82772

Table 2 Wear rate of Carbide pin sliding against Sample 1, for variable speeds and loads

The data from the table is interpolated and plotted in MATLAB, to obtain the plots below:

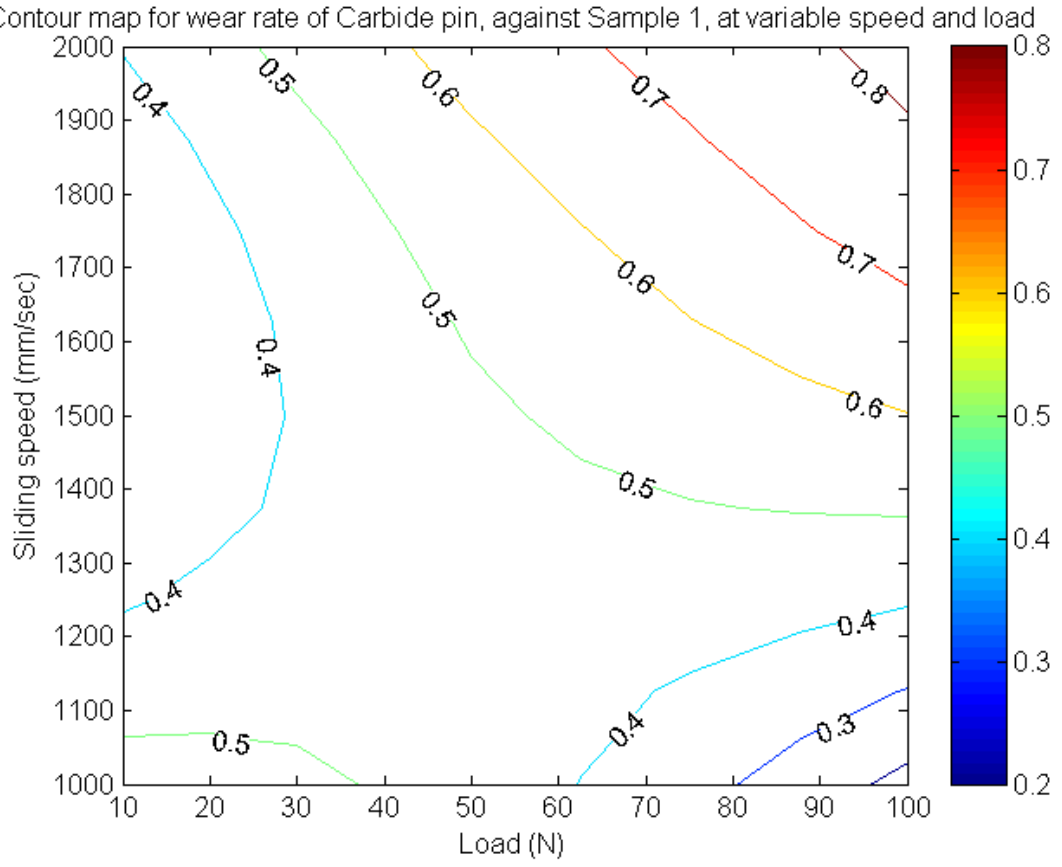

Figure 34 Contour map for wear rate of Carbide pin, while drilling Sample 1, at variable speed and load

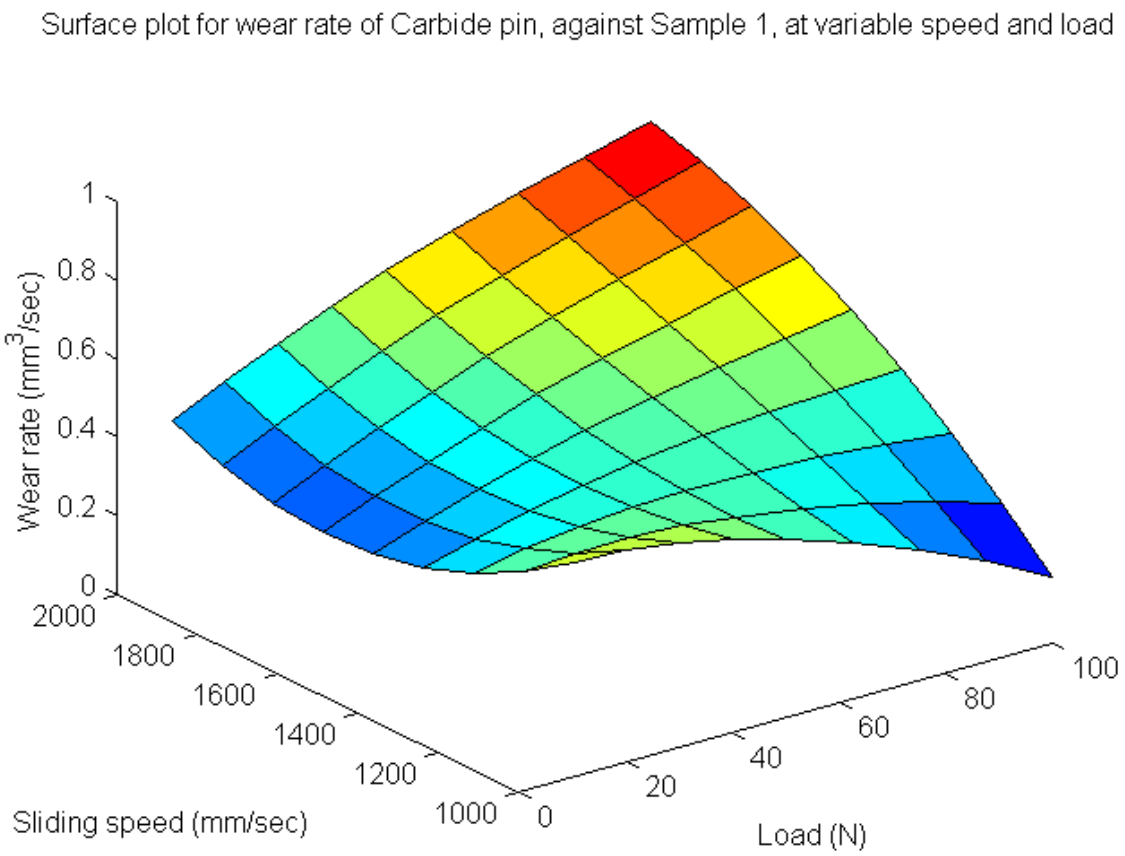

Figure 35 Surface plot wear rate of from Carbide pin, while drilling Sample 1, at variable speed and load

Table: Experimental data of wear rate of Sample 1 disk, sliding against Carbide pin

Speed (mm/sec) **Load (N)**	**1000**	**1500**	**2000**
10	3.04313	2.85707	1.5326
50	2.5108	4.98333	13.0706
100	0.52183	1.5	8.43293

Table 3 wear rate of Sample 1 disk sliding against Carbide pin, for variable loads and speeds

The data in Table 3 is plotted in MATLAB to obtain the following,

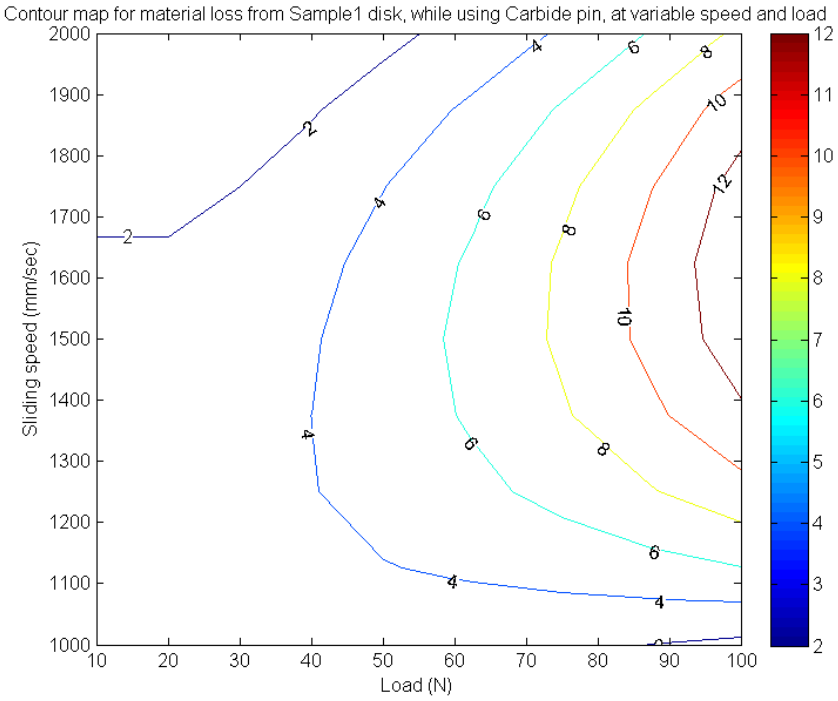

Figure 36 Contour map wear rate of from Sample 1, using Carbide pin, at variable speed and load

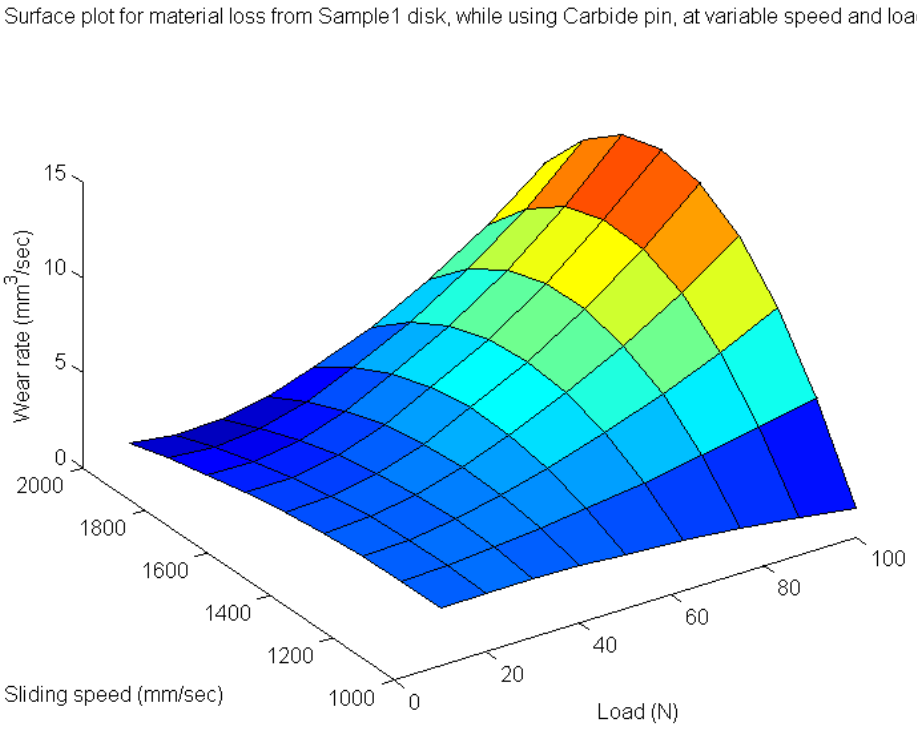

Figure 37 Surface plot for wear rate of Sample 1, using Carbide pin, at variable speeds and loads

As we are more interested in the tool efficiency, therefore, from the pin wear rate contour map, we can observe that the minimum tool loss rate occurs at 1800-2000 mm/sec speed

range and 10-20 N load range, which corresponds to a wear-rate of approximately 2 mm^3/sec of wear-rate on the disc, and a pin wear rate of approximately 0.2 mm^3/sec.

5.2. EXPERIMENT SET B : "S-GREY" AND HSS PIN

A set of experiments for varying speeds and loads were performed for a disk of rock sample 1, with HSS pin. The experimental data is tabulated as follows:

Table: Experimental data of wear rate of HSS pin sliding against Sample 1

Speed (mm/sec) **Load (N)**	**1000**	**1500**	**2000**
10	0.41832	0.54375	0.66917
50	0.87454	0.69285	0.54509
100	1.28771	0.94982	0.68313

Table 4 wear rate of HSS pin sliding against Sample 1

The data from the table is interpolated and plotted in MATLAB, to obtain the plots below:

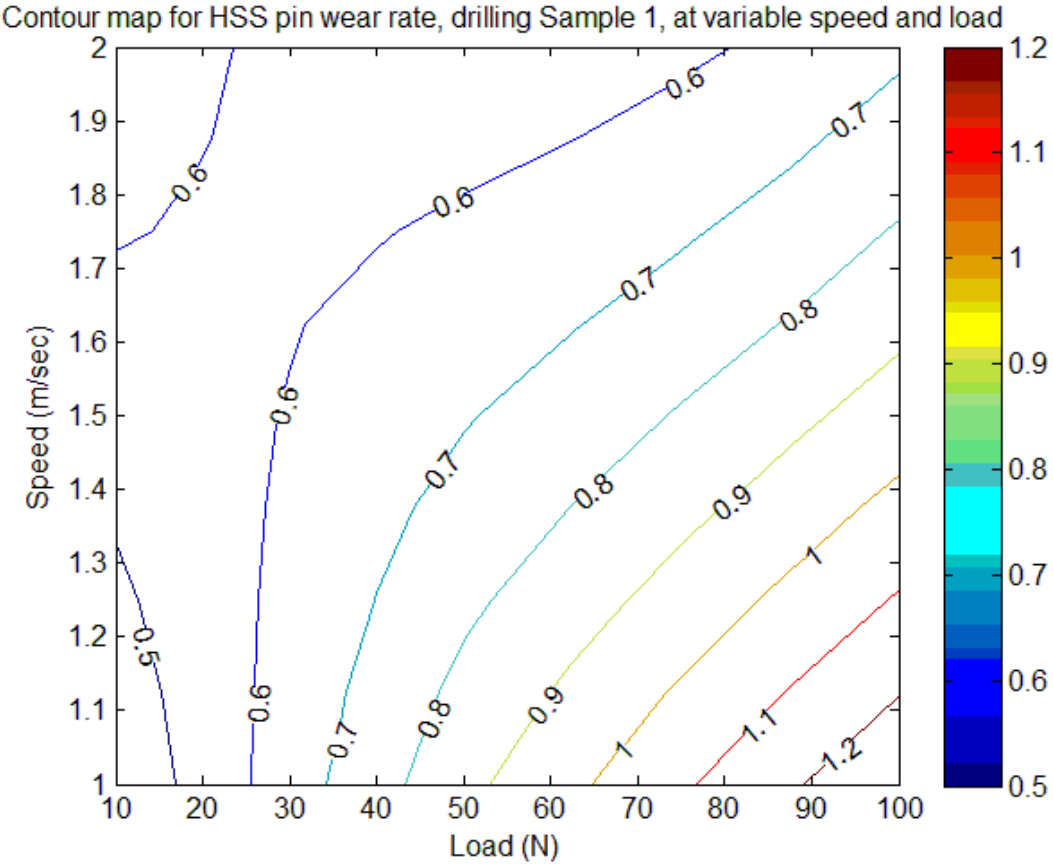

Figure 38 Contour map for wear rate of HSS pin, drilling Sample 1, at variable speed and load

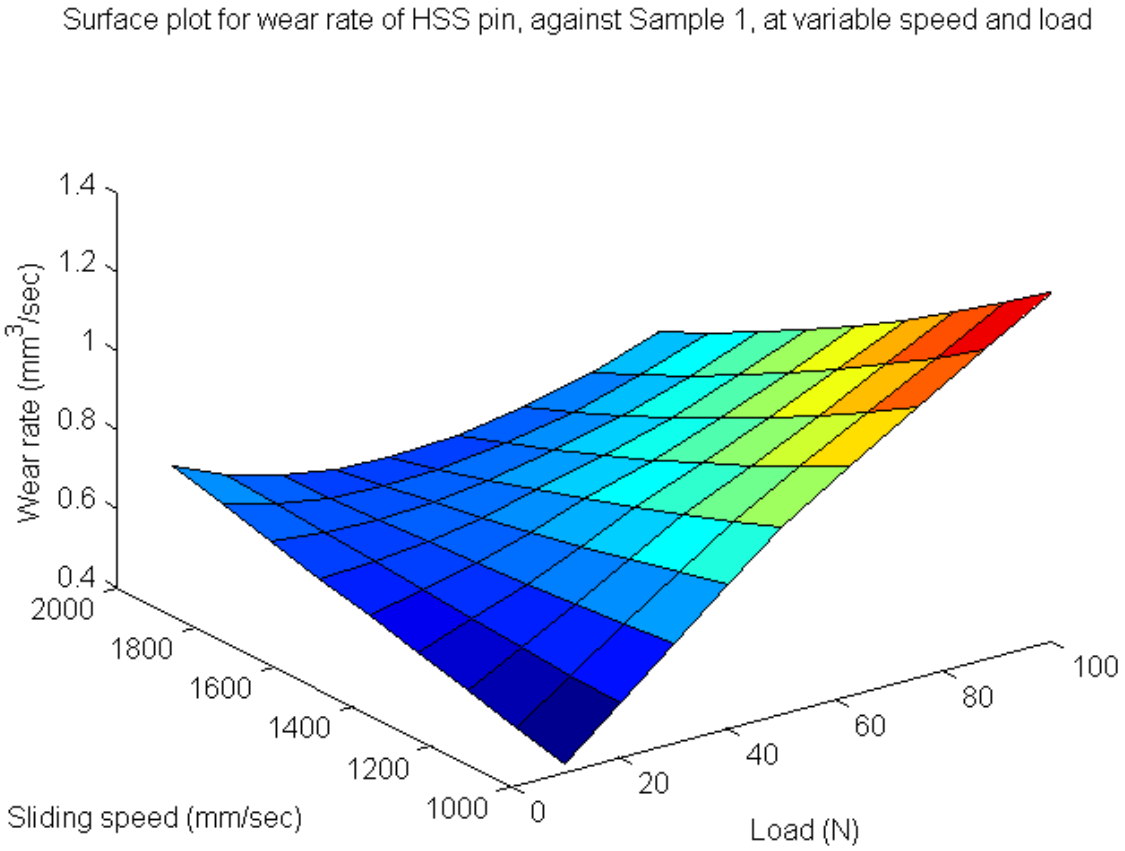

Figure 39 Surface plot wear rate of HSS pin, drilling Sample 1, at variable speed and load

Table: Experimental data of wear rate of Sample 1 disk, sliding against HSS pin

Speed (mm/sec) **Load (N)**	**1000**	**1500**	**2000**
10	11.7798	21.8515	25.632
50	35.001	18.8556	4.8991
100	1.83333	4.83333	22.039

Table 5 wear rate of Sample 1 disk sliding against HSS pin, for variable loads and speeds

The date from above table is plotted in MATLAB to obtain the following,

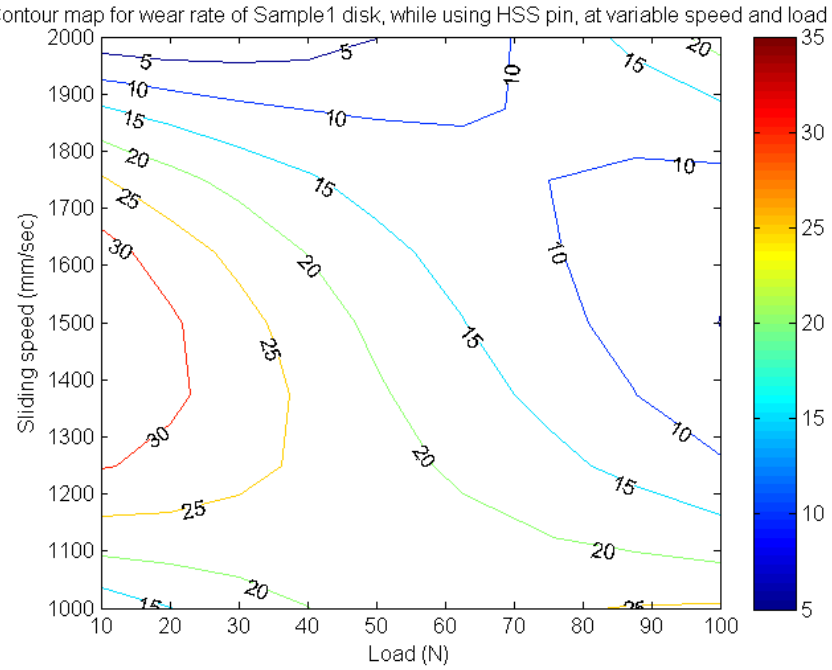

Figure 40 Contour map for wear rate of Sample 1, using HSS pin, at variable speed and load

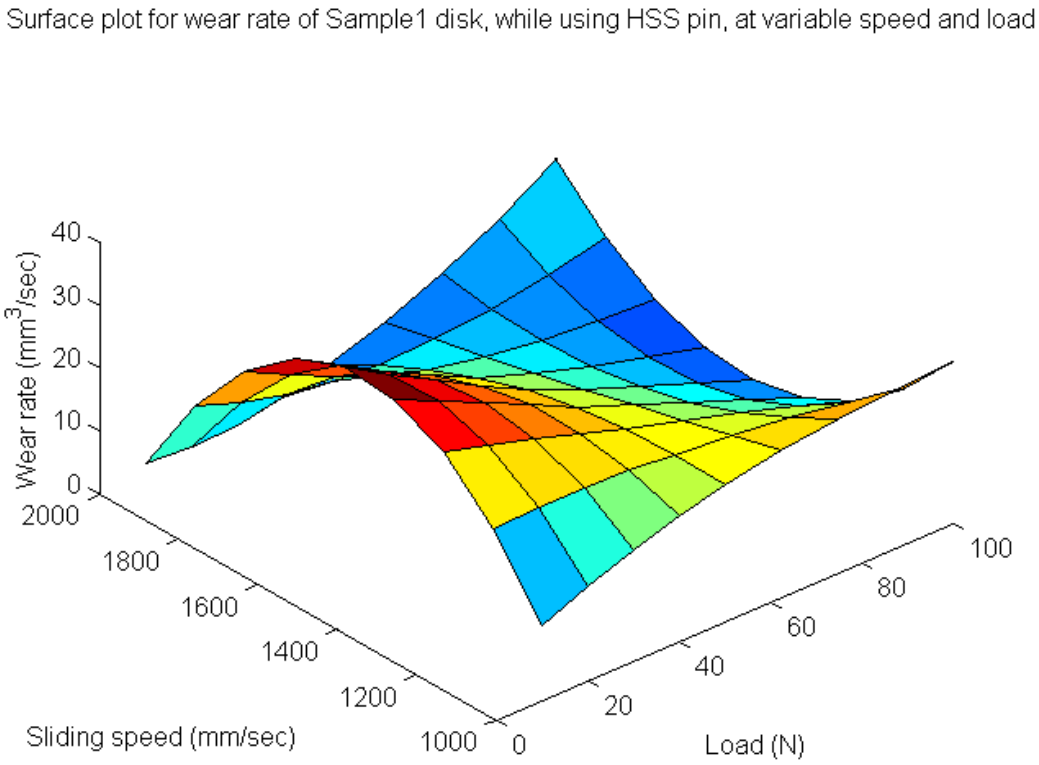

Figure 41 Surface plot for wear rate of Sample 1, using HSS pin, at variable speed and load

From the pin wear rate contour map, we can observe that the minimum tool loss (MRR~ 0.42 mm^3/sec) occurs in the range of 1000-1300 mm/sec and 10-15 N load range, which

corresponds to the medium wear rate for the sample disc, being in the range 15-20 mm^3/sec. The region of avoidance for this experiment set occurs for the speed range <500 mm/sec, and the load range >90N.

Tool Optimization for S-grey rock sample:

From experiment sets A and B, it is concluded that the optimum tool material for drilling through S-grey rocks is the HSS pin, because even though the minimum MRR for HSS pin is 0.42 mm^3/sec, and that of the Carbide is 0.2 mm^3/sec, but even for a pin MRR of ~0.4 mm^3/sec, the disc MRR using the Carbide pin is very less (i.e. ~0.52 mm^3/sec), whereas for the same pin MRR, the disc MRR using HSS pin is of the range 15-20 mm^3/sec. The optimum conditions for using HSS pin on S-grey rock are:

- speed range: 1000-1300 mm/sec
- load range: 10 – 15N.

The comparison can also be made by obtaining the ratio of the disc wear rate produced at the minimum tool wear rate for any combination. The ratio shall be termed as "bit efficiency coefficient".

$$Bit\ efficiency\ coefficient\ (B) = \frac{Disc\ MRR\ at\ minimum\ tool\ MRR}{Minimum\ tool\ MRR}$$

Then,

- $B_{WC,\ S\text{-}grey}$ is 1.53 / 0.17 = 9
- $B_{HSS,\ S\text{-}grey}$ is 11.78 / 0.42 = 28

Thus, HSS is the selected tool.

5.3. EXPERIMENT SET C: "GRANITE" AND CARBIDE PIN

A set of experiments for varying speeds and loads were performed for a disk of rock sample 2, with a Carbide pin. The experimental data is tabulated as follows:

Table: Experimental data of wear rate of Carbide pin sliding against Sample 2

Speed (mm/sec) **Load (N)**	**1000**	**1500**	**2000**
10	0.39808	0.31936	0.33459
50	0.37642	0.33888	0.31831
100	0.86425	0.67228	0.51081

Table 6 wear rate of Carbide pin sliding against Sample 2

The data from the table is interpolated and plotted in MATLAB, to obtain the plots below:

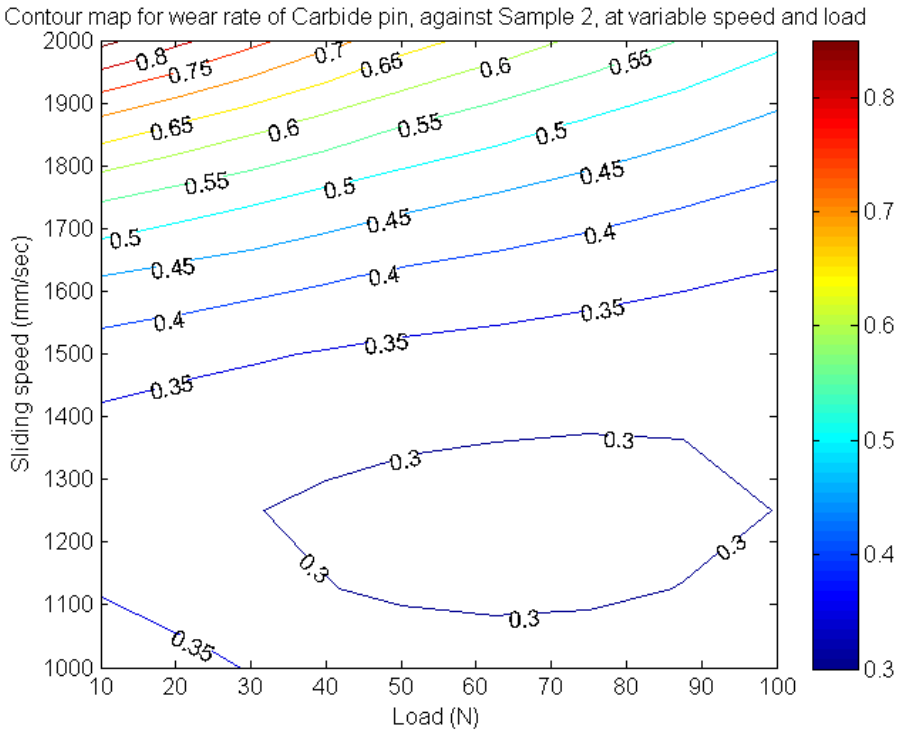

Figure 42 Contour map for wear rate of Carbide pin while drilling Sample 2, at variable speed and load

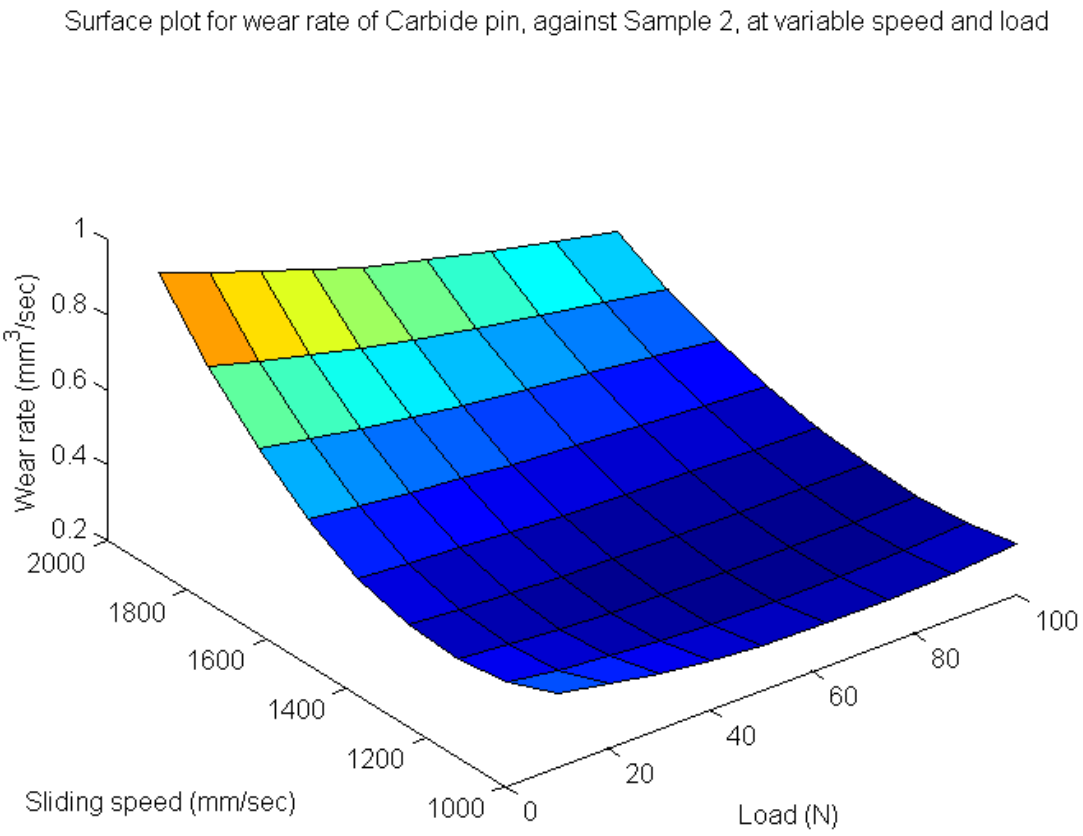

Figure 43 Surface plot for wear rate of Carbide pin while drilling Sample 2, at variable speed and load

Table: Experimental data of wear rate of Sample 2 disk, sliding against Carbide pin

Speed (mm/sec) **Load (N)**	**1000**	**1500**	**2000**
10	0.95934	1.67934	2.39933
50	6.86916	8.20516	9.54116
100	4.86953	4.94382	5.17583

Table 7 wear rate of Sample 2 disk sliding against Carbide pin, for variable loads and speeds

The date in above table is plotted in MATLAB to obtain the following,

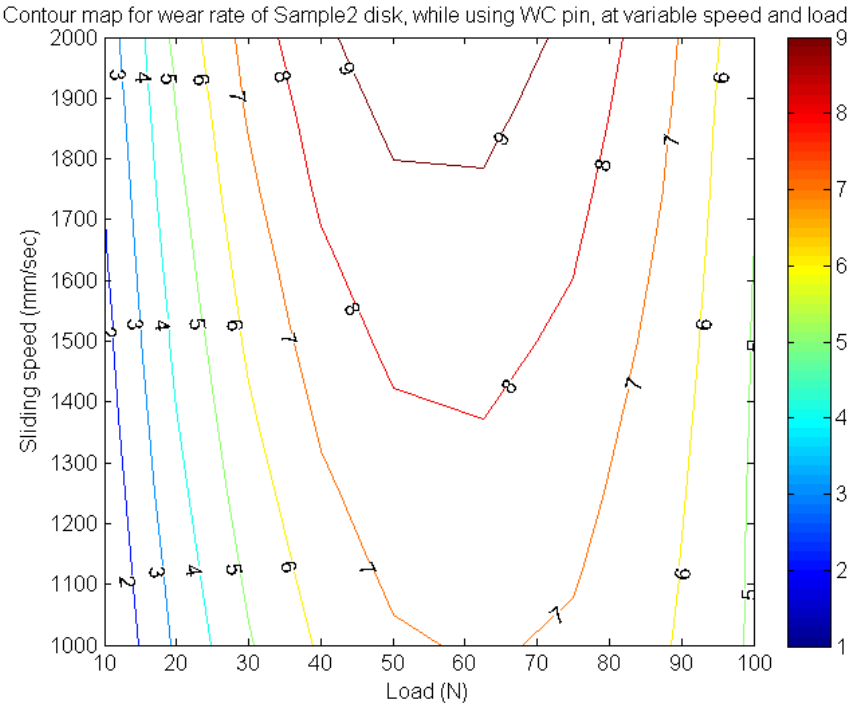

Figure 44 Contour map for wear rate of Sample 2, using Carbide pin, at variable speed and load

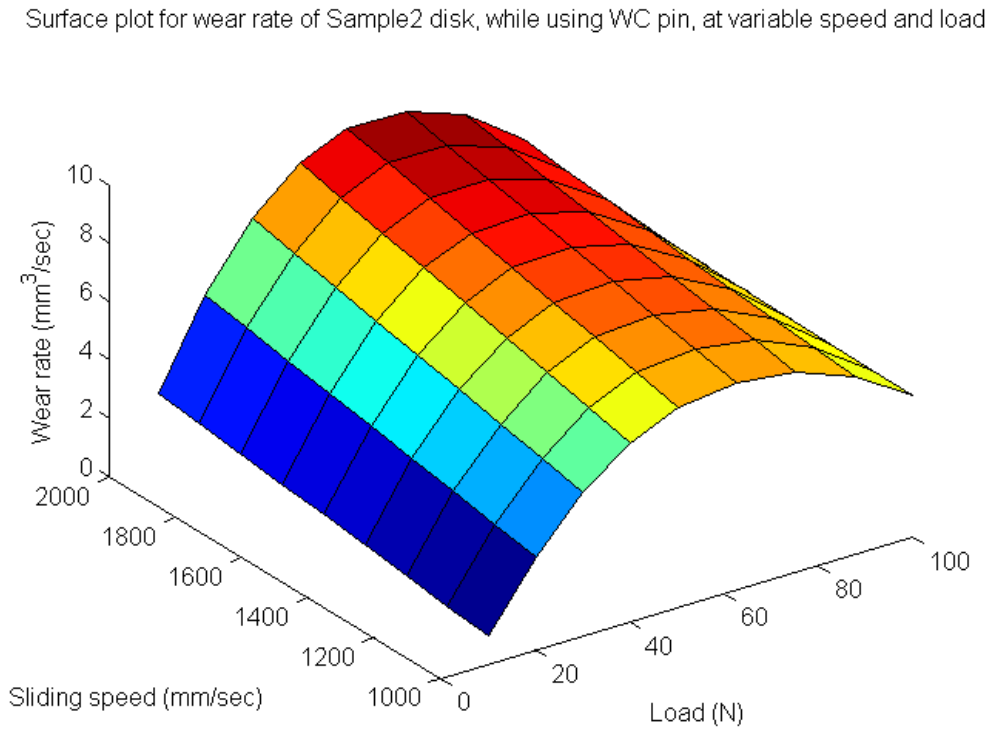

Figure 45 Surface plot wear rate of Sample 2, using Carbide pin, at variable speed and load

From the contour map for the pin wear rate, we notice that the minimum tool loss for this combination occurs in the load range 20-40 N, and the speed range 1200 – 2000 mm/sec; this

region corresponds to the medium-wear region on the disc-wear map, ranging from 3 to 6 mm^3/sec. The region of avoidance for this set of experiments is the speed range > 2000mm/sec, and the load range < 25N, corresponding to a tool MRR of ~0.9 mm^3/sec.

5.4. EXPERIMENT SET D: "GRANITE" AND HSS PIN

A set of experiments for varying speeds and loads were performed for a disk of rock sample 2, being slid against HSS pin. The experimental data is tabulated as follows:

Table: Experimental data of wear rate of HSS pin sliding against Sample 2

Speed (mm/sec) Load (N)	**1000**	**1500**	**2000**
10	0.27283	0.16211	0.3332
50	0.04729	0.30406	0.49296
100	0.58733	0.54606	0.50479

Table 8 wear rate of HSS pin sliding against Sample 2

The data from the table is interpolated and plotted in MATLAB, to obtain the plots below:

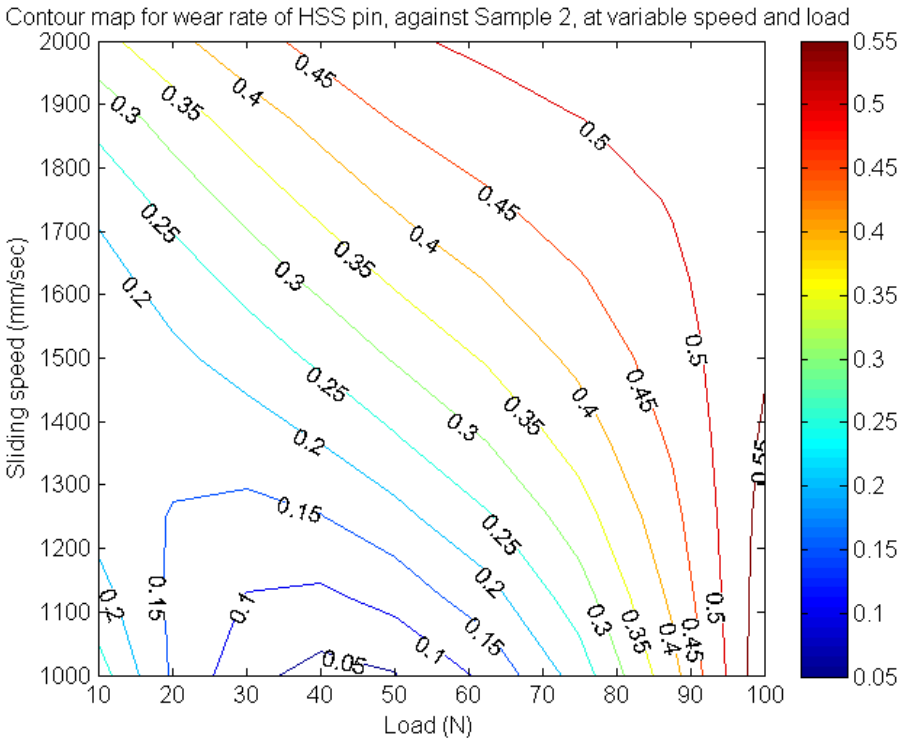

Figure 46 Contour map for wear rate of HSS pin, while drilling Sample 2, at variable speed and load

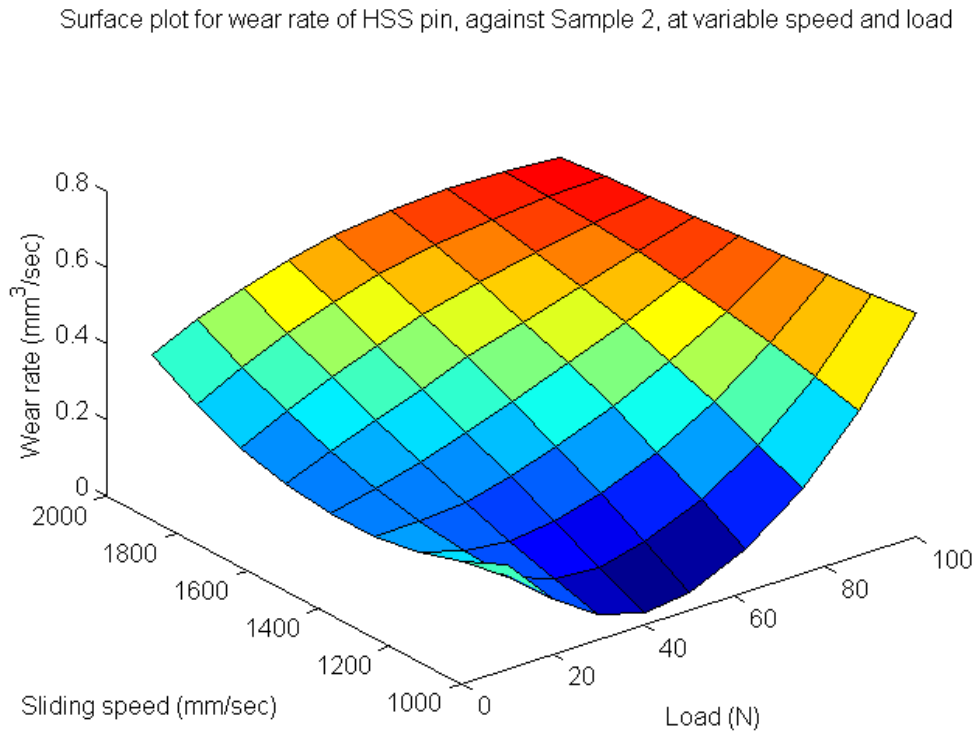

Figure 47 Surface plot for wear rate of HSS pin, while drilling Sample 2, at variable speed and load

Table: Experimental data of wear rate of Sample 2 disk, sliding against HSS pin

Speed (mm/sec) **Load (N)**	**1000**	**1500**	**2000**
10	0.72	1.08	1.44
50	10.5511	10.1004	9.85345
100	18.344	15.6312	13.2732

Table 9 wear rate of Sample 1 disk sliding against HSS pin, for variable loads and speeds

The date in above table is plotted in MATLAB to obtain the following,

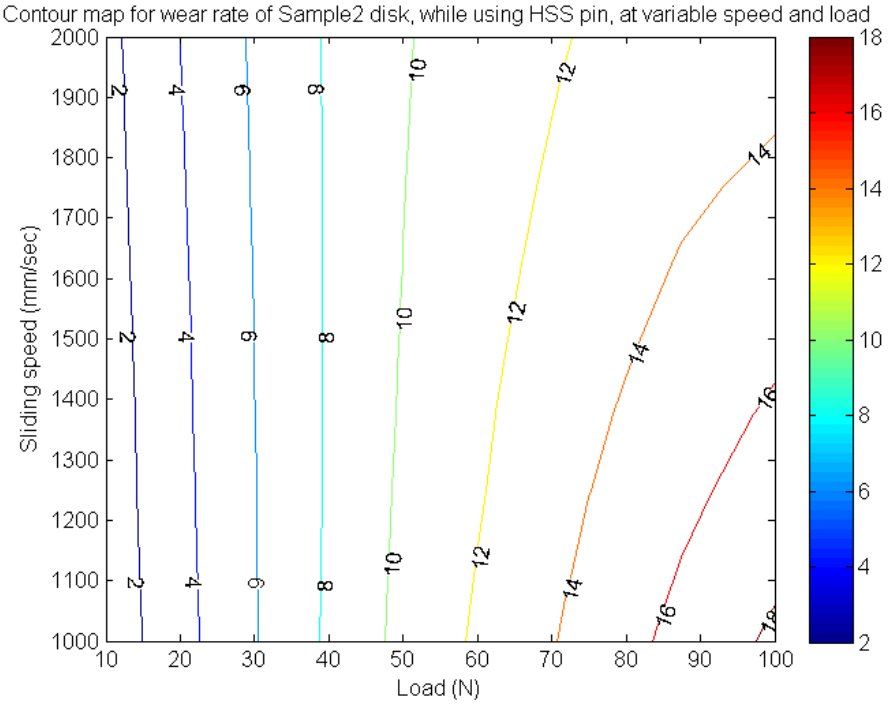

Figure 48 Contour map for wear rate of Sample 2, using HSS pin, at variable speed and load

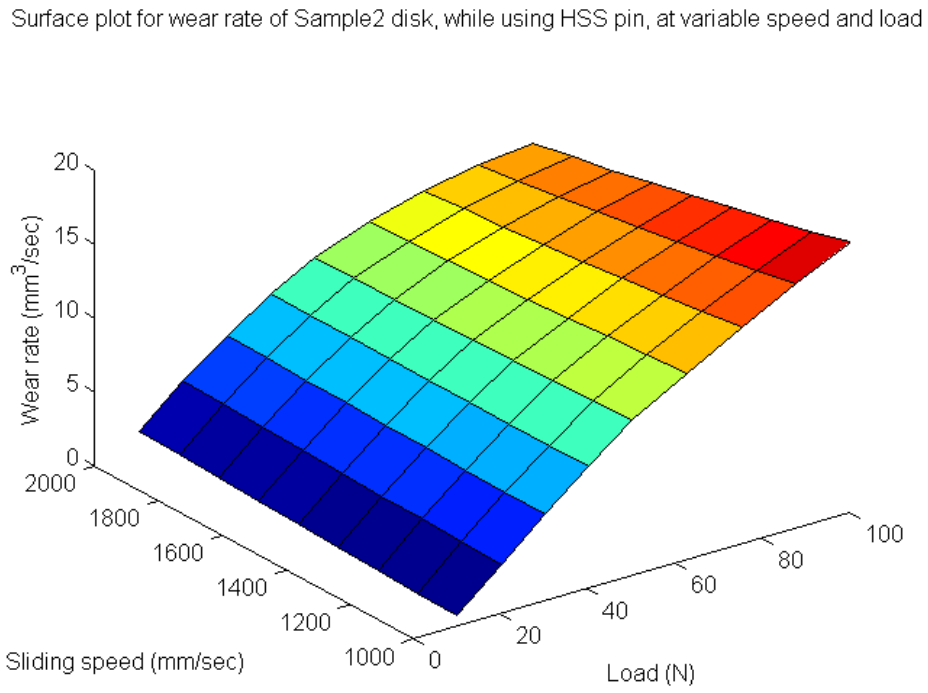

Figure 49Surface plot for wear rate of Sample 2, using HSS pin, at variable speed and load

From the contour map, it is visible that the minimum tool loss (~0.1 mm^3/sec) for this combination lies in the range 30-50 N, at a speed of 1000 – 1300 m/sec; which corresponds to

the mild disc loss rate in the range of 10 – 12 mm^3/sec. The region of avoidance for this set of experiments is the load range >100N, for all speeds, especially above 1500 mm/sec.

Tool Optimiztion for Granite sample:

From the experiment sets C and D, it is concluded that the optimum tool required to drill through Granite rock is HSS pin, running at 50 N load, and 1000 mm/sec. The selection is based on the observation that the minimum (optimum) pin MRR for Carbide pin is ~0.3 mm^3/sec, corresponding to the disc MRR of 9.5 mm^3/sec, whereas the minimum pin MRR for the HSS pin is 0.1 mm^3/sec, corresponding to a disc MRR > 10 mm^3/sec.

Determining the bit efficiency co-efficient (B) for the minimum bit MRR,

- $B_{WC,Granite} = 9.54 / 0.32 = 29.8$
- $B_{HSS,Granite} = 10.55 / 0.05 = 211$

Thusly, the HSS pin produces more material wear on the disc with lesser pin wear. The optimum drilling conditions for HSS are:

- Speed: >1500 mm/sec
- Load: >100N

5.5. EXPERIMENT SET E: "LORALAI" AND CARBIDE PIN

A set of experiments for varying speeds and loads were performed for a disk of rock sample 3, with a Carbide pin. The experimental data is tabulated as follows:

Table: Experimental data of wear rate of Carbide pin sliding against Sample3

Speed (mm/sec) **Load (N)**	**1000**	**1500**	**2000**
10	0.46053	0.55395	0.83526
50	1.04201	0.86032	0.71256
100	0.18601	0.26375	0.33133

Table 10 wear rate of Carbide pin sliding against Sample 3

The data from the table is interpolated and plotted in MATLAB, to obtain the plots below:

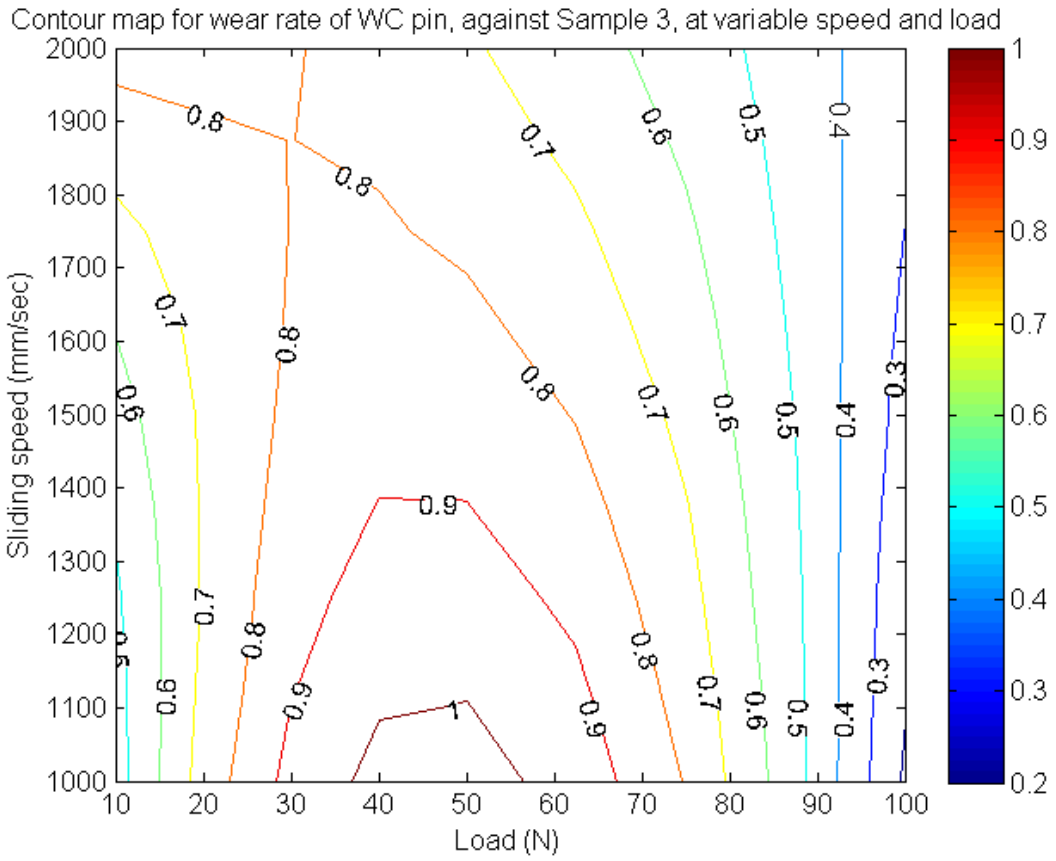

Figure 50 Contour map for wear rate of Carbide pin, while drilling Sample 3, at variable speed and load

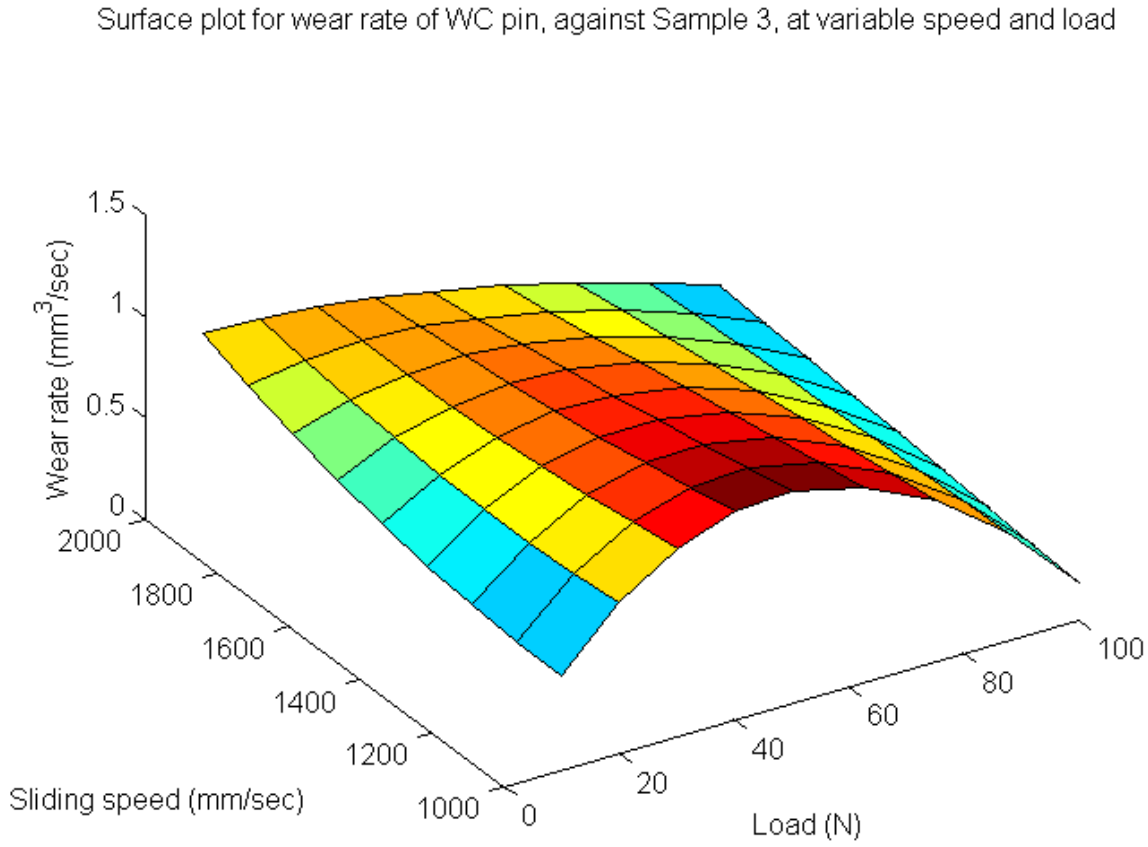

Figure 51 Surface plot for wear rate of Carbide pin, while drilling Sample 3, at variable speed and load

Table: Experimental data of wear rate of Sample 3 disk, sliding against Carbide pin

Speed (mm/sec) **Load (N)**	**1000**	**1500**	**2000**
10	3.84419	5.19589	13.2883
50	19.4091	18.7837	20.0682
100	59.8588	40.0666	24.6214

Table 11 wear rate of Sample 3 disk sliding against Carbide pin, for variable loads and speeds

The date in above table is plotted in MATLAB to obtain the following,

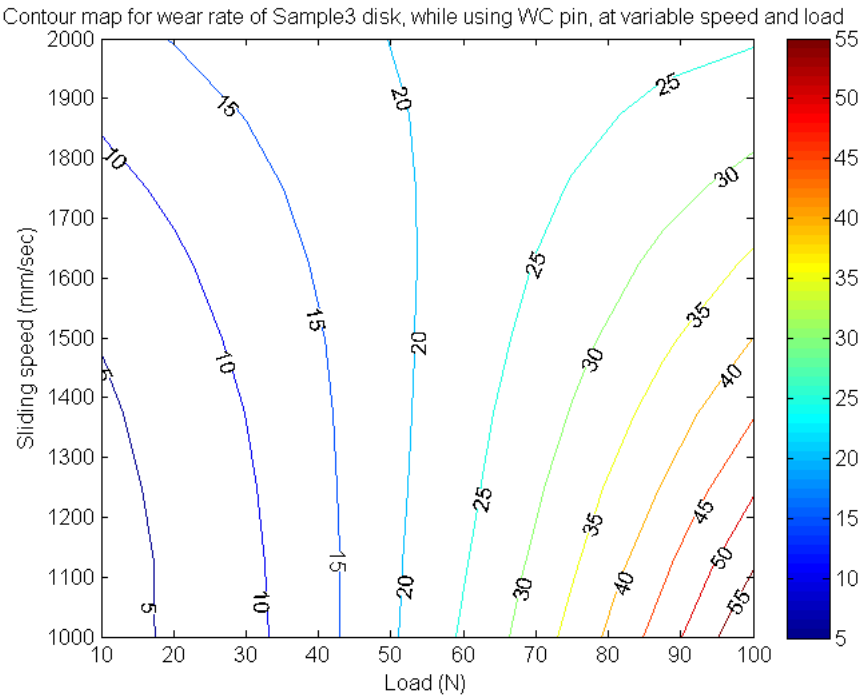

Figure 52 Contour map for wear rate of Sample 3, using Carbide pin, at variable speed and load

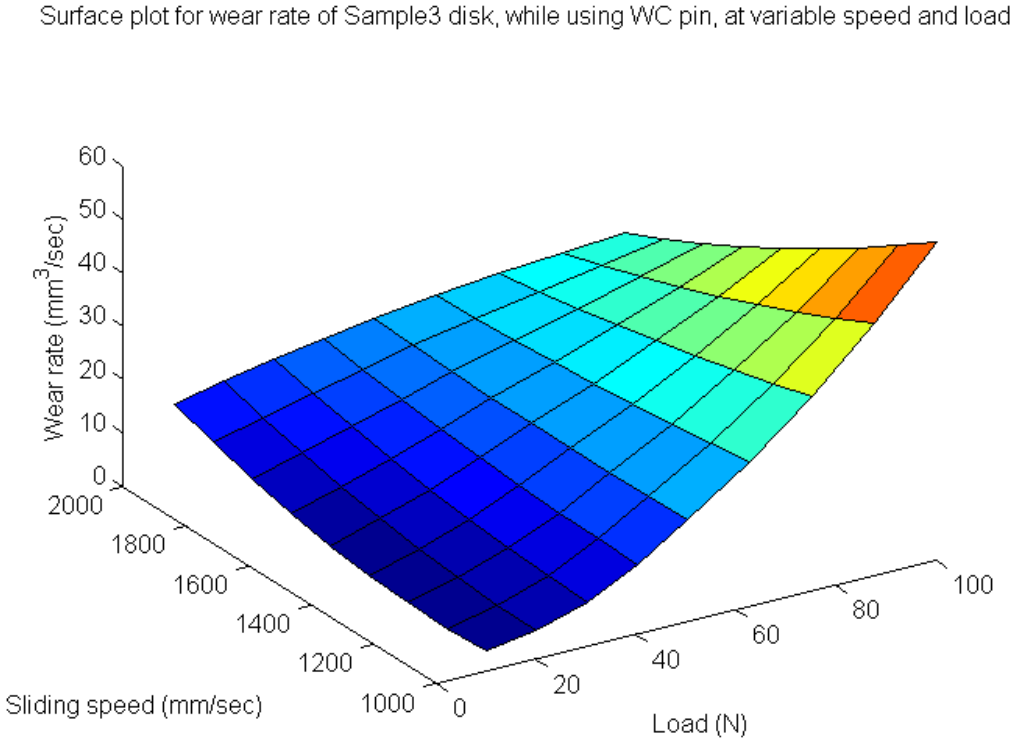

Figure 53 Surface plot for wear rate of Sample 3, using Carbide pin, at variable speed and load

From the contour map for pin-wear rate, we can determine the ranges for minimum tool loss rate (MRR ~0.2 mm^3/sec), which occurs above a load of 95N, and minimum speed i.e. 1000

mm/sec; this region corresponds to the maximum disc wear region, lying in the range of 50 – 55 mm^3/sec. The selected region is the optimum drilling region for this combination.

5.6. EXPERIMENT SET F: "LORALAI" AND HSS PIN

A set of experiments for varying speeds and loads were performed for a disk of rock sample 3, with an HSS pin. The experimental data is tabulated as follows:

Table: Experimental data of wear rate of HSS pin sliding against Sample 3

Speed (mm/sec) **Load (N)**	**1000**	**1500**	**2000**
10	0.04799	0.06486	0.16587
50	0.10297	0.09965	0.10647
100	0.24585	0.16456	0.10113

Table 12 wear rate of HSS pin sliding against Sample 3

The data from the table is interpolated and plotted in MATLAB, to obtain the plots below:

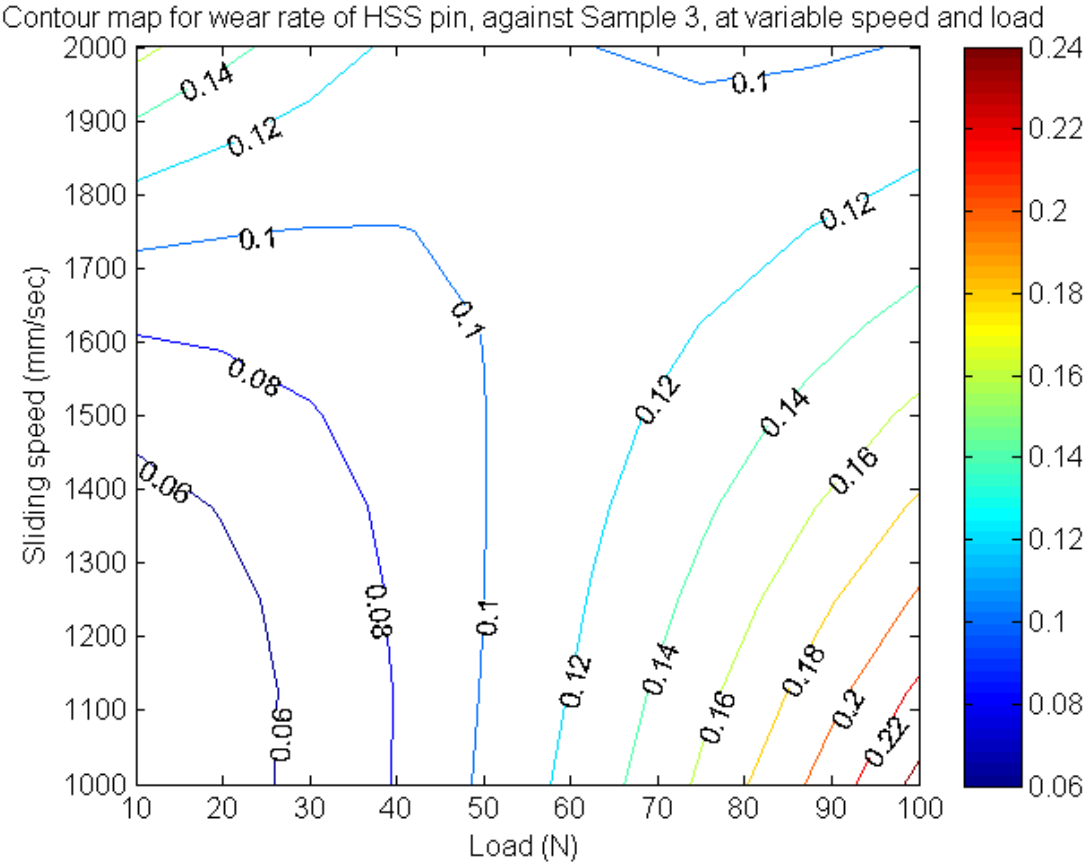

Figure 54 Contour map for wear rate of HSS pin, while drilling Sample 3, at variable speed and load

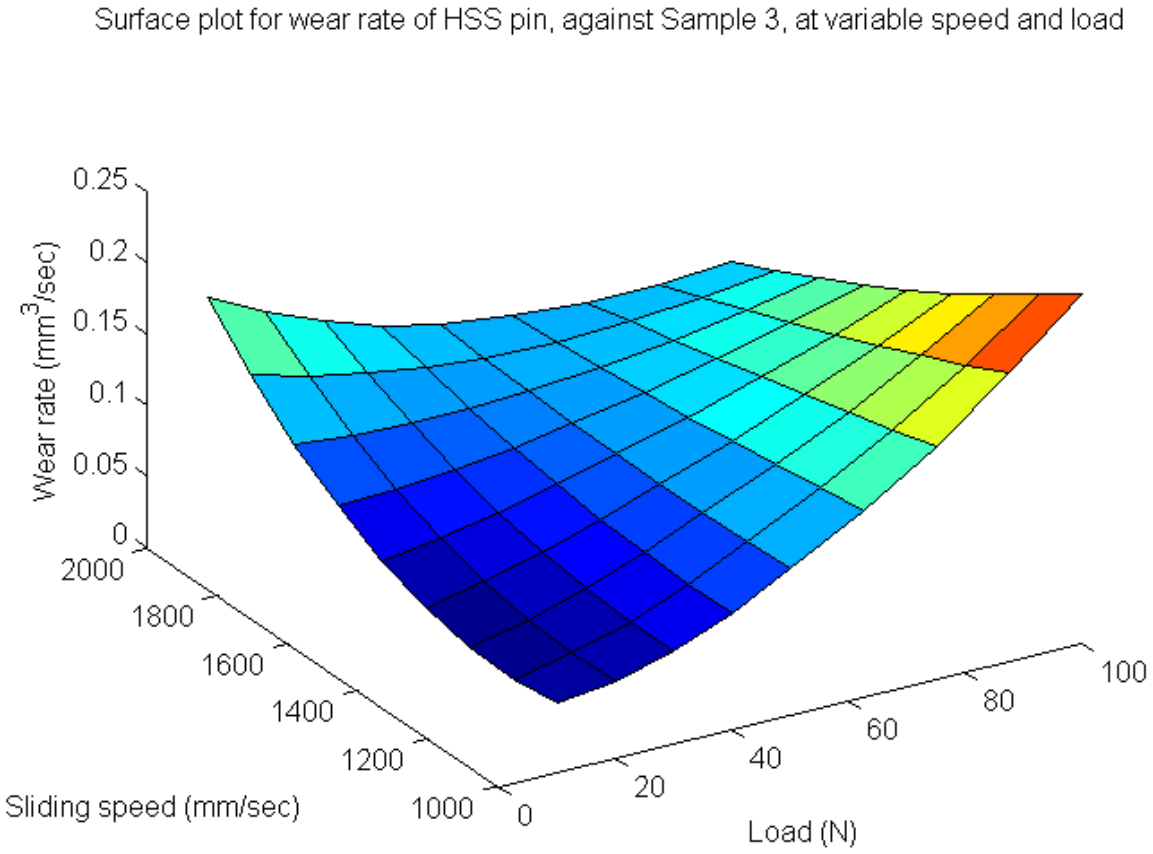

Figure 55 Surface plot for wear rate of HSS pin, while drilling Sample 3, at variable speed and load

Table: Experimental data of wear rate of Sample 3 disk, sliding against HSS pin

Speed (mm/sec) **Load (N)**	**1000**	**1500**	**2000**
10	15.7271	5.45118	2.66494
50	3.36834	7.10355	9.69284
100	25.7109	21.061	17.239

Table 13 wear rate of Sample 3 disk sliding against HSS pin, for variable loads and speeds

The date in above table is plotted as below,

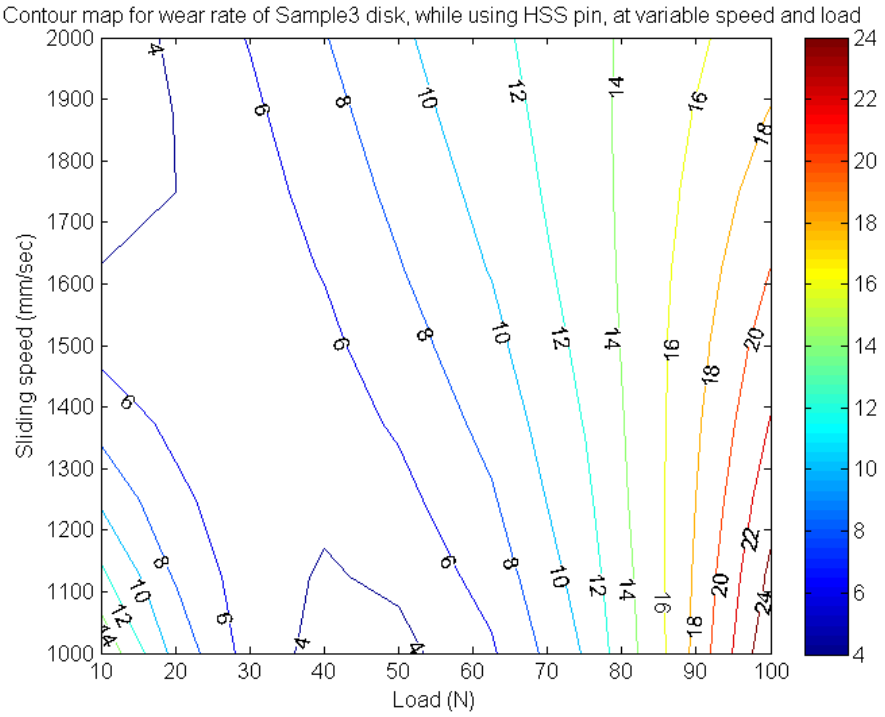

Figure 56 Contour map for wear rate of Sample 3, using HSS pin, at variable speed and load

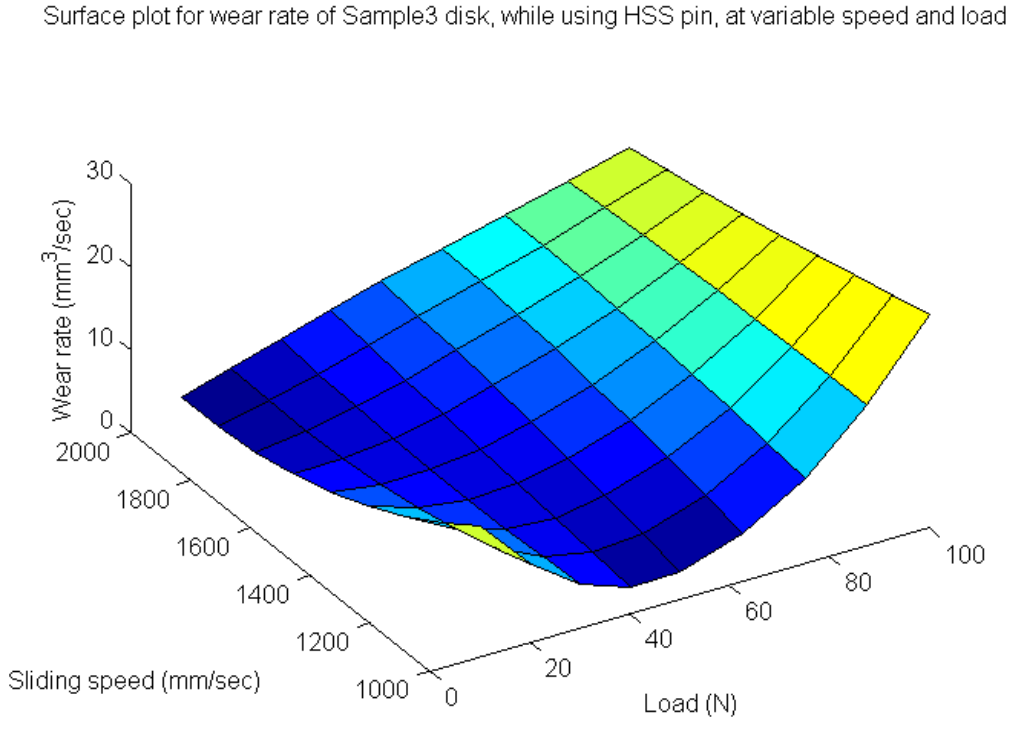

Figure 57 Surface plot for wear rate of Sample 3, using HSS pin, at variable speed and load

From the contour map for the tool loss rate, we can observe that the minimum tool loss for this combination (MRR ~ 0.05 mm^3/sec) occurs in the range 10-25 N, at minimum speed i.e.

approximately 1 m/sec. This corresponds to the mild disc wear region, with wear rates in the range of 10 – 12 mm^3/sec.

Tool Optimization for Loralai sample:

From the experiment sets E and F, it is concluded that the optimum tool required to drill through Loralai rock is HSS. This selection is based upon the observation that the minimum tool wear for HSS pin (MRR ~ 0.05 mm^3/sec) corresponds to a MRR of approximately 10 mm^3/sec in the disc; whereas the minimum tool wear for the Carbide pin (MRR ~0.2 mm^3/sec) corresponds to a MRR of approximately 55 mm^3/sec.

Determining the bit efficiency co-efficient for the respective minimum tool MRR:

- $B_{WC,Loralai}$ = 59.86/0.19 = 315
- $B_{HSS,Loralai}$ = 15.73/0.05 = 314.6 ~ 315

But, the minimum tool MRR for HSS (0.05 mm^3/sec) is much lower and safer than the minimum tool MRR for Carbide pin.

The optimum drilling conditions for HSS against Loralai are:

- Speed: ~ 1000 mm/sec
- Load: 10 – 25 N

5.7. EXPERIMENT SET G: "TAVERA" AND CARBIDE PIN

A set of experiments for varying speeds and loads were performed for a disk of rock sample 4, with a Carbide pin. The experimental data is tabulated as follows:

Table: Experimental data of wear rate of Carbide pin sliding against Sample 4

Speed (mm/sec) **Load (N)**	**1000**	**1500**	**2000**
10	0.27213	0.41227	0.83422
50	0.37642	0.33888	0.31831
100	0.378	0.34632	0.33497

Table 14 wear rate of Carbide pin sliding against Sample 4

The data from the table is interpolated and plotted in MATLAB, to obtain the plots below:

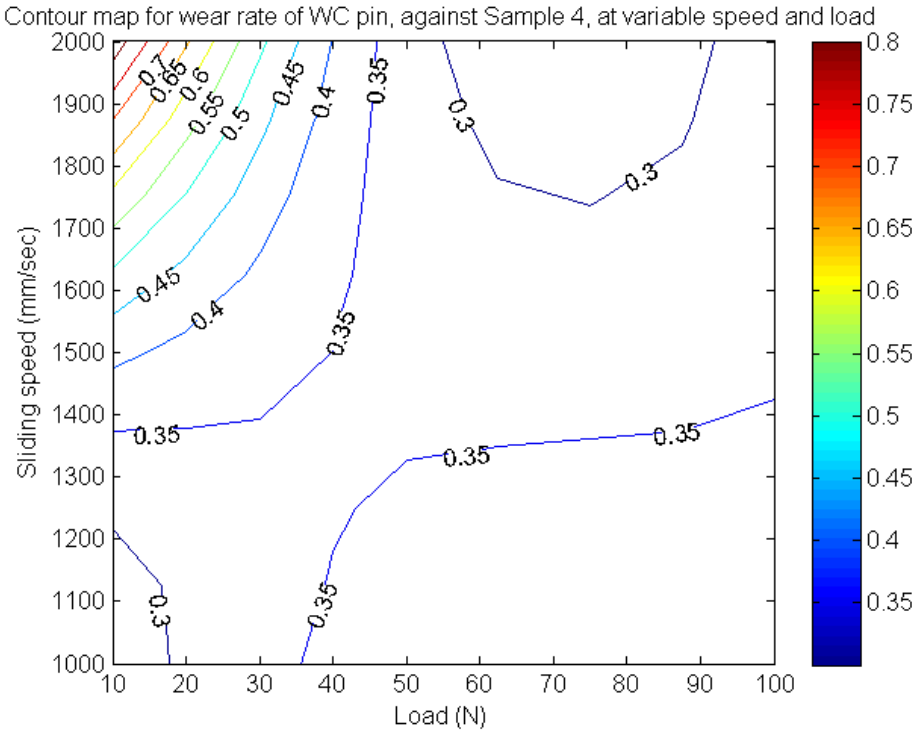

Figure 58 Contour map for wear rate of Carbide pin, while drilling Sample 4, at variable speed and load

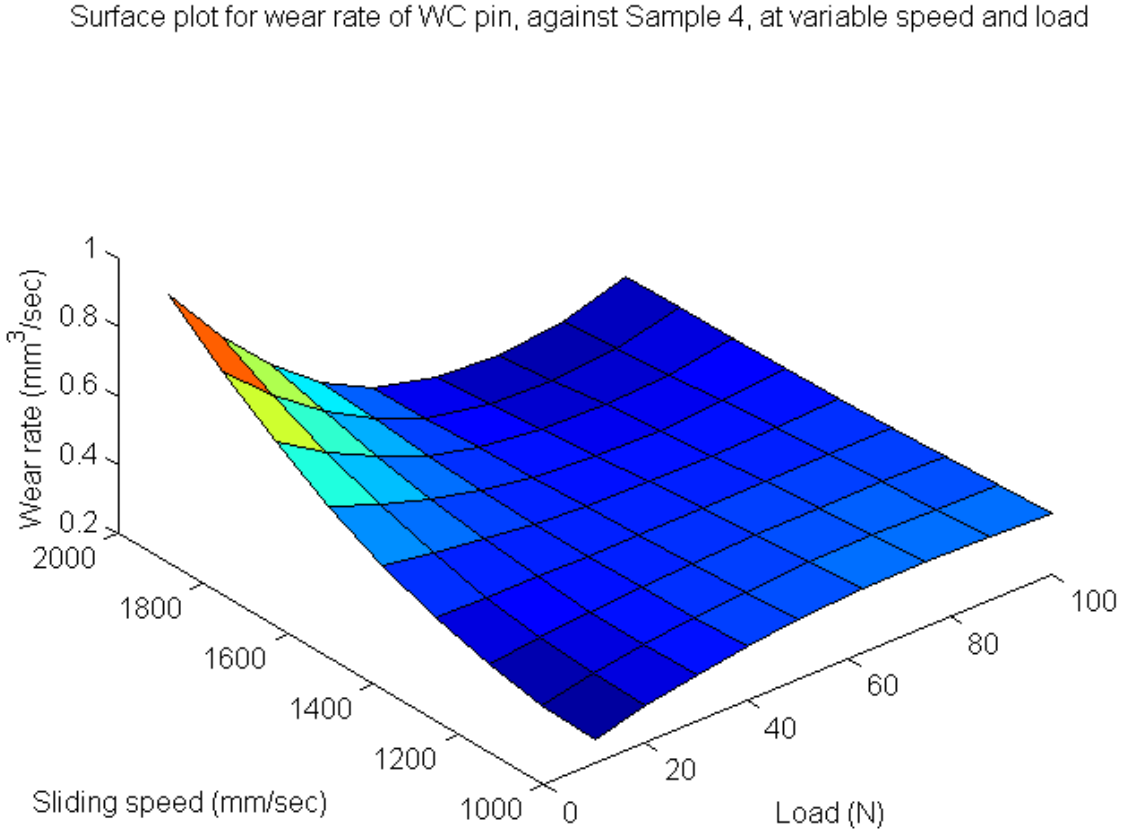

Figure 59 Surface plot for wear rate of Carbide pin, while drilling Sample 4, at variable speed and load

Table: Experimental data of wear rate of Sample 4 disk, sliding against Carbide pin

Speed (mm/sec) **Load (N)**	**1000**	**1500**	**2000**
10	5.52423	5.1104	15.931
50	39.4525	26.5933	18.1905
100	2.5	5.45938	18.7792

Table 15 wear rate of Sample 4 disk sliding against Carbide pin, for variable loads and speeds

The date in above table is plotted in MATLAB to obtain the following,

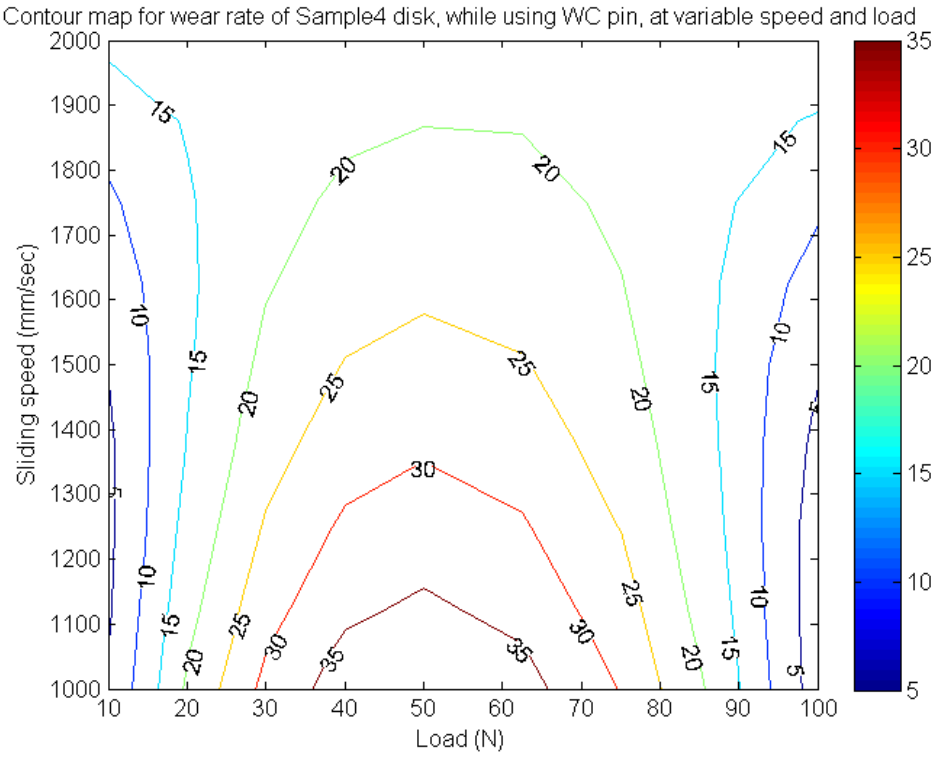

Figure 60 Contour map for wear rate of Sample 4, using Carbide pin, at variable speed and load

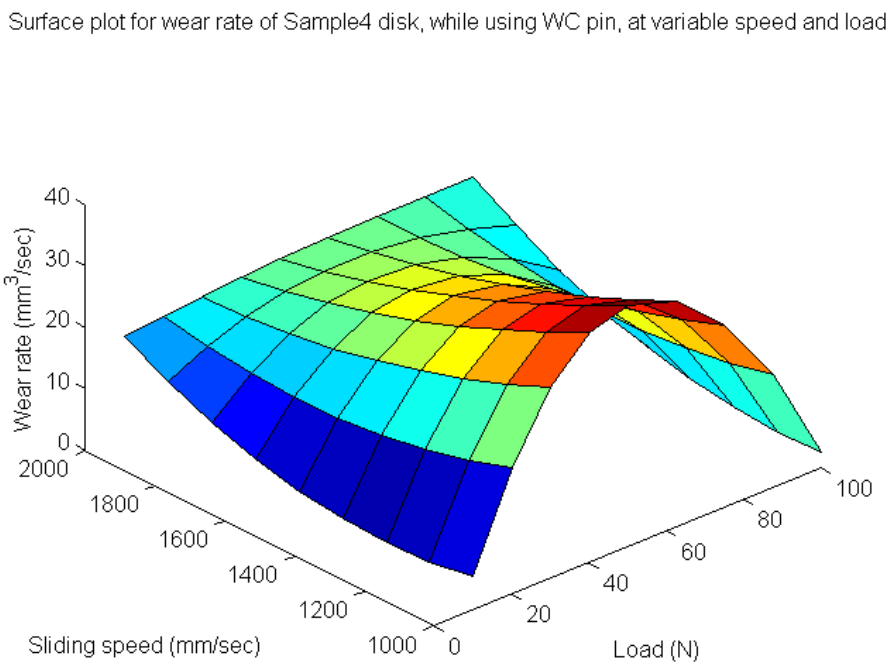

Figure 61 Surface plot for wear rate of Sample 4, using Carbide pin, at variable speed and load

The experimental data shows that minimum tool loss (MRR ~0.3 mm^3/sec) occurs in the whole load range from 0 – 100N, below 1400 mm/sec. This region on the pin wear map corresponds to the high disc-wear range from 25 – 35 mm^3/sec, and thus provides the optimal drilling parameters for this combination.

5.8. EXPERIMENT SET H: "TAVERA" AND HSS PIN

A set of experiments for varying speeds and loads were performed for a disk of rock sample 4, with an HSS pin. The experimental data is tabulated as follows:

Table: Experimental data of wear rate of HSS pin sliding against Sample 4

Speed (mm/sec) **Load (N)**	**1000**	**1500**	**2000**
10	0.33493	0.33493	0.33493
50	0.7722	0.68136	0.60748
100	0.02692	0.16506	0.32652

Table 16 wear rate of HSS pin sliding against Sample 4

The data from the table is interpolated and plotted in MATLAB, to obtain the plots below:

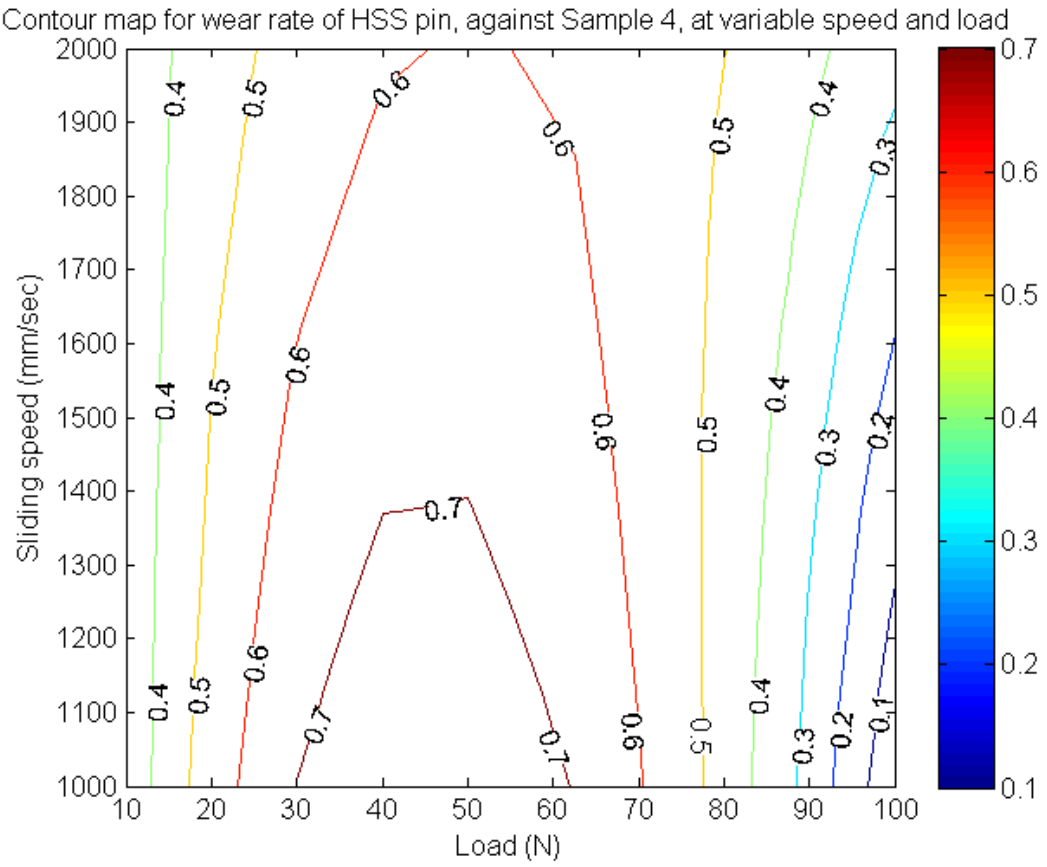

Figure 62 Contour map for wear rate of HSS pin, while drilling Sample 4, at variable speed and load

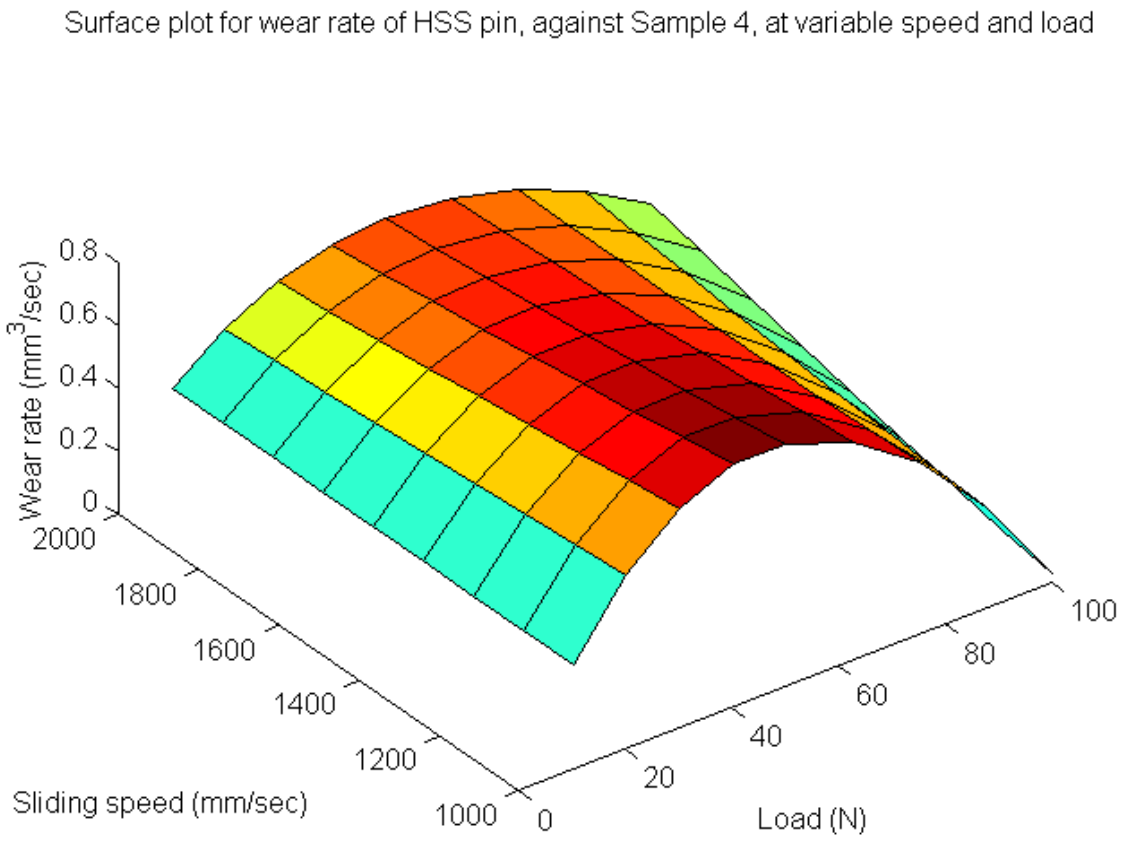

Figure 63 Surface plot for wear rate of HSS pin, while drilling Sample 4, at variable speed and load

Table: Experimental data of wear rate of Sample 4 disk, sliding against HSS pin

Speed (mm/sec) **Load (N)**	**1000**	**1500**	**2000**
10	8.00828	7.51863	4.03313
50	18.406	15.9975	14.2257
100	9.73893	9.73893	9.73893

Table 17 wear rate of Sample 4 disk sliding against HSS pin, for variable loads and speeds

The data is plotted as below,

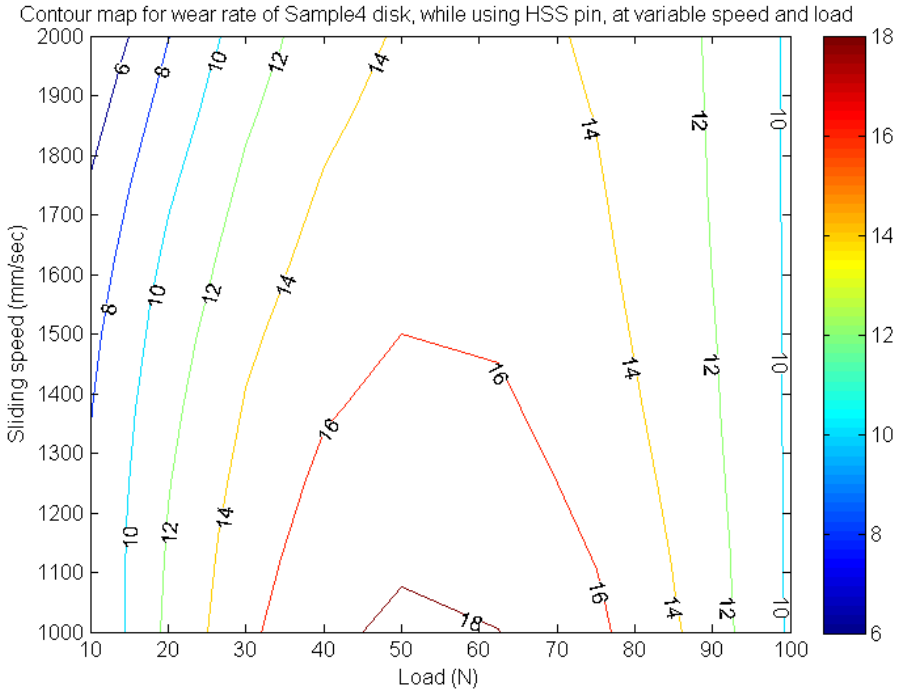

Figure 64 Contour map for wear rate of Sample 4, using HSS pin, at variable speed and load

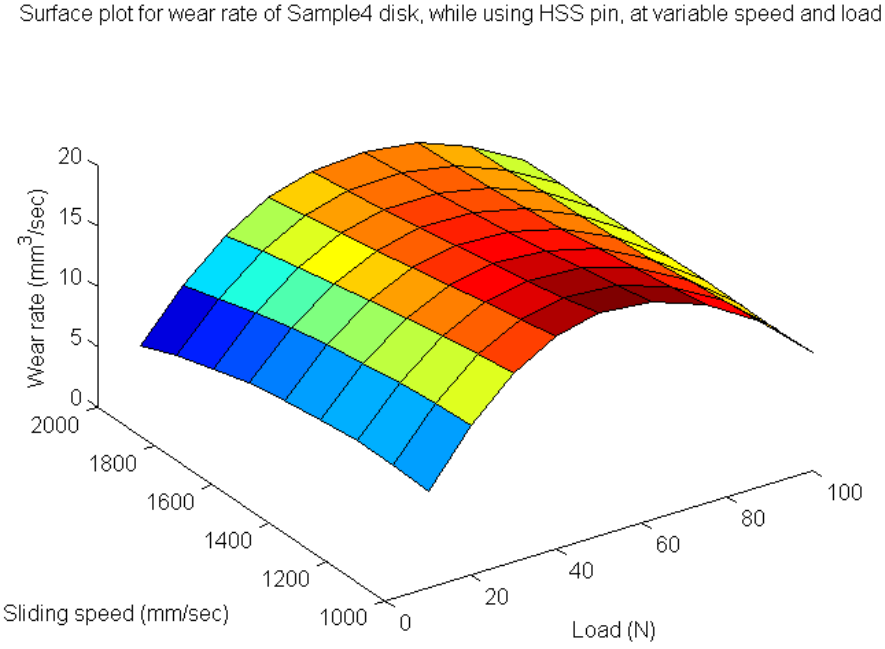

Figure 65 Surface plot for wear rate of Sample 4, using HSS pin, at variable speed and load

The experimental data shows that minimum tool loss (MRR 0.03 mm^3/sec) occurs above the 90-100 N load range at minimum speeds, i.e. near 1000 mm/sec. This region corresponds to the mild disc wear region, where the wear rate is of the range 10 mm^3/sec.

Tool Optimization for Tavera sample:

From the experiment sets G and H, it is concluded that the optimum tool required to drill through Tavera rock is HSS, because for the minimum tool wear rate (MRR ~0.03 mm^3/sec), the wear produced in the disc at a rate of approximately 10 mm^3/sec; whereas for the minimum Carbide pin wear rate (MRR ~0.3 mm^3/sec), the wear produced in the disc is at the rate of approximately 20 mm^3/sec, which is not a very high value as compared to the pin wear rate.

Determining the bit efficiency co-efficients for each pin, at the respective minimum pin wear rate:

- $B_{WC,Tavera} = 5.52/0.27 = 20$
- $B_{HSS,Tavera} = 9.73/0.1 = 97$

Therefore, HSS is the selected tool. The optimal range of conditions for the HSS pin are:

- Speed: < 1000 mm/sec
- Load: > 100 N

5.9. WORST CASES FOR PIN-WEAR

The two worst cases for HSS and Carbide pins are observed and the contour plots are extended through further experimentation.

5.9.1. Worst HSS Pin-Wear Case:

The maximum wear rate for HSS pin is observed for Sample 1 (S-grey). From the contour plot, it is observed that the maxima spreads above the load 100N, and below the speed 1m/sec. Therefore, the plot is extended to a load of 150N, and a speed of 0.5 m/sec. The experimental results are tabulated as follows:

Speed (mm/sec) Load (N)	**500**	**1000**	**1500**	**2000**
10	1.50796	0.41832	0.54375	0.66917
50	2.01062	0.87454	0.69285	0.54509
100	2.51327	1.28771	0.94982	0.68313
150	2.51327	1.50796	3.01593	2.51327

Table 18 Extended table for HSS pin wear rate, mm^3/sec, sliding against Sample 1

The tabulated values are presented as a scatter plot below:

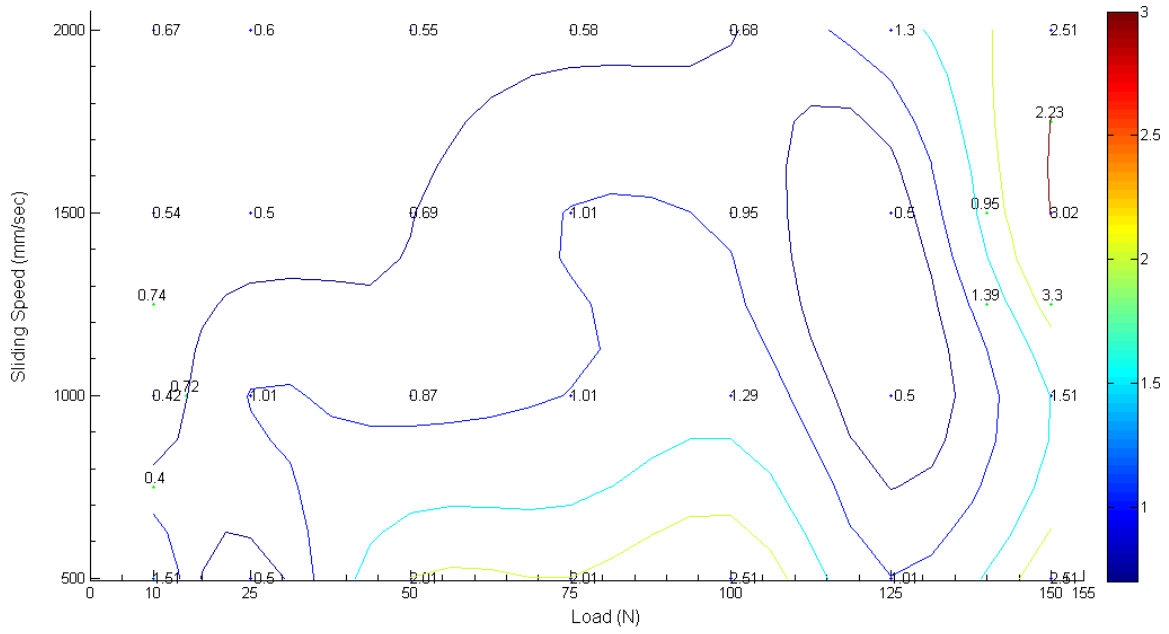

Figure 66 Scatter plot for HSS pin wear rate, sliding against Sample 1 for variable speeds and loads

The contour plot follows the previous trend with the maxima extending beyond 100N and 1m/sec, and a new maxima is observed in the range 1500 – 2000 mm/sec, for the load range above 140 N. This maxima is therefore the region of avoidance, whereas the region of safety remains the same, i.e. the speed range 1000 – 1500 m/sec, and load range 10N.

The corresponding disc wear rates are also recorded, calculated and tabulated as below:

Speed (mm/sec) **Load (N)**	**500**	**1000**	**1500**	**2000**
10	12.00088	11.7798	21.8515	25.632
50	7.20053	35.001	18.8556	4.8991
100	12.0009	1.83333	4.83333	22.039
150	16.8012	16.8012	9.88345	9.588141

Table 19 Extended disc wear rates (mm^3/sec) for Sample 1 disc, sliding against HSS pin

A scatter plot represents the aforementioned data:

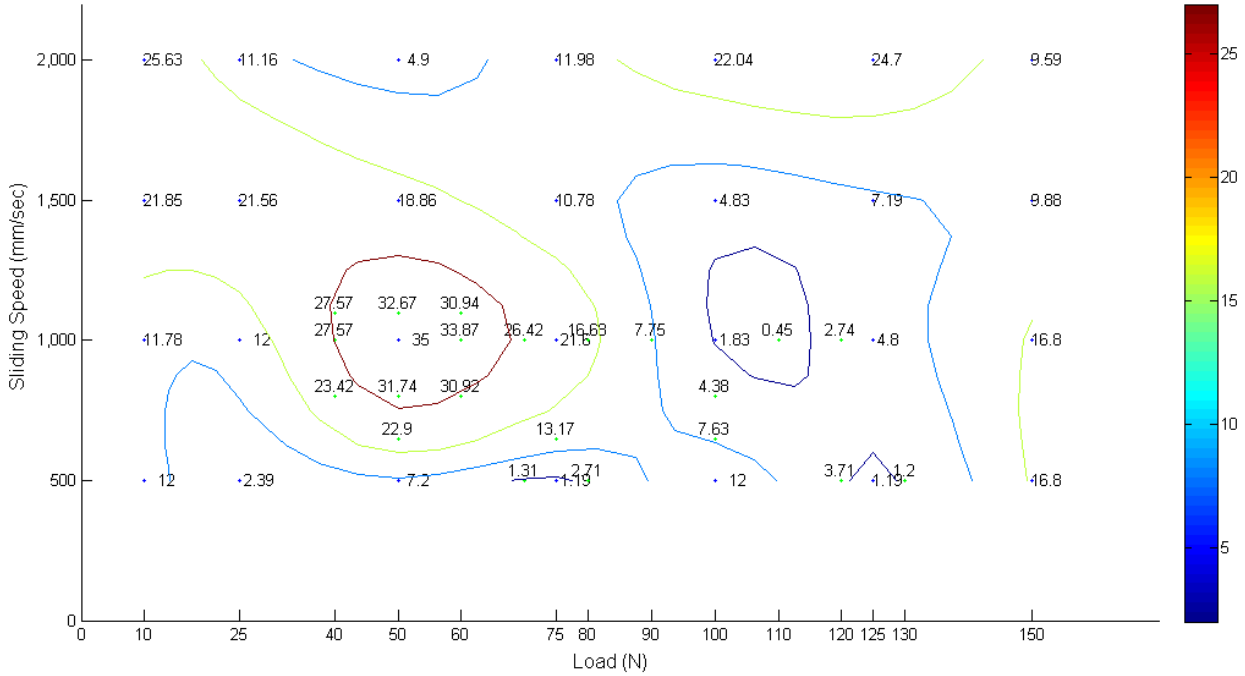

Figure 67 Scatter plot for Sample 1 disk wear rate, against HSS pin, for variable speeds and loads

The maxima remains the same as the previous plot i.e. speed around 1000m/sec, and load range around 40 – 60 N.

5.9.2. Worst Carbide Pin-Wear Case:

The maximum wear rate for Carbide pin is observed for Sample 3 (Loralai). From the contour plot, it is observed that the maxima spreads around the load 50N, and below the speed 1.5m/sec, and continues on beyond 1m/sec. Therefore, the plot is extended to a speed of 0.5 m/sec. The experimental results are tabulated as follows:

Speed (mm/sec) **Load (N)**	**500**	**1000**	**1500**	**2000**
10	1.00531	0.46053	0.55395	0.835255
50	0.50265	1.04201	0.86032	0.71256067
100	0.50265	0.18601	0.26375	0.33133267

Table 20 Extended table for Carbide pin wear rate, mm^3/sec, sliding against Sample 3

The tabulated values are presented as a scatter plot below:

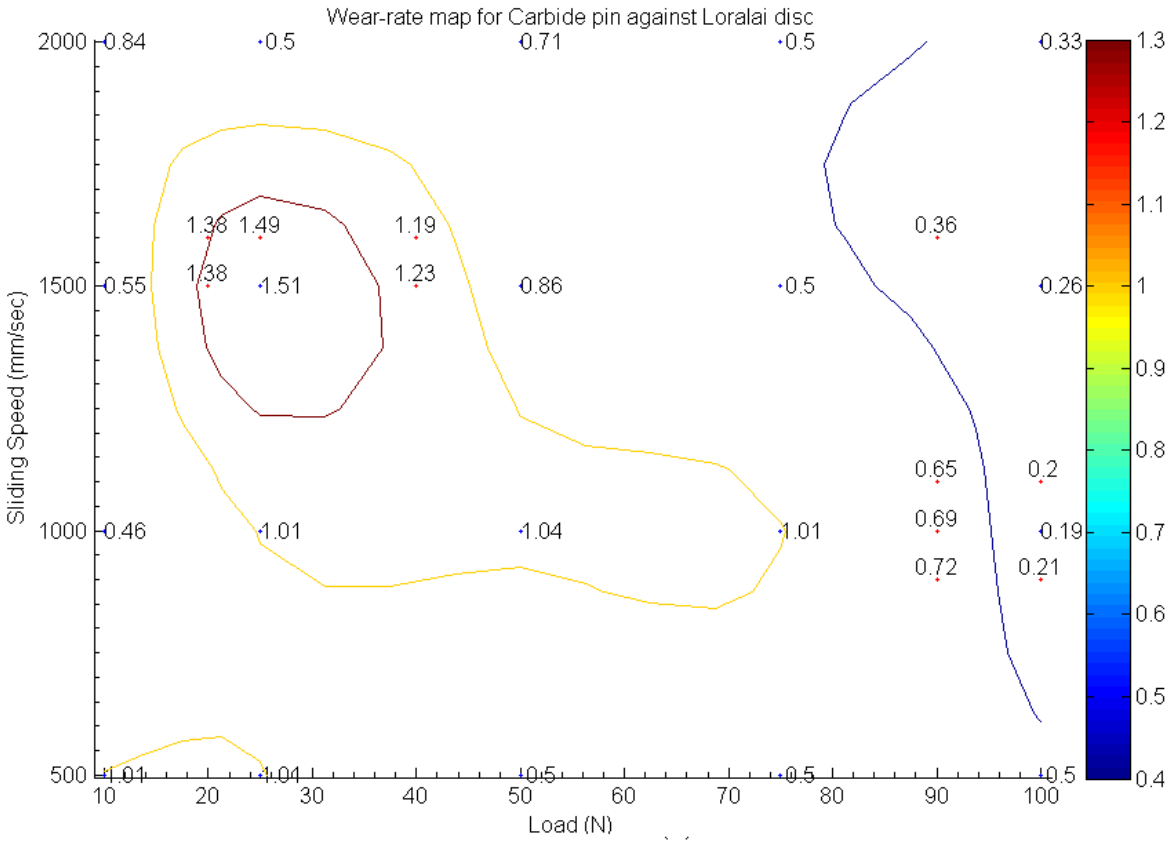

Figure 68 Scatter plot of Carbide pin wear rate, sliding against Sample 3 at variable speed and load

From the contour plot it is observed that the maxima is around the 1000 mm/sec speed range, and 20 – 25 N load range. This is the region of avoidance, whereas, the region o safety lies above the speed 750 mm/sec, and in the load range ~ 100N.

The corresponding disc-wear rate is recorded and tabulated as follows:

Speed (mn/sec) **Load (N)**	**500**	**1000**	**1500**	**2000**
10	8.356636	3.84419	5.19589	13.28826
50	7.162831	19.4091	18.7837	20.06824
100	10.74425	59.8588	40.0666	24.62139

Table 21 Extended table for Sample 3 disc wear rate, against Carbide pin

The data is presented as a scatter plot below:

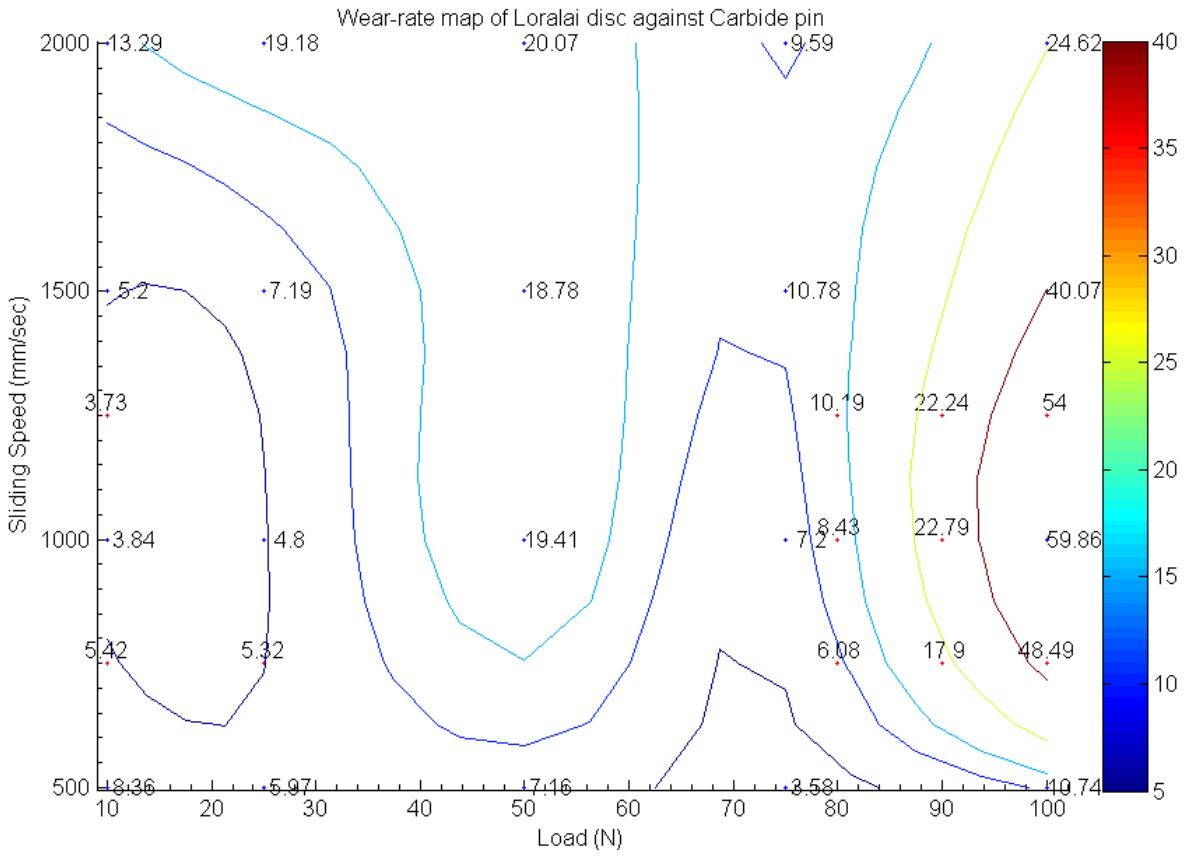

Figure 69Scatter plot for Sample 3 disc wear rate, using Carbide pin at various speeds and loads

From the contour plot, it is observed that the maxima stays in the same region, i.e. around 1000 mm/sec speed range, and above 100 N load.

5.10. LINEARITY OF WEAR-RATES

The wear for s-gray with Carbide pin at 1000mm/s, 10N load, are plotted as a sample to show that the volume loss due to wear, rises linearly with the increase in load:

Table: Wear loss for Carbide pin and "S-gray" disc in sliding contact at 1000mm/s, 10N

Time (sec)	Pin-wear (mm^3)	Disc-wear (mm^3)
3	1.50796	7.61051
13	3.01593	13.6989
23	5.02655	18.2652
33	7.03717	25.8757
43	8.54513	33.4862

Table 22 Wear volume loss for Carbide pin and S-gray disc in sliding contact at 1000 mm/s, 10N

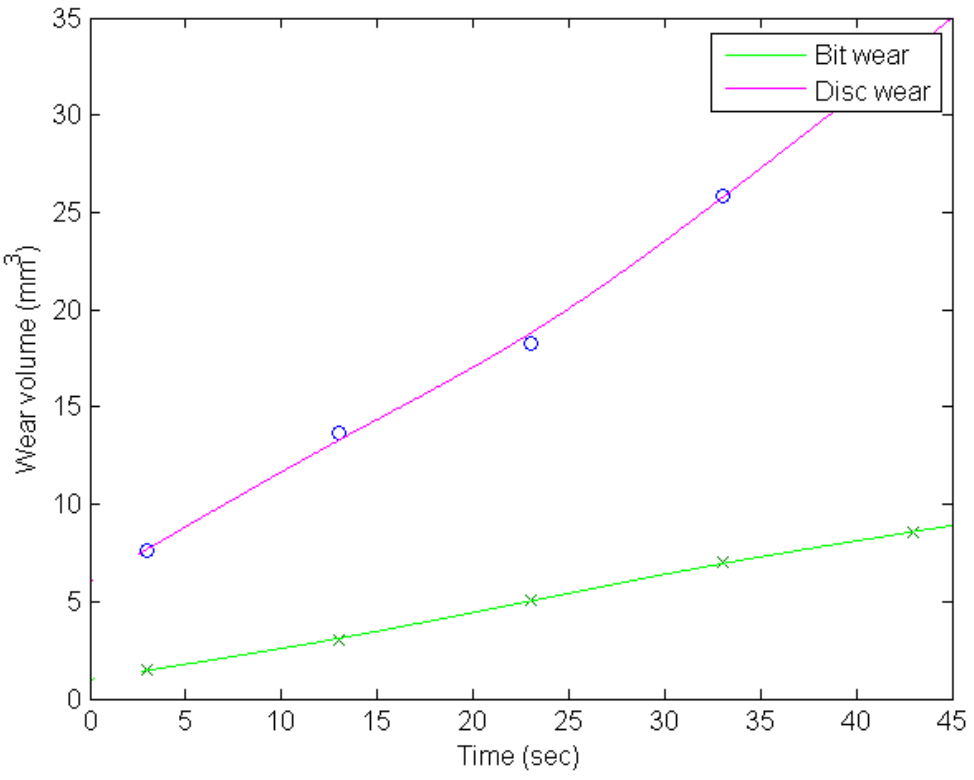

Figure 70 Wear rate comparison for pin-wear(x) and disc-wear (o) for carbide pin and s-gray disc at 1000mm/s, 10N

The wear for s-gray with HSS pin at 1000mm/s, 10N load are plotted as a sample to show that the wear volume rises linearly with the increase in load:

Table: Wear volume rates for HSS pin and s-gray disc in sliding contact at 1000mm/s, 10N

Time (sec)	Pin-wear (mm^3)	Disc-wear (mm^3)
3	0.50265	9.6132
13	1.00531	14.4199
23	2.01062	24.0332
33	2.51327	28.8398
43	3.01593	38.4531

Table 23 Wear volume loss for HSS pin and s-gray disc in sliding contact at 1000mm/s, 10N

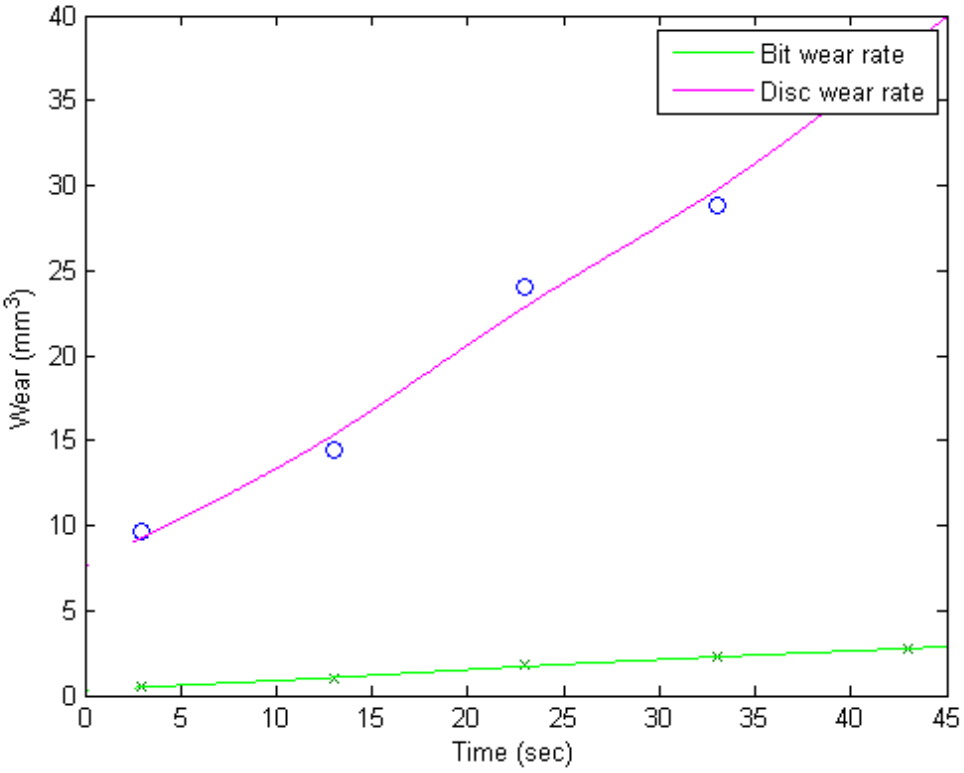

Figure 71 Wear rate comparison for pin-wear(x) and disc-wear (o) for HSS pin and s-gray disc at 1000mm/s, 10N

The wear for s-gray with carbide pin at 1500mm/s, 10N are plotted as a sample to show that the wear-rate rises linearly with the increase in load:

Table: Wear volume rates for Carbide pin and s-gray disc in sliding contact at 1500mm/s, 50N

Time (sec)	**Pin-wear (mm^3)**	**Disc-wear (mm^3)**
3	2.01062	65.9734
13	3.51858	122.522
23	5.5292	193.208
33	7.03717	259.181
43	9.04779	325.155

Table 24 Wear volume loss for carbide pin and s-gray disc in sliding contact at 1500mm/s, 50N

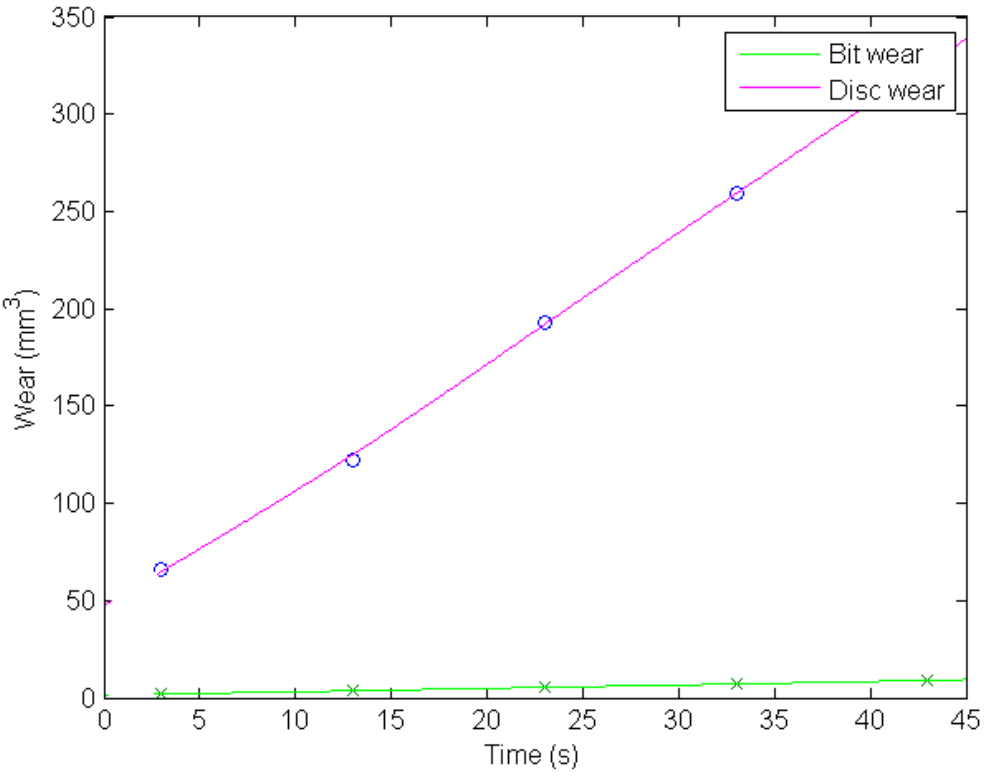

Figure 72 Wear rate comparison for pin-wear (x) and disc-wear (o) for carbide pin and s-gray disc at 1500mm/s,50N

The wear for s-gray with HSS pin at 1500mm/s, 50N are plotted as a sample to show that the wear-rate rises linearly with the increase in load:

Table: Wear volume loss for HSS pin and s-gray disc in sliding contact at 1500mm/s, 50N

Time (sec)	**Pin-wear (mm^3)**	**Disc-wear (mm^3)**
3	1.00531	19.6035
13	2.01062	49.0088
23	3.51858	78.4142
33	5.02655	98.0177
43	6.03186	117.621

Table 25 Wear volume loss for HSS pin and s-gray disc in sliding contact at 1500mm/s, 50N

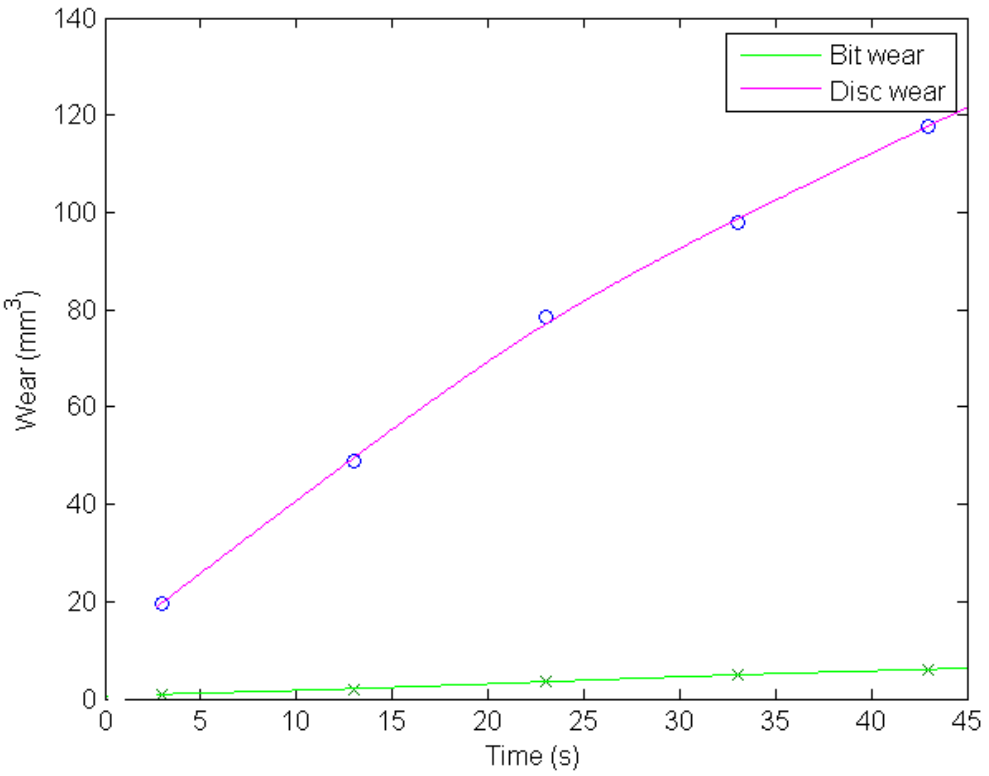

Figure 73 Wear rate comparison for pin-wear (x) and disc-wear (o) for HSS pin and s-gray disc at 1500 mm/sec,50N

The wear for s-gray with carbide pin at 2000mm/s, 100N are plotted as a sample to show that the wear-rate rises linearly with the increase in load:

Table: Wear volume loss for carbide pin and s-gray disc in sliding contact at 2000mm/s, 100N

Time (sec)	Pin-wear (mm^3)	Disc-wear (mm^3)
3	2.01062	29.2168
13	3.51858	68.1725
23	5.5292	107.1283
33	7.03717	136.3451
43	9.04779	165.5619

Table 26 Wear volume loss for carbide pin and s-gray disc in sliding contact at 2000mm/s, 100N

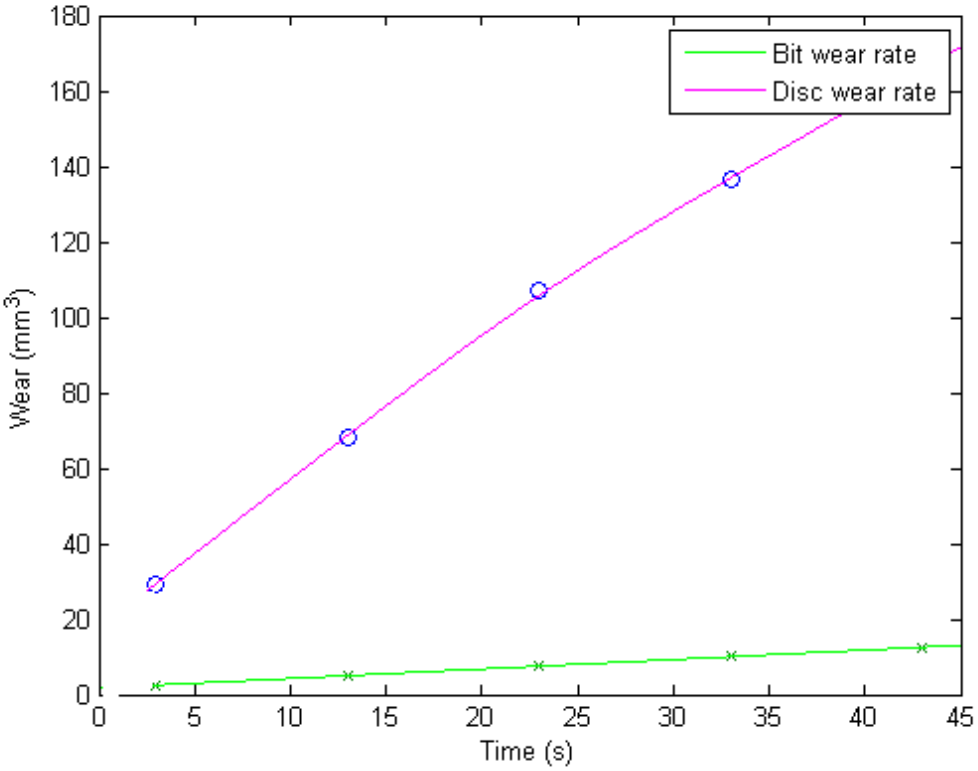

Figure 74 Wear rate comparison for pin-wear (x) and disc-wear (o) for carbide pin and s-gray disc at 2000mm/s,100N

The wear for s-gray with HSS pin at 2000mm/s, 100N are plotted as a sample to show that the wear-rate rises linearly with the increase in load:

Table: Wear volume rates for HSS pin and s-gray disc in sliding contact

Time (sec)	**Pin-wear (mm^3)**	**Disc-wear (mm^3)**
3	2.01062	65.9734
13	3.51858	122.522
23	5.5292	193.208
33	7.03717	259.181
43	9.04779	325.155

Table 27 Wear volume loss for HSS pin and s-gray disc in sliding contact at 2000 mm/s, 100N

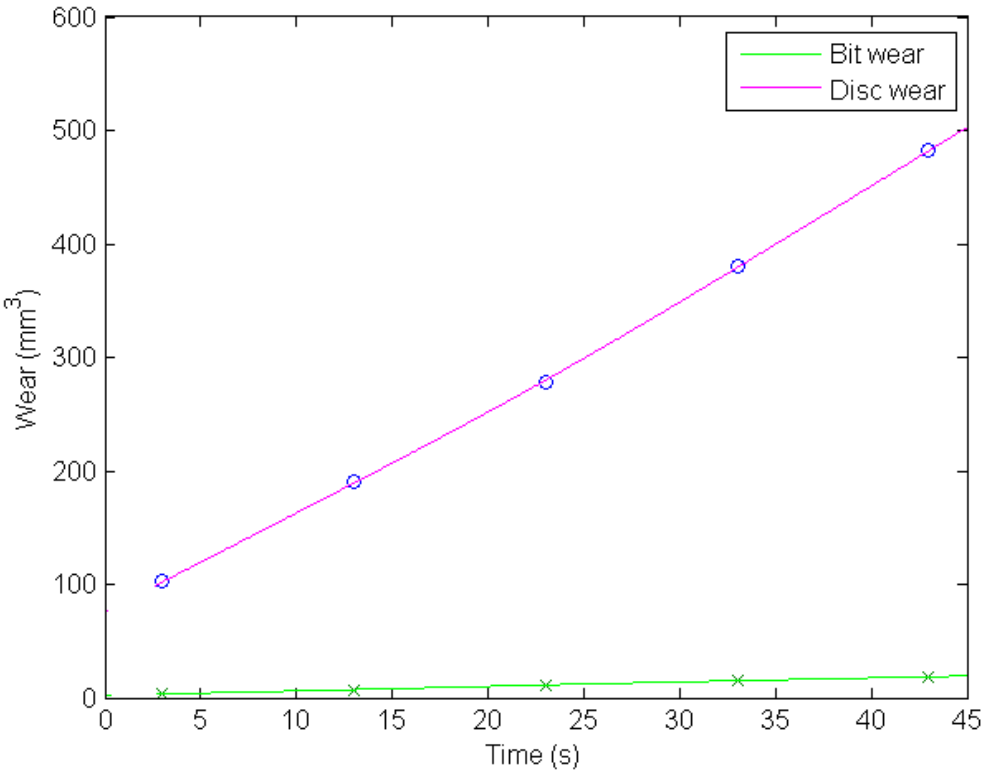

Figure 75 Wear rate comparison for pin-wear (x) and disc-wear (o) HSS pin and s-gray disc at 2000 mm/s, 100N

CONCLUSIONS

The optimal operating regions for different rocks samples were identified in the rsults section.Hence it gives the guideline for a optimal drilling range for the specific rock samples at Indigenous tribometers for the study of rock drilling are a future requirement. The experiments conducted in this study show that different rocks have different wear response to different drill-bit material at different loads and speeds, hence the factors required for drilling optimization can be identified, and tweaked for maximum results. Petroleum exploration companies like OGDCL require such equipment to maximize the outcome obtained from minimum investment, and save on precious drilling time, if the optimized factors are known.

RECOMMENDATIONS FOR FUTURE WORK

1. Since very little literature is available on the wear behavior of different rocks, this is a topic that can be explored further.
2. Use of SEM, EDS and XRD, is recommended to study the composition and morphology of the sliding materials to better identify the wear mechanisms involved.
3. Detailed wear mechanism maps of drill-bits and rocks may then be constructed to summarize different regimes of wear, such as mild, severe etc. (as in this study) and the mechanisms associated with each regime, such as delamination, abrasion, chipping, etc. This can give an insight into not only the material of the drill bit but also the type of drill bit that can be used most effectively in a specific area.
4. The response of different rocks to advanced drill bit inserts and coatings, and vice versa, can be further explored for the purpose of optimization.
5. Derivation of an analytical relation between different factors involved in wear, and the wear volume or wear rate, is a topic that needs detailed investigation.
6. 3D stylus profilometry, in combination with the single-trace method (36), can be used to obtain a better estimate of the wear volumes and rates.
7. Since rock-drilling is not a simple bit-contacting-rock processs, and involves other complications, like underground water reservoirs, presence of different debris, rise in temeperature, etc., the simple tribometer is only first step towards rock-drilling tribology studies. The tribometer can be rigged with further instrumentation to simulate further complicated scenarios, like the introduction of environmental factors, such as pressure, temperature, humidity, lubrication, contamination, etc. These will allow for a better understanding of wear behavior of different drill bit and rock sample combinations in different environmental conditions.

REFERENCES

1. *Overview no. 55 Wear-Mechanism Maps.* **Lim, S. C. and Ashby, M. F.** s.l. : Elsevier, 1987, Acta Metallurgica, Vol. 35, pp. 1-24.

2. **Watanabe, H.** Drilling Machines. *Encyclopedia of Life Suppport Systems.* [Online] Sample Chapter. http://www.eolss.net/Sample-Chapters/C05/E6-37-06-03.pdf.

3. **Wikipedia.** Drilling rig. *Wikipedia.com.* [Online] http://en.wikipedia.org/wiki/Drilling_rig.

4. **Lundell, Lars-Gunnar.** *Diamond Enhanced Rock Drill Bit For Percussive Drilling. 5,947,215* Sandviken, Sweden, September 7, 1999.

5. *Rock penetration into cemented carbide drill buttons during rock drilling.* **Beste, Ulrik, Jacobson, Staffon and Hogmark, Sture.** 2008, Wear, Vol. 264, pp. 1142-1151.

6. **Oskarsson, J.** *Tribological testing of drill bit inserts.* Uppsala University. Uppsala, Sweden : s.n., 2011. Master Thesis.

7. **Angseryd, Jenny, et al., et al.** On a wear test for rock drill inserts. *Wear.* [Accepted Manuscript, to appear in Wear]. 2012. http://dx.doi.org/10.1016/. WEA100372.

8. *Tribology of unlubricated sliding contact of ceramic materials and amorphous carbon.* **Khurshudnov, Andrew G., Olsson, Mikael and Kato, Koji.** 1997, Wear, Vol. 205, pp. 101-111.

9. *Tribological design methods for minimum surface damage of HDD slider.* **Kim, D. -E., Chung, K. -H. and Cha, K. -H.** 2003, Tribology International, Vol. 36, pp. 467-473.

10. *Pole tip recession studies of thin-film rigid disk head sliders: I. Mechanisms of pole tip recession growth.* **Xu, Junguo and Bhushan, Bharat.** 1998, Wear, Vol. 219, pp. 16-29.

11. *Tribological investigations on micromachined silicon sliders.* **Gatzen, Hans H. and Beck, Michael.** 2003, Tribology International, Vol. 36, pp. 279-283.

12. *An environmental tribometer for the study of rubbing surface reactivity.* **Adamou, A. S., et al., et al.** 2006, Wear, Vol. 261, pp. 311-317.

13. *Low temperature tribology at the B.Verkin Institute for Low Temperature Physics and Engineering.* **Ostrovskaya, Y. L., et al., et al.** 4, 2001, Tribology International, Vol. 34, pp. 265-276.

14. *Tribological tests in ceramics materials development: a pin-on-disk tribometer for high temperature and controlled atmosphere.* **Palmonari, C., Esposito, L. and Toscano, E. H.** Milano, Italy : s.n., 1989. Conference Evolution of Advanced Materials. pp. 633-638.

15. **Platon, F.** *Standard Tribological Tests for Engineering Ceramics, Ceramic Materials and Components for Engines.* s.l. : D. Keram. Ges. Publications, 1986. pp. 735-757.

16. *Tribology at high temperatures.* **Semenov, A. P.** 1, 1995, Tribology International, Vol. 28.

17. *Seizure and wear rate testing of wheel–rail contacts under lubricated conditions using pin-on-disc methodology.* **Sundh, Jon, Olofsson, Ulf and Sundvall, Krister.** s.l. : Elsevier, 2008, Wear, Vol. 65.

18. **Bowden, F. P. and Tabor, D.** *The Friction and Lubrication of Solids.* Oxford : Clarendon Press, 1950.

19. —. *The Friction and Lubrication of Solids - Part II.* Oxford : Clarendon Press, 1950.

20. *Friction-induced vibration, chatter, squeal and chaos:Part I. Mechanics of contact and friction; Part II. Dynamics and modeling.* **Ibrahim, R. A.** 1994 : s.n., Applied Mechanics Reviews, Vol. 47, pp. 209-253.

21. *Friction-induced oscillations of a pin-on-disk slider: analytical and experimental studies.* **Tworzydlo, W. Woytek, et al., et al.** 1999, Wear, Vol. 236, pp. 9-23.

22. *Significance of the normal degree of freedom and natural normal vibrations in contact friction.* **Tolstoi, D. M.** 1967, Wear, Vol. 10, pp. 199-213.

23. *Friction Oscillations with a pin-on-disc tribometer.* **Godfrey, Douglas.** 2, 1995, Tribology International, Vol. 28, pp. 119-126.

24. **Tworzydlo, W. W., et al., et al.** Numerical modeling of friction-induced vibrations and dynamic instabilities. [ed.] R. A. Ibrahim and A. Soom. *Friction-Induced Vibration, Chatter, Squeal and Chaos.* New York : ASME, 1992. Vol. 49, pp. 13-32.

25. *A new design for the pin and V-blocks tribometer.* **Sebastian, K. Savio and Bhaskar, V. R.** 4, s.l. : Elsevier Science, Ltd., 1995, Tribology International, Vol. 28, pp. 219-223.

26. *Development of a high-speed cryogenic tribometer: Design concept and experimental results.* **Subramonian, B. and Basu, Bikramjit.** 2006, Material Science and Engineering A, Vol. 415, pp. 72-79.

27. *An experimental study of ball-on-flat wear on a newly developed rotational tribometer.* **De Moerlooze, Kris, Al-Bender, Farid and Van Brussel, Hendrik.** 2011, Wear, Vol. 271, pp. 1005-1016.

28. *A new tribometer for friction and wear studies of dental materials and hard tooth tissues.* **Kulesza, Zbigniew and Sajewicz, Eugeniusz.** 2007, Tribology International, Vol. 40, pp. 885-895.

29. *Construction and evaluation of a new tribometer for polymers.* **Kashani, Mehdi Razzaghi, Behazin, Ehsan and Fakhar, Afsaneh.** 2011, Polymer Testing, Vol. 30, pp. 271-276.

30. *A rig test to measure friction and wear of heavy duty diesel engine piston rings and cylinder liners using realistic lubricants.* **Truhan, John J., Qu, Jun and Blau, P. J.** 3, 2005, Tribology International, Vol. 38, pp. 211-218.

31. *Design and development of an advanced linear reciprocating tribometer.* **Mohan, C. B., et al., et al.** 2009, Wear, Vol. 267, pp. 1111-1116.

32. *A new tribometer for friction drives.* **Sinha, Sujit K., Thia, Shi-Ling and Lim, L. C.** 2007, Wear, Vol. 262, pp. 55-63.

33. *New micro tribometer for rolling friction.* **Olaru, Dumitru N., et al., et al.** 2011, Wear, Vol. 271, pp. 842-852.

34. *Sliding wear map for the magnesium alloy Mg-9Al-0.9 Zn (AZ91).* **Chen, H. and Alpas, A. T.** 2006, Wear, Vol. 246, pp. 106-116.

35. *A comparison of methods for determining wear volumes and surface parameters of spherically-tipped sliders.* **Whitenton, E. P. and Blau, P. J.** 1988, Wear, Vol. 124, pp. 291-309.

36. *An efficient method for accurately determining wear volumes of sliders with non-flat wear scars and compound curvatures.* **Qu, Jun and Truhan, John J.** 2006, Wear, Vol. 261, pp. 848-855.

37. *Recent developments in wear mechanism maps.* **Lim, S. C.** 1-3, s.l. : Elsevier Science Ltd., 1998, Tribology International, Vol. 31, pp. 87-97.

38. *Researches on the mechanism of abrasion. Report III, mechanism of abrasion of cast iron and steel.* **Okoshi, M. and Sakai, H.** 1941, Trans. JSME, Vol. 7, pp. 29-47.

39. *Wear maps for grey cast iron.* **Riahi, A. R. and Alpas, A. T.** 2003, Wear, Vol. 255, pp. 401-409.

40. *Subsurface sliding wear damage characterization in Al–Si alloys using focused ion beam and cross-sectional TEM techniques.* **Meng-Burany, X., et al., et al.** 2011, Wear, Vol. 270, pp. 152-162.

41. *Wear mechanism maps for TiN-coated high speed steel.* **Wilson, S. and Alpas, A. T.** 1999, Surface and Coatings Technology, Vols. 120-121, pp. 519-527.

42. *Wear Mechanism Maps for Thermal-Spray Steel Coatings.* **Edrisy, A., Perry, T. and Alpas, A. T.** October 2005, Metallurgical and Material Transactions A, Vol. 36A, pp. 2737-2750.

43. *A wear mechanism map for the diamond polishing process.* **Hird, J. R. and Field, J. E.** s.l. : Elsevier, 2005, Wear, Vol. 258, pp. 18-25.

44. ASTM Standard G 99-05, Standard Test Method for Wear Testing with a Pin-on-Disk Apparatus. *Annual Book of ASTM Standards.* 2005. Vol. 03.02. DIN 50 324.

45. *Role of Atmospheric Oxidation in High Speed Sliding Phenomena.* **Cocks, M.** s.l. : The American Institute of Physics, 1957, Journal of Applied Physics, Vol. 28, pp. 835-843.

46. *Processes of Metal Transfer and Wear.* **Antler, M.** 1964, Wear, Vol. 7, pp. 181-204.

47. *The Relationship Between Load and Sliding Distance in the Initiation of Mild Wear in Steels.* **Farrell, R. M. and Eyre, T. S.** 5, 1970, Wear, Vol. 15, pp. 359-372.

48. *The Delamination Theory of Wear and the Wear of a Composite Metal Surface.* **Jahanmir, S., Suh, N. P. and Abrahamson II, E. P.** 1976, Wear, Vol. 32, pp. 33-49.

49. *Wear of Metals at high sliding speeds.* **Saka, N, Eieiche, A. M. and Suh, N. P.** 1977, Wear, Vol. 44, pp. 109-125.

50. **Bhattacharyya, S.** 1980, Wear, Vol. 61.

51. *Vacuum sliding behaviour of thermally oxidized Ti–6Al–4V alloy.* **Yazdanian, M. M., Edrisy, A. and Alpas, A. T.** 2007, Surface & Coatings Technology, Vol. 202, pp. 1182-1188.

52. **Kinsella, F. H. and Childs, T. H.** 1978. Inst. of Mechanical Engineers Conference Publications 1978. Vol. 55.

APPENDIX-A

The motor-controller wiring sequence is as follows. The terminals U,V,W on the controller are to be connected with the terminals U1,V1,W1 on the motor. The motor connection box has two connection configurations. However the connection has to be made with the delta connection terminals. It is indicated with the symbol Δ in the connection box.The terminals R,S,T are used for connecting the controller to the main three phase power.

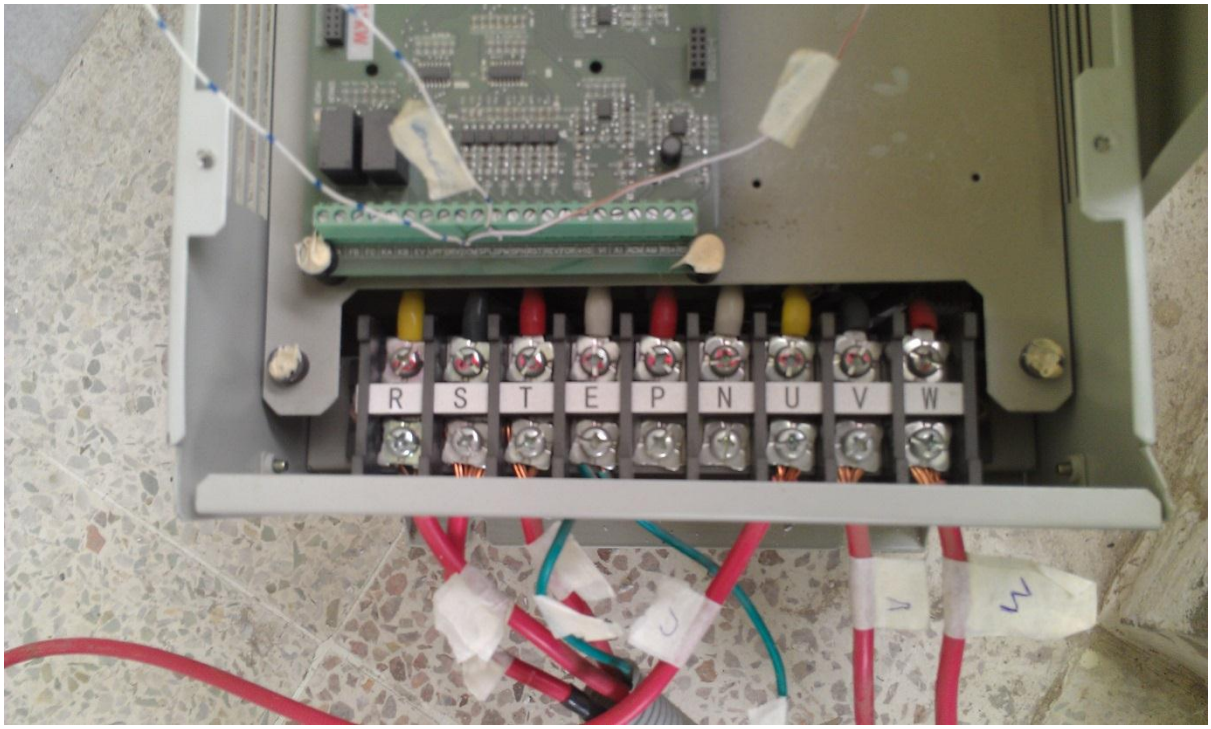

Figure 76 wiring connections on the controller

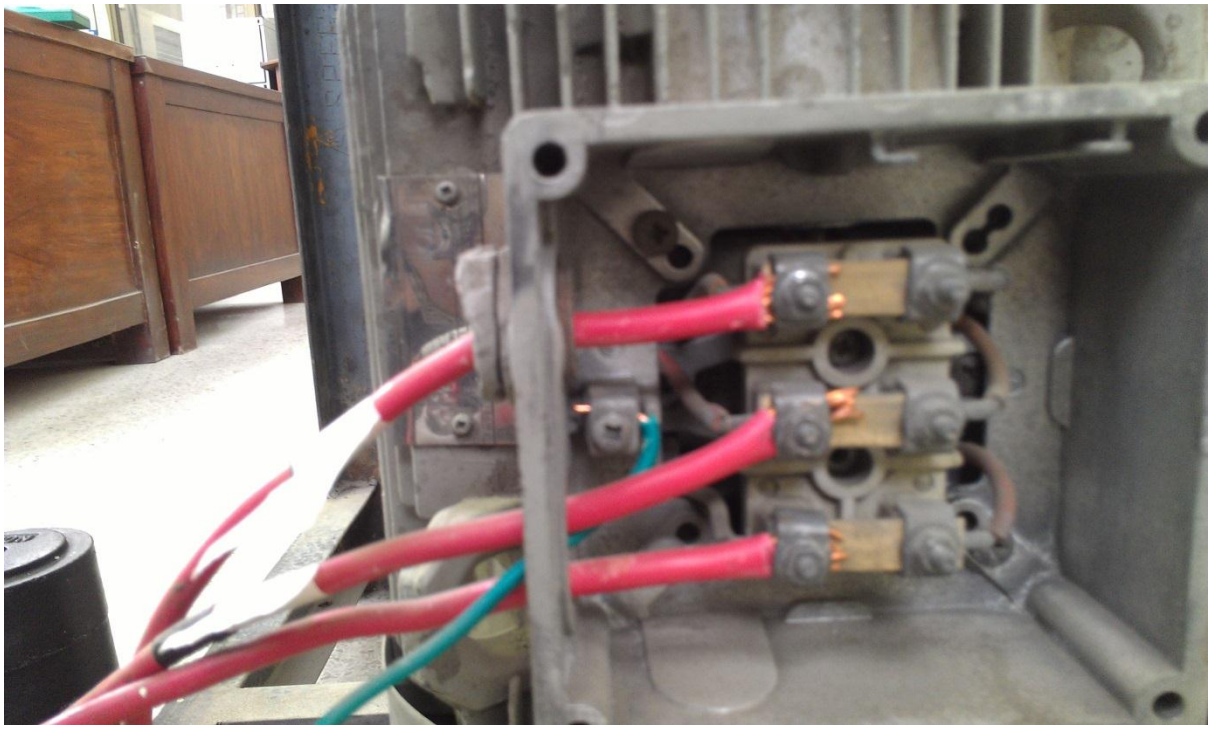

Figure 77 wiring connections on the motor

APPENDIX-B

MATLAB CODE FOR PLOTTING WEAR DATA

```
clear all
clc
clf

wear=[0.299896015 0.281559703 0.151033846;
0.292940282 0.254608601 0.226409038;
0.12    0.12    0.12];

%Interpolating load and speed matrices

load(1,1:5)=10:40/4:50;
load(1,5:9)=50:50/4:100;
speed=1:1/8:2;

%creating the contour plot
figure;
%interp2 code is used to interpolate the wear data using cubic spline
[C,h] = contour(load, speed, interp2(wear,2,'cubic'));
text_handle3 = clabel(C,h);
xlabel('Load (N)')
ylabel('Speed (m/sec)')
zlabel('Wear volume (mm^3)')
title('Contour map for material loss from Sample1 disk, while using HSS
pin, at variable speed and load ')
colorbar;

figure
surface(load,speed,interp2(wear,2,'cubic'));
title('Surface plot for material loss from Sample1 disk, while using HSS
pin, at variable speed and load ')
xlabel('Load (N)')
ylabel('Surface speed (m/sec)')
zlabel('Wear volume (mm^3)')
```

MATLAB CODE FOR PLOTTING WEAR-RATES

```
time=[3 13 23 33 43]';
disc=[0.064
0.226
0.612
0.69
0.779
];
bit=[1.215428577
4.768255
9.594828616
12.32428577
14.78514292
];
```

```
fitdisc=fit(time,disc,'smoothingspline');
fitbit=fit(time,bit,'smoothingspline');

figure
plot1=plot(time,disc,'o',time,bit,'x');
hold on
plot2(1)=plot(fitbit,'g');
hold on
plot2(2)=plot(fitdisc,'m');

set(plot2(1),'DisplayName','Bit wear rate');
set(plot2(2),'DisplayName','Disc wear rate');
xlabel=('Time (sec)' );
ylabel=('wear rate (mm^3/sec)');
Title=('Disc and bit wear rates v/s time');
```

MATLAB CODE FOR PLOTTING SCATTER PLOTS

```
clf

%loadx is the load matrix,speedx matrix is the speed matrix
%wearn is the wear rate matrix to be plotted

scatter(loadx(1,:),speedx,5,'b','filled'); %scattering the dots
text(loadx(1,:),speedx,cellstr(num2str(wearn(1,:)'))); %adding text
hold on %holding on to the figure for further dots
for i=2:7
scatter(loadx(i,:),speedx,5,'b','filled');
text(loadx(i,:),speedx,cellstr(num2str(wearn(i,:)')));
end

%for crowding, every set of experiments is saved as a separate load, speed
and wear matrix
for i=1:length(load1)
scatter(load1(i),speed1,5,'g','filled');
text(load1(i),speed1,cellstr(num2str(wear1(i))),'horizontal','center','vert
ical','bottom');
end
for i=1:length(load2)
scatter(load2(i),speed2,5,'g','filled');
text(load2(i),speed2,cellstr(num2str(wear2(i))),'horizontal','center','vert
ical','bottom');
end
for i=1:length(load3)
scatter(load3(i),speed3,5,'g','filled');
text(load3(i),speed3,cellstr(num2str(wear3(i))),'horizontal','center','vert
ical','bottom');
end
for i=1:length(load4)
scatter(load4(i),speed4,5,'g','filled');
text(load4(i),speed4,cellstr(num2str(wear4(i))),'horizontal','center','vert
ical','bottom');
end
%v is the vector which defines the levels of contours
[C,h]=contour(loads',speeds,interp2(wearn,2,'cubic')',v); %superimposing
the contour plot
```